universität wien

MASTERARBEIT / MASTER'S THESIS

Titel der Masterarbeit / Title of the Master's Thesis

„Immune System Engagers With Tuneable Properties“

verfasst von / submitted by

Ricarda Mauthner, BSc

angestrebter akademischer Grad / in partial fulfilment of the requirements for the degree of

Master of Science (MSc)

Wien, 2022 / Vienna 2022

Studienkennzahl lt. Studienblatt / degree programme code as it appears on the student record sheet:	A 066 862
Studienrichtung lt. Studienblatt / degree programme as it appears on the student record sheet:	Masterstudium Chemie UG2002
Betreut von / Supervisor:	Univ.-Prof. Dr. Christian Friedrich Wilhelm Becker
Mitbetreut von / Co-Supervisor:	

Acknowledgements

First and foremost, I want to thank my supervisor Christian Becker for having me as one of his master students. Thank you for the guidance, the welcoming work environment and the possibility to work on such an interesting topic. I had lots of fun and was able to learn a lot during my practical work.

I also want to say a special thanks to Manuel Felkl. Thank you for the time you took when I had questions during my practical work. Thank you for all the nice calls we had, when I needed guidance and thank you for your patience with me.

Of course, I need to thank all the members of the Becker Group, Alanca Schmid, Leopold Dürrauer, Oliver Gajsek, Somnath Mukherjee and all the others. Thank you for welcoming me in your office, for the scientific expertise you provided me with, and also for the occasional meeting outside the work environment. I really appreciate all the help I received and hopefully you were not to annoyed with my many questions.

It goes without saying, that all my friends, who supported me through the highs and lows of writing a master thesis also deserve a mention here. Thanks Robert T. for the hours of online conversations about a variety of very scientific topics. Thanks Christian D. for always having an open ear, even when I was frustrated with my work and thanks for the continuous support, even when I was annoying from time to time. A special thanks to Michael M. for the occasional distraction from work, for listening to my complaints and for being there for me no matter what. I also need to thank Athenais L., Stephan S., Rainer B. and all the others, for supporting me outside the university and continuously taking loads of my shoulders if I needed you to. Thank you for making this time unforgettable and supporting me, no matter what, you are real ones.

At last, I want to thank my family, especially my parents and grandparents, for supporting me through my whole study. Thank you for always being there for me, for the emotional and financial support and always having an open ear.

Danke Billy Oma und Opa, Danke Mama und Papa, Bussi.

1. Table of contents

2. Abstract

According to GLOBOCAN 2020 19.3 million new cases of cancer were diagnosed in one year and 10 million people died of this disease. It is predicted, that by 2040 there might be as much as a 47% increase in new cancer cases. With this statistic in mind, the search for better cancer therapeutics becomes even more urgent. In addition to well-established cancer drugs, like cis-Platin, monoclonal antibodies (mAbs) have found their way in cancer treatment. The latter display many advantages over small molecule drugs, like their ability to selectively target cancer cells while leaving healthy cells unharmed or to activate the body's immune response. As of today, more than 14 mAbs are approved as cancer therapeutics. On the flip side, mAbs also show some disadvantages, such as their size, difficulty in generating them at large scales, limited stability and fewer possibilities of modification. To create more suitable drugs, which compensate for some of these disadvantages, so called "Immune system engagers" (ISErs) are being designed. They possess an intermediate size between mAbs and small drug molecules as well as having more modification possibilities. ISErs can also activate the innate immune system and specifically target cancer cells.

The goal of this work was to synthesize new ISErs and optimizing them with regard to their structure, bioavailability and ability to activate the innate immune system. To achieve this, Fmoc solid phase peptide synthesis (SPPS) was combined with chemical ligation techniques. As starting structure for the synthesis and optimisation, a known ISEr called Y9 was used. The efficiency of this ISEr has already been proven in cell culture studies and in a guinea pig model. The structure of Y9 consists of an formylated effector and two binders. The latter are linked via polyethylene glycol (PEG) chains to the effector. The formylated short amino acid sequence can also be found in *Staphylococcus aureus* and activates the *N*-formyl peptide receptors on immune cells. The binders target with high affinity the integrin α3 chain, which is overexpressed on the cell surface of many tumours.

For the synthesis of the novel ISErs, first the core structure of Y9 was modified by coupling PEG chains of different molecular weighs via copper(I)-catalyzed alkyne-azide cycloaddition (CuAAc) to the structure, producing so-called tuneable ISErs (t-ISErs). Furthermore, activatable ISERs (a-ISErs) with a cleavable effector were designed to increase effector concentration in tumor tissue and the corresponding immune response. Two different strategies were applied here. First, the effector was linked to the larger scaffold with a hydrazone, which should be cleaved in the hypoxic low pH environment of cancer cells. Secondly, two non-proteinogenic amino acids, valine and citrulline, were introduced into the structure with the goal of being cut by matrix metalloproteinases (MMP), which are also overexpressed by tumour cells.

During this thesis three novel ISErs were successfully synthesized and additionally tested regarding their effector and binder activity. One ISEr, with an introduced hydrazone linkage, proved to be unstable during analysis and purification and was therefore difficult to synthesize. Additionally, cleavage experiments with MMP2 were performed on one of the ISErs with a novel Val-Cit cleavage site but no cleavage from the chosen MMP could be observed.

3. Zusammenfassung

Krebs ist in der heutigen Zeit eine der häufigsten Krankheiten, wobei laut GLOBOCAN 2020 19,3 Millionen Menschen im Jahr 2020 an Krebs erkrankten und 10 Millionen Menschen an den Folgen dieser Krankheit starben. Schätzungen dieser Studie prognostizieren eine Steigerung um 47% an Krebsneuerkrankungen bis zum Jahr 2040. Diese Fakten machen die Notwendigkeit einer zielgerichteten und erfolgreichen Behandlung umso offensichtlicher. In der Krebstherapie finden heutzutage Antikörper bereits ein breites Einsatzgebiet, aufgrund ihrer Fähigkeit einzelne Ziele selektiv anzugreifen und das Immunsystem zu aktivieren, ohne gesunden Zellen dabei zu schaden. Über 14 monoklonale Antikörper sind bereits in der Krebstherapie zugelassen.

Antikörper besitzen jedoch bestimmte Nachteile, wie beispielsweise ihre Größe, Schwierigkeit der Herstellung in großem Maßstab, beschränkte Selektivität, beschränkte Stabilität und geringe Anzahl von Modifikationsstellen. Um einige dieser Nachteile ausgleichen zu können, werden sogenannte „Immune system engagers“ (ISErs) synthetisch hergestellt, die eine geringere Größe und breitere Modifikationsmöglichkeiten bieten. ISErs kombinieren die Fähigkeit von Antikörpern spezifische Ziele im Körper anzugreifen sowie deren Fähigkeit das Immunsystem zu stimulieren und umgehen dabei weitgehend die Größen- und Stabilitätsprobleme.

Ziel dieser Arbeit war, die Synthese neuer, synthetischer ISErs und die Verbesserung dieser hinsichtlich ihrer Struktur, biologischen Verfügbarkeit sowie ihrer Fähigkeit das angeborene Immunsystem zu aktivieren. Hierfür wurde klassische Fmoc- Festphasenpeptidsynthese mit verschiedenen chemischen Ligationsmöglichkeiten kombiniert. In dieser Arbeit wurde als Ausgangsstruktur ein bereits literaturbekannter ISEr namens Y9 verwendet dessen Effizienz, sowohl des Effektors als auch der beiden Binder, bereits in Zellstudien und im Meerschweinmodell nachgewiesen wurden.

Y9 setzt sich aus einem formylierten Effektor und zwei Bindern zusammen. Die zwei Binder sind über monodisperse Polyethylenketten (PEG) an den Effektor gebunden. Die formylierte Sequenz des Effektors wird beispielsweise im Bakterium *Staphylococcus aureus* angetroffen und aktiviert bekannterweise die *N*-formyl Peptidrezeptoren an Immunzellen. Die Binder binden mit einer hohen Affinität an die Integrin α3 Kette, welche von gewissen Tumorarten an der Zelloberfläche überexprimiert wird.

Zur Synthese der neuen ISErs wurden zunächst verschieden lange PEG Ketten an die Grundstruktur von Y9 mittels Kupfer(I)-katalysierte Azid-Alkin-Cycloaddition (CuAAc) gekoppelt, um die sogenannten „tuneable“ ISErs (t-ISErs) herzustellen. Weiters wurden „activatable“ ISErs (a-ISErs) hergestellt, die einen spaltbaren Effektor besitzen, um die Effektor-Konzentration im Tumorgewebe zu erhöhen und damit auch die einhergehende Immunantwort. Hier wurden zwei verschiedene Ansätze verfolgt, erstens sollte ein pH labiler Effektor generiert werden, der spezifisch in den hypoxischen Tumorzellen bei niedrigen pH-Werten abgespalten wird. Zweitens wurden zwei nicht proteinogene Aminosäuren, Valin und Citrullin, in die Sequenz eingebaut, die spezifisch von Matrixmetalloproteasen (MMP) gespalten werden sollen, welche in gewissen Tumoren überexprimiert sind.

Im Rahmen dieser Arbeit konnten drei neue ISErs erfolgreich synthetisiert werden. Beide t-ISErs sowie ein a-ISEr konnten zusätzlich auf die Aktivität der Binder und des Effektors getestet werden. Weites wurde ein a-ISEr mit einer Hydrazonbindung hergestellt. Hier gab es allerdings Probleme mit dessen Stabilität während der Aufreinigung, daher konnte diese Verbindung nicht vollständig hergestellt werden. Während den zusätzlich durchgeführten Experimenten zur Spaltung des a-ISErs mit Val-Cit mithilfe von MMP2 und HT29 Zellen, konnten keine Spaltprodukte beobachtet werden.

4. List of Abbreviations

GLOBOCAN	Global cancer statistics-online Database
Fmoc	Fluorenylmethoxycarbonyl
t-ISEr	Tuneable-Immune system engager
a-ISEr	Activatable-Immune system engager
SPPS	Solid phase peptide synthesis
Boc	tert-butyloxycarbonyl
AA	Amino Acid
DMF	Dimethylformamid
TFA	Trifluoroacetic acid
mmol	milli Mole
M	Mole
DIPEA	Diisopropylethylamin
TFA	Trifluoroacetic acid
TIS= TiPS	Triisopropylsilane
Mtt	4-methyltrityl
HATU	Hexafluorophosphate Azabenzotriazole Tetramethyl Uronium
ACN	Acetonitrile
PBS	Phosphate buffered saline
Trt	Trityl
tBu	Tert-butyl
Asc	Ascorbic acid
TBTA	Tris(benzyltriazolylmethyl)amine
HBTU	Hexafluorophosphate Benzotriazole Tetramethyl Uronium
PEG	Polyethylene glycol
ISEr	Immune system engager
mAb	Monoclonal antibody
MP	Main pool
SP	Side pool
CuAAc	Cupper-alkyne-azide-cycloaddition
MMP	Matrix metalloproteinase

DMEM	Dulbecco's Modified Eagle's Medium
FBS	Fetal Bovine Serum
MT-MMP	Membrane type matrix matalloproteinases
PMA	Phorbol-12-myristat-13-acetat
PAMP	Pathogen associated molecular pattern
MHC	major histocompatibility complex
FPR	formyl peptide receptors
TIMPs	Tissue inhibitors of matrix metalloproteinases
DHR	Dihydrorhodamine

5. Introduction

5.1 Peptides and Proteins

Proteins belong, together with carbohydrates and nucleic acids, to the core molecules responsible for biological life as we know it. The main advantage of proteins, compared to the other two, is their versatility which makes them best suited for the involvement in a great number of biological processes like working as catalysts, neurotransmitters, transporters for smaller molecules, immune defence, growth, movement and many more.[1] Peptides have consecutively gained attention in the scientific community due to their involvement in life science. Especially their applications in the medical field, for example the development of new drugs, has put peptides in the spotlight. The ease of use of recombinant methods, compared to the time consuming and expensive isolation of peptides or proteins from their natural sources, has contributed to the progress in this field. [2]

5.1.1 Building Blocks

Chemically speaking proteins are oligo- or polypeptides constructed from different amino acids, which are connected by a condensation reaction as seen in *Figure **1***. The transition between peptides and proteins is not a clear cut, rather than a formal classification, stating, that a polypeptide with a sequence longer than 100 amino acids is referred to as a protein. [2] The condensation leads to the formation of the amide bond between the carboxy group of one amino acid and the amino group of the following one, via release of water. The sequence, in which the amino acids are connected is called the primary structure.

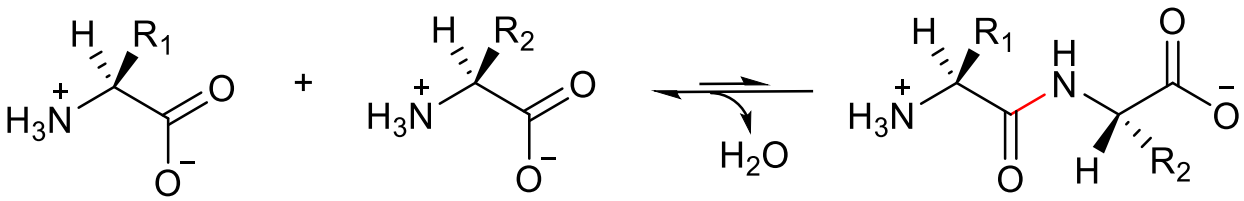

Figure 1 Condensation (from left to right) between two amino acids. Formation of a new amide bond (red)

As proven in 1953 by Pauling and Corey, via X-ray crystallography, the C-N bond possesses a partial double bound character through delocalisation electrons between the carbonyl group and the nitrogen. Therefore movement around the C-N bond is restricted. [3] The conformation of the peptide backbone is determined by the two torsion angles: φ [phi] and ψ [psi] as seen in *Figure **2***. As a result the peptide bond is planar leading to a *cis* and a *trans* conformer where the *trans* conformation is more common, because it places the two α-carbons on the opposite sides of the amide bond. [1]

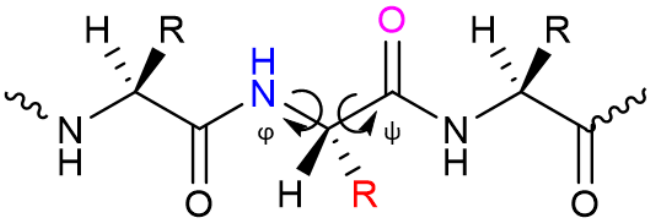

Figure 2 Amide bond with both torsion angles phi and psi

20 proteinogenic amino acids are known today, meaning that all naturally occurring peptides and proteins are constructed of these few monomers. Amino acids consist of a central, chiral carbon atom, which is connected to one amino group, one carboxyl moiety, one hydrogen and the representative side chain. The only exception from this rule is glycine with another hydrogen atom as a side chain and therefore no chiral carbon atom, as can be seen in the figure below [1]. All natural occurring amino acids have the L-conformation.

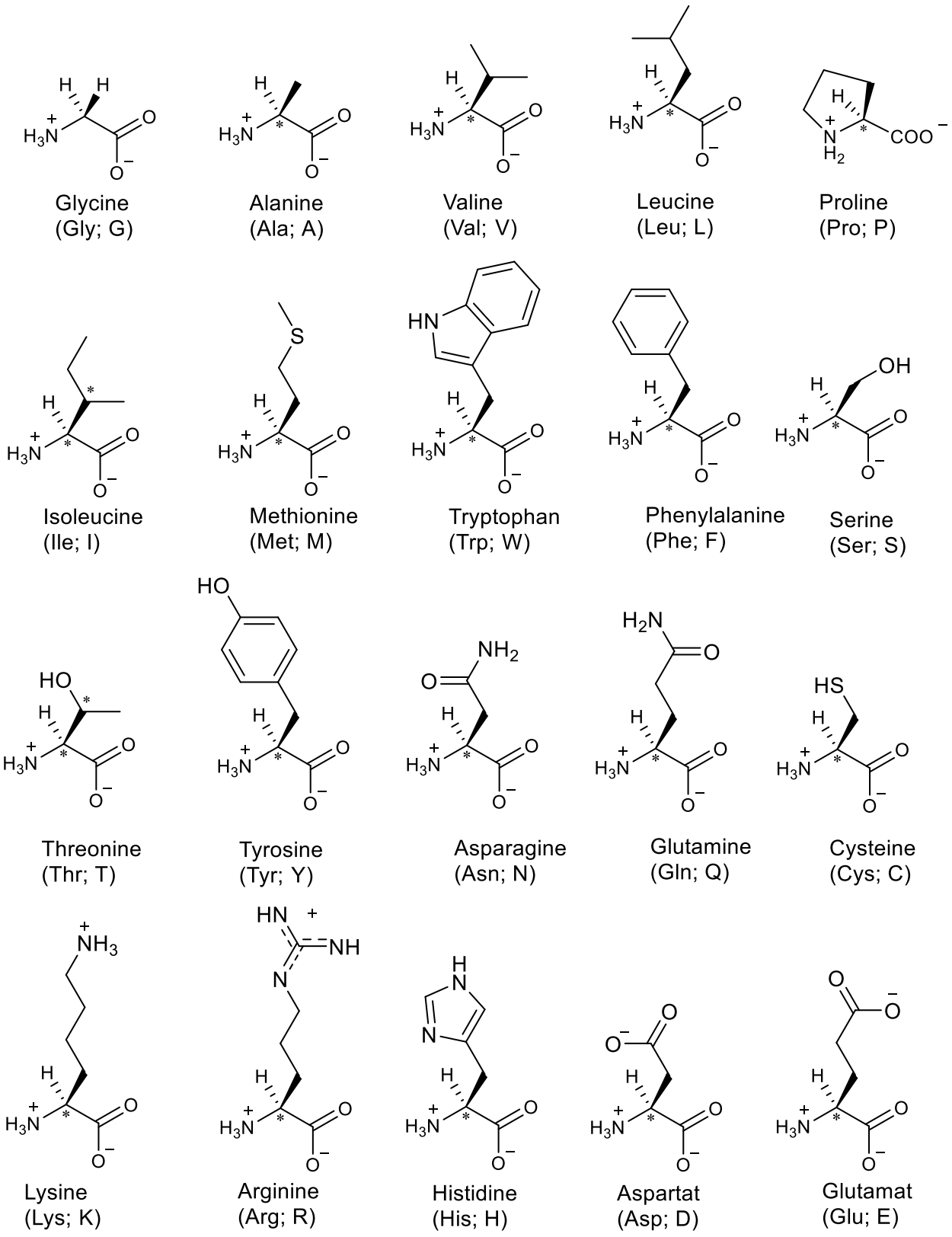

Figure 3 The 20 proteinogenic amino acids, with their full names as well as their three and one letter codes

Due to the amino and carboxyl group, the ionisation state of one amino acid is pH dependent, ranging from both groups being protonated at a low pH, the zwitterionic state, as seen in ***Figure 3*** at neutral pH and both groups being deprotonated at a high pH. The side chains can be divided into four subcategories, *hydrophobic*, *polar*, *positively* and *negatively charged* at physiological pH. [1]

Oligopeptides can fold into a secondary structure, which normally presents as an α-helix or an β-pleated sheet. Other formations, like a β-turn or Ω-loop are also possible. These secondary structures are mainly held together by hydrogen bonds between the N-H and C=O groups of the amino acids. [1] The final 3-dimensional structure of a large peptide or protein is defined by the amino acid primary sequence, as it can have a stabilising or destabilising effect.

5.1.2 Peptide Synthesis

The concept of synthesizing peptides on a solid phase was introduced in 1963 by Merrifield, making peptides easily accessible for the broad scientific community.[4] For the modern mechanism of solid phase peptide synthesis (SPPS), a combination of permanent as well as temporary protection groups comes into play. The peptide is bound to a solid phase with the use of a bifunctional linker, which is inert during the coupling conditions and also serves as a permanent protection group for the first carboxyl-group. The permanent protection groups are generally designed to protect the side chains of the different amino acids and remain on the molecule during the whole synthesis and the temporary groups are generally attached to the *N*-terminal amine and removed each coupling cycle. [5] Two main strategies are used today, depending on the temporary protection group for the *N*-terminal amine of the peptide, the Boc or Fmoc strategy. Fmoc SPPS prevailed against the Boc strategy because of the milder reaction conditions, like the avoidance of HF for cleavage, the availability and low cost of building blocks and the range of orthogonal protecting groups involved in the reaction. Fmoc is used as a protection group for the *N*-terminal amine side of the peptide and is labile against bases.[5] The deprotection strategy for Fmoc is the use of piperidine resulting in the cleavage product dibenzofulvene, which has an UV absorption and can therefore be easily used for reaction monitoring or resin modification monitoring, as performed in this work later on.

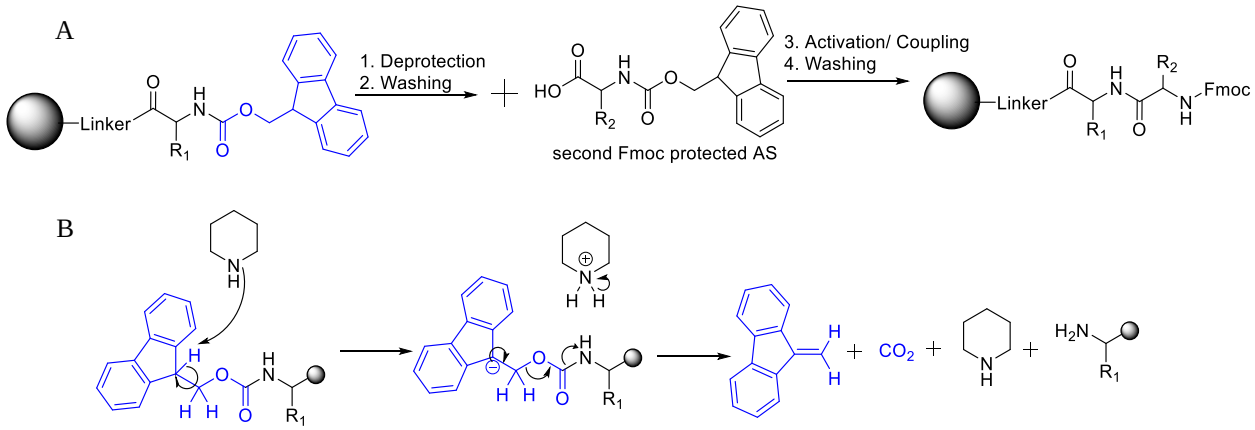

Figure 4 ***A)*** *General working steps of the coupling for the classic Fmoc strategy, with the deprotection of the Fmoc group, the removal of the dibenzofulvene by washing, the activation of the second amino acid followed by coupling and the last washing step for removal of the uncoupled amino acid* ***B)*** *Reaction mechanism for deprotection of the Fmoc group with piperidine*

The yield of SPPS depends on the success of every coupling step, as the efficiency of each complete cycle has an increasing influence on the final yield, the longer the amino acid chain becomes. For the Boc deprotection the acid TFA is used, which could cleave off small amounts of the side chain protection groups as well. This leads to a limitation of the peptide length as the success of the synthesis is bound to the efficiency of each step.[4]

5.2 The immune system

Proteins have a variety of tasks in the human body, for example they play an important role in the function of the immune system. Because of their ability to fold into complex three-dimensional structures, proteins are the ideal building blocks for antibodies.[6] The immune response of the human body can be broadly divided into two categories, first the innate and second the adaptive immune system. Both systems are responsible for detection as well as elimination of foreign pathogens in the body. The innate immune system is present in all animals and is designed to target the most common threats and has a 500-million-year evolutionary history. The adaptive immune system is a feature, present in most vertebrates and relies heavily on the production of antibodies. It can specifically react to novel invaders and produce antibodies, which are able to recognise their target again, in case of a second exposure.[6] Antibodies are produced by B cells, which are part of white blood cells, derived from the bone marrow, and are divided into five classes: IgG, IgM, IgA, IgD and IgE, with IgG being the most common. (Ig= immune globulin).

5.2.1 The innate immune system

All cells involved in the innate immune response are formed from stem cells in the bone marrow and are part of the leukocytes, the white blood cells.

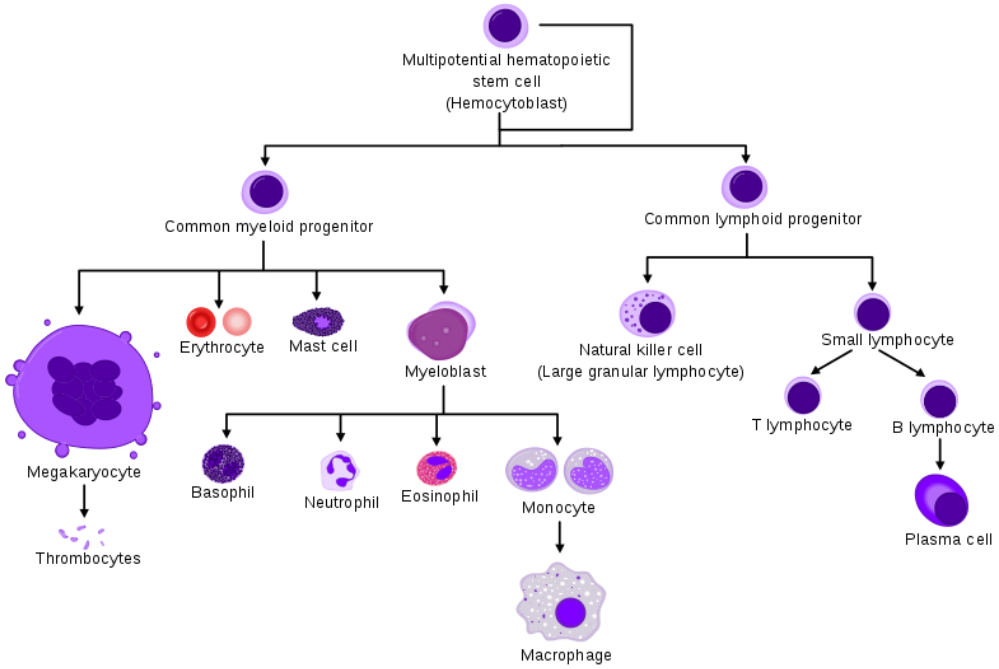

Figure 5 Simplified schematic description of the haematopoiesis, or the formation of different blood cell types from one stem cell in the bone marrow[7]

These cells are omnipresent in every tissue of the body and detect, with different cell surface receptors, foreign invaders. Those receptors are designed to recognize pathogen-associated molecular patterns (PAMPs)[8]. PAMPs are conserved molecular structures, which are very common in microbial pathogens and often responsible for the survival of the invading microbe. Immune cells use these PAMPs to differentiate between healthy cells of the body and the disease. A major part of leukocytes are the myeloid cells, which are part of the blood cells, that don't belong to the lymphatic system, as can be seen in *Figure **5***. One of the most important cells from the myeloid subcategory, are the macrophages, which are present in all tissue types exposed to the environment. These cells are produced as monocytes and are transported through the blood stream. Upon entering a tissue, the monocytes mature into macrophages. Macrophages are generally the first line of defence against pathogens. After recognition of a PAMP from a macrophage, they activate and will do two things. First, they release cytokines, which are hormone like signalling molecules designed to attract other members of the innate immune system, like neutrophils. Interleukins are an example of such molecules. Those cytokines also activate endothelial cells, which start producing the glycoprotein selectin, which is designed to slow neutrophiles from the blood

steam down, so they can successfully invade the inflamed tissue. Secondly, they start a process called phagocytosis, where the macrophages encapsulate the pathogen presenting the PAMPs. During this process the pathogen gets incapsulated in a phagosome from the macrophage, once inside the cell, the phagosome fuses with the lysosome, another capsule inside the macrophage, containing different proteases and other degrading chemicals. This process degrades the pathogen and the remaining fragments can be presented as antigens for the adaptive immune system on the surface of the macrophage with the class two major histocompatibility complex (MHC) molecules. Therefore, macrophages are part of the antigen presenting cells. The activated macrophage also increases production of reactive oxygen species (ROS), like hydrogen peroxide. [6]
Neutrophiles are short lived killer cells of the innate immune system with an average life span of just about five days. Upon detecting a cytokine in the blood stream, they invade the inflamed tissue and destroy pathogens as well as healthy tissue. During this process neutrophiles also produce cytokines to attract other immune cells. The invasion and movement of different cells due to a stimulus is called cytotaxis.

5.2.2 The adaptive immune system

The adaptive immune system is designed to adapt against pathogens after the first contact and recognize them if a repeated exposure occurs. This is achieved with the former mentioned different types of antibodies. 75% of the total amount of antibodies are IgG. Antibodies are built from two heavy and two light chains and are generally structured to possess a constant region (Fc) and a more variable region (Fab), as will be discussed later in this work. The Fc region is different for the types of antibodies and therefore used to classify them. Antibodies are formed from B-cells, which are part of the lymphatic system, as can be seen in *Figure **5***. They are derived from the bone narrow and after maturing can be found in every part of the human body. Ideally, B-cells produce antibodies for every possible pathogen to be available in case of an invasion. With just about 25 000 genes in the human body it is mathematically impossible to have a gene decoding an antibody for every pathogen. The nobel prize winner Susumu Tonegawa discovered in 1977 that the DNA of immature and mature B-cells differentiates from each other[9]. He also discovered that only four gene segments are responsible for the formation of the heavy chain of an antibody, which he dubbed V, D, J and C. There are a different number of variations from each segment and during maturation the B-cell ends up with just one possibility. Light chains follow the same principle of gene segments and through random matching in the mature B-cell, a large library of different antibodies can be created with only a small amount of starting gene segments.[6] Proteins follow the same strategy, forming complex, diverse structures with just 20 amino acid building blocks. After the B-cell matures it produces a small number of its antibodies and presents them on its surface to form the so-called B-cell receptors (BCRs). If the corresponding antigen to the antibody comes into contact with the BCRs, the B-cell starts to proliferate and all clones start to produce the specific antibody to eliminate the pathogen.[6] Together with the antibody producing B-cells the killer T-cells, or T-lymphocytes, are also a part of the adaptive immune system. The difference between B and T cells is that T-cells mature in the thymus and after activation and proliferation the T-cells do not produce antibodies but eliminate infected cells.

5.3 Immune oncology

Immune oncology is defined as the artificial, drug induced immune stimulation to treat cancer. Two classes of molecules belonging to this category are of interest for this work. On the one hand the monoclonal antibodies, which have been in use as cancer therapeutics for the past 15+ years, and on the other hand a novel class of potential cancer therapeutics, the immune system engagers (ISEr). ISErs follow the same basic mode of action but are designed to overcome some of the flaws present in the use of mAbs. There are other therapeutics falling in the category of immune oncology, for example the “Checkpoint Inhibitors”. Compared to the former two mentioned classes, the Checkpoint Inhibitors target the adaptive immune system, specifically the T-cells. To avoid a strong immune response, the immune system has different “Checkpoints” in place for regulation, for example CTLA-4 and PD-1.[10] Cancer cells often down regulate these Checkpoints to avoid detection. With special designed antibodies, like the drug Ipilimumab, these Checkpoints can be inhibited and therefore a stronger T-cell immune response can be observed.

5.3.1 Antibodies for cancer therapy

The success of antibodies as cancer therapeutics was based on the discovery of the highly differentiated cell surface structure of cancer cells in comparison to normal cells.[11] Those structures have proven to be well suited as antigens for antibodies and mark the malignant cells, as cancer is normally "invisible" to the immune system. The most commonly used antibodies are part of the IgG subfamily and comprise two heavy chains and two light chains, which are linked via disulfide bridges and a Fab and Fc region.[12]

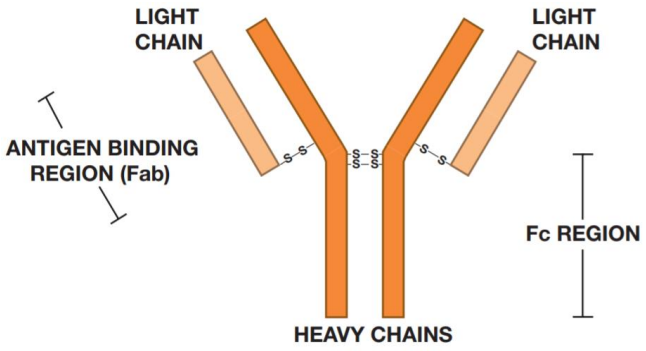

Figure 6 Structural overview of the most common parts from an IgG antibody[6]

The Fab region of an antibody is responsible for the accurate detection of the antigen while the highly conserved Fc tail region of the antibody allows specific binding and therefore activation of the different cells involved in the immune response. The mode of action for an antibody-based drug is the direct targeting of a cell surface receptor with the Fab region. Afterwards, the antibody can eliminate the tumor cell with one of three possible mechanisms: First, the direct blocking or activation of an essential receptor, leading to apoptosis. Secondly, the activation of the immune system with the Fc region, leading to infiltration of immune cells into the tissue and eventual phagocytosis and lastly, the attack of vasculature and stroma cells of the tumor.[11] The activation of the immune system involves complement-dependent cytotoxicity (CDC), antibody-dependent cellular cytotoxicity (ADCC) and the regulation of T-cell function.[13] The ideal target for an mAb is overexpressed, easily accessible and virtually not present on healthy cell surfaces or is a free antigen in the tissue or blood stream. The most commonly used antigens can be divided into seven categories, regarding their function in the cell. The three most common categories for cancer targeting antigens are haematopoietic differentiation antigens, glycoproteins, and growth and differentiation signalling targeting antigens.

With the use of antibodies, some disadvantages have also been reported. For the synthesis of mAbs, different strategies can be used, like a display of different single chain fragments by phages or the use of a transgenic mouse for antibody isolation.[14] For the first synthesis method, different genes are incorporated in the genome of the bacteriophage and the produced antigens as result are displayed on the surface of the phage, allowing the generation of a large library as well as targeted screening. For the second method, different laboratory mice are genetically modified to express human IgGs. After exposure of the desired antigen, they produce the corresponding IgG, which can be obtained from the animal through isolating its micelles. There are many other methods present for the synthesis of mAbs and this should just serve as an example of the complexity. All strategies known today require highly qualified personnel, are expensive and a long adaptation time is needed to introduce changes to the antibody. [14]

5.4 Immune System Engagers

In this chapter, I will cover the theoretical basis of the ISErs as well as the necessary background information of all cell surface receptors or proteinases targeted by the novel ISErs used in this thesis.

The approved cancer therapeutics in use today can be divided into two categories, regarding their mass. The small molecule drugs, with a mass range of 300 to 1000 Da and the mAbs with a mass over 25 kDa. The established mode of action for the small molecule drugs, like cis-Platin, is based on their ability to enter the cell while the mAbs target cell surface receptors, as mentioned before. ISErs follow the same basic mode of action like antibodies, with targeting cell surface receptors and activating the immune system, but they possess an

intermediate size between small molecule drugs and antibodies. ISErs are synthetic, peptide-based compounds and were designed with the idea to overcome some of the former mentioned disadvantages of antibodies, such as their large size, production costs or limited stability.[13]

5.4.1 ISEr-Structure

ISErs contain three main moieties: An effector, designed to activate the innate immune system, binders, designed to bind to specific cell surface receptors on cancer cells and PEG chains, which link the former two. The PEG chains were chosen because of their non-immunogenic properties as well as their chemically inertness. They are monodisperse and normally possess a length of 10 nm (PEG_{27}) to mimic the distance between two paratopes in antibodies.[13] Different binders for ISErs have been reported, which are able to target different cell surface receptors. Examples of such binders would be **B9**, designed to target the integrin α3 chain or **B59**, targeting ephrin A2 receptor. Two different effectors, called **F1** (fMFL) and **F2** (fMIFL) have been investigated for the ISEr synthesis. The **F2** proved to induce a higher level of oxidative burst response in human leukocytes after being integrated into the ISEr structure, while the **F1** showed a reduced potency by two numbers of magnitude[13]. The number of effectors and binders present in the structure can vary but for optimal binding at least two binders are necessary. Regarding the number of effector and binder moieties, different multivalent as well as multispecific ISErs have been reported to increase the avidity of the product, as can be seen in *Figure **7***.[15] The avidity of a molecule is defined as the combined strength of all different binding interactions present in the structure. The most commonly used effector structures **F1** and **F2** include an *N*-formylated sequence activating the formyl peptide receptors (FPRs) of the myeloid immune cells. FPRs are G protein-coupled receptors, meaning they can bind the guanine nucleotides GDP and GTP and are coded by three different genes in the human body (FPR1-3). FPR1 and 2 possess a high structural identity and are both expressed on non-myeloid cells as well, like epithelial cells or neuroblastoma cells. FPR1 receptors were found to be the main binding point for the **F2** in previous studies.[16] After activation, these receptors are responsible for cell migration, superoxide production as well as cytokine release, making them the perfect target. The recognition of *N*-formylated methionine, which is a structure, most common in different bacteria, is important for identification and defence against those pathogens.[17]

The most common structure of ISErs is the trivalent nature with one effector and two binders, mimicking the structure of mAbs. But also, bi-and multispecific antibodies as well as smaller single chain antibodies, “minibodies” and multiple-armed antibodies as new formats are being developed. An example of a single-chain antibody is blinatumomab, which can bind to the CD19 and leads to the T cell invasion in the tumor tissue. [18]

As also new valency in antibodies is tested in the clinic, the design of ISErs with different structures was not far-fetched. This design faces similar problems like the design of similar antibodies, including the distribution of cell surface targets or the “binding-site barrier”. [19]

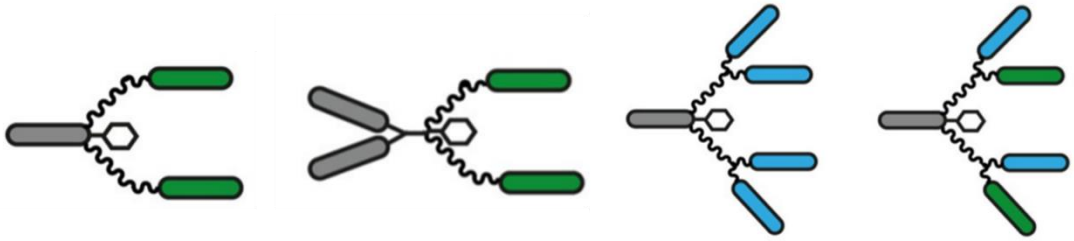

Figure 7 Schematic description of C-terminal biotin marked ISErs with different number of binders (blue and green) and effectors (grey), where the binders can target different cell surface structures[15]

One of the main advantages of ISErs is the possibility to synthesize them by SPPS on resin and therefore eliminate the use of time and cost intensive recombinant methods used in antibody synthesis. Anne C. Conibear et.al. reported the synthesis of different multivalent ISErs with two binders dubbed **B9** and **B59** as well as the effector **F2**. [15] Their findings were consistent with the reported problems of multivalent antibodies, as the X scaffold with two effectors showed lower activity in human leukocytes, indicating the binding to the FPRs is limited by steric hindrances. They tested the ISErs with different number of binders on the cell line PC-3 and observed an

increased avidity from the **B59** binders but not the **B9** binders, indicating that the density of the cell surface receptor also plays a large role in the design.

5.4.2 Mode of action

As the function of the innate immune system has already been described, this chapter focuses on providing a short summary of the so far known mode of action of ISErs in general.
As already been mentioned before, the structures of the binders can vary in their design and have different targets based on their sequence.

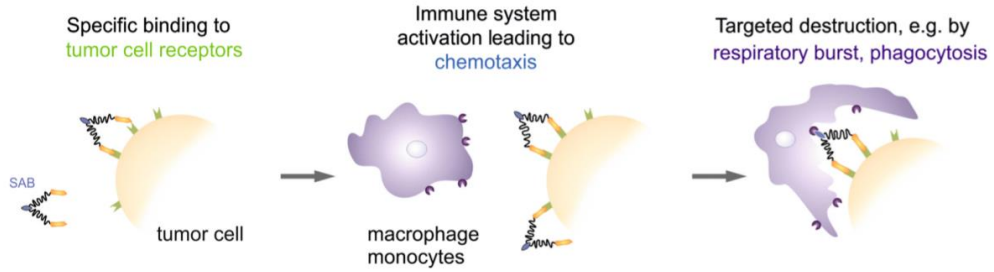

Figure 8 Simplified schematic mechanism of the activation of the innate immune system by an trivalent ISEr[13]

After the synthetic antibody is administered, either via injection into the blood stream or direct injection into the tumor tissue, the binders connect with their intended target, as seen in *Figure **8*** on the first panel. After being bound on the cell surface, the cancer cells present the effectors, which can be recognized by the members of the myeloid immune cells, like macrophages, monocytes or granulocytes. For the initial binding the receptor density, the accessibility as well as possible dimerization of the receptor come into play. As already mentioned before, the integrin α3 as well as the ephrin A2 receptors are the most used targets for ISErs. Both form dimers on the cell surface, but the integrin forms heterodimers with the β1 subunit and the ephrin forms homodimers with another A2 subunit which might facilitate stronger bindings with multivalent ISErs.[15] The effector binds to the FPR receptor on the myeloid cells, which leads to cytokine release, chemotaxis, respiratory burst, and eventually phagocytosis of the tumor cell. The respiratory burst is achieved by activation of the NADPH oxidase, a membrane bound enzyme, which reduces O_2 to O_2^-. The superoxide anion can produce other reactive oxygen species like hydroxyl radicals or with the help of the enzyme superoxide dismutase, H_2O_2[16]. In addition, neutrophils are attracted increasing the inflammatory response. As the activation of the FPR1 receptor, which is the main target of the effector, normally leads to internalization of the target, a bead-based study was performed to test if the bead-bound ISErs would activate the FPR1 as strongly as free ISErs. At the same time it was important to establish, if tumor bound ISErs were still able to activate the innate immune system. Pötgens *et. al.* demonstrated, that ISErs were still able to induce an immune system response when bound to beads, ruling out the possibility of internalisation. They observed the expected response from the myeloid cells such as chemotaxis, change in shape of the cells from round to irregular or activation of NADPH oxidase. They also demonstrated, a secondary mode of action, namely the release of immune stimulating fragments after incubation of tumor cells with the ISEr Y9. Here either the complete ISEr or *N*-formylated fractions are responsible for the leukocyte activtion. This could lead to a concentration gradient of effector in the tumor tissue, further increasing the desired immune response.[16] The binding of the effector to its receptor is strongly influenced by steric hindrances, as suggested by previously obtained data. [13,15]

5.4.3 ISEr-Y9

One example for an ISEr is the trivalent compound Y9. This ISEr has already been successfully synthesized and tested regarding its effectiveness, stability and safety. As can be seen in *Figure **9***, the used effector was the **F2** with the formylated methionine, isoleucine, phenylalanine and leucine (fMIFL). These *N*-formylated sequences are common in bacteria and can stimulate the FPR receptors in myeloid cells. This sequence can also be found in *Staphylococcus aureus* and can already induce chemotaxis at a concentration of 10 pM. After incorporating the

sequence into the larger scaffold, a decrease in potency can be observed. Experiments with **F2** coupled to the two PEG_{27} chains revealed, that after a subcutaneous injection of 100 nM in mice and guinea pigs sufficient cytokine concentrations of IL-1β could be detected after 6h and 24h.[13]

The effector sequence is followed by two glycine, which function as spacers and two lysine residues, which link the effector scaffold with the designed binders via PEG chains.

The binders, marked in blue in the sequence, were identified via one bead one compound screenings (OBOC) to bind specifically to the integrin α3 chain.[20] They are one of the two former mentioned common binders for the ISErs, **B9,** and were the base for the Y9 nomenclature. Their 8-mer sequence consists of non-proteinogenic amino acids as well as peptidomimetics and is cyclised with two D-cysteines. They were tested beforehand with biotin-streptavidin flow cytometry on A431 tumor cells producing a K_D of ~90 nM. [13]

Integrins belong to the family of transmembrane cell surface receptors and comprise 24 heterodimeric combinations consisting of α1-18 and β1-8. [21] A further division can be made based on their recognition sequence where they can be divided into four sub-categories: collagen-binding, Arg-Gly-Asp (RGD)-binding, laminin-binding, and leukocyte binding. They rely on Mg^{2+}, or other divalent cations, to induce their active state. Integrins play a role in cell adhesion, survival of cells and in the interaction with extracellular environments. The α3 chain is connected to the β1 and the ligand, in healthy cells, is laminin. Many integrins are overexpressed by different tumors to assist in the process of metastasis as well as invasion of foreign tissue, making them an ideal target for a cancer therapeutic. Different studies also reported a correlation between the β1 subunit and malignancy in neuroblastomas.[22] A loss of expression of this subunit leads to an increased tumorigenicity of the tumors.

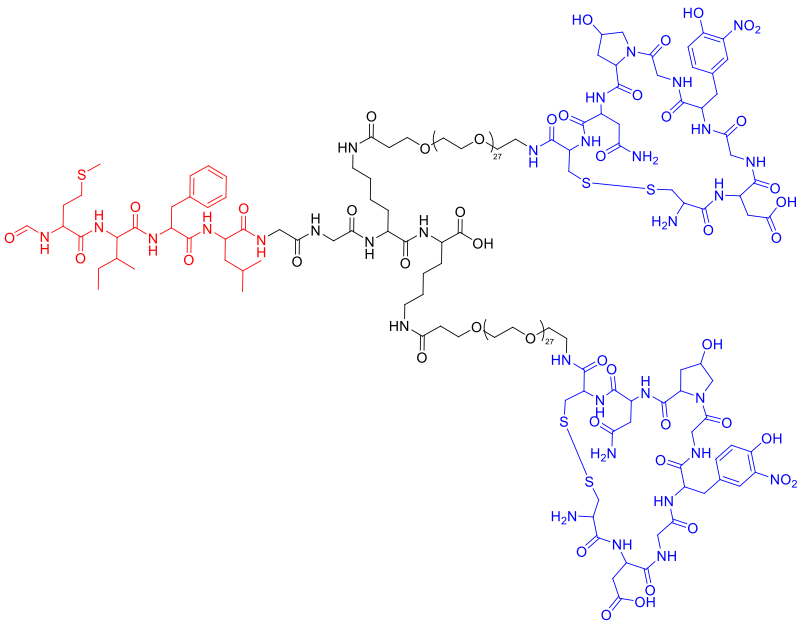

Figure 9 Structure of the ISEr Y9, with the effector marked in red and both binders marked in blue (structure shown without stereochemistry)

Activation of the immune system *in vivo* by Y9 was tested in guinea pigs as well as immune deficient Balb/$c^{nu/nu}$ mice by injecting 100 nm subcutaneously. The guinea pig was chosen, as previous data suggests an immune response after injection of a formylated amino acid sequence coupled with an IgG.[23] In both animal cases, immune cell infiltration in the tissue was observable, but a higher dose was needed for the immune suppressed animals as the immune response is weakened in these animals.

The stability of the compound had also been tested *in vitro* with mouse serum, where HPLC-analysis revealed that after 48h only 20% of Y9 were degraded. The high stability of the compound comes from a variety of factors like the PEG chains protecting the Y9 from proteolysis, the inclusion of non-proteinogenic amino acids as well as the cyclic structure of the binders. For the stability test *in vivo*, a subcutaneous injection of different concentrations in the nM scale were performed on mice and samples analysed with a special designed dot-blot method. With this method a clearance half-life of about 2h was established. [13]

The effectiveness of Y9 to inhibit or prevent tumor formation was tested *in vivo* in the guinea pig model, where GPC-16 tumor cells were injected in Dunkin Hartley guinea pigs together with a single dose of 200 nM Y9. This experiment revealed after 35 days 3 out of 10 guinea pigs treated with Y9 grew tumors but 9/10 pigs in the control group experienced observable tumor growth. [13]

The safety of the Y9 ISEr was tested on Balb/c mice with dose escalation studies, revealing, that negative side effects, besides the expected inflammatory reaction at the injection site, were only observed at 800 nM concentration with negative effects on the kidney and the liver. [13]

5.5 Matrix Metalloproteinases

In this thesis an a-ISEr was designed with a novel cleavage site for matrix metalloproteinases (MMPs) between the effector and the binders. Matrix metalloproteinases were first discovered in 1962[24] and are Zn^{2+} dependent endopeptidases. MMPs possess a highly conserved, three histidine containing sequence in their active centre, chelating the Zn^{2+}. In addition to the active centrum, most MMPs possess a Hemopexin domain and these two structures are linked by a proline-rich amino acid linker. 23 human, zinc depended MMPs have been identified to this day (MMP1-23) and they can be divided into five major sub-families, regarding their preferred substrate, although many MMPs can cleave overlapping substrates. The collagenases, gelatinases, membrane type MMPs (MT-MMPs), matrilysins and stromelysins. Some MMPs cannot be sorted into these categories and are summarized in a small sixth sub-family as others.[25] The MT-MMPs have an additional transmembrane domain linked to the Hemopexin to anchor themselves in the cell membrane. In healthy cells MMPs are responsible for the degradation of extra cellular matrix (ECM). Due to the involvement in ECM degradation, the expression of MMPs is highly regulated to avoid damage to healthy cells and tissue. Different safety mechanisms come into play, such as, their production in small amounts, additional activation by interleukins, growth factors or MT-MMPs and the use of tissue inhibitors of matrix metalloproteinase (TIMPs). The MMPs are produced as pro-enzymes (=zymogens), where the active site of the zinc containing catalytic domain is obstructed and need to be proteolytically activated to gain the active MMP[25].This activation process, as can be seen in *Figure **10***, can take place either inside the cell in the Golgi-apparat by serine proteinases, after secretion from the cell by MT-MMPs on the cell surface or in the extracellular matrix. [26]

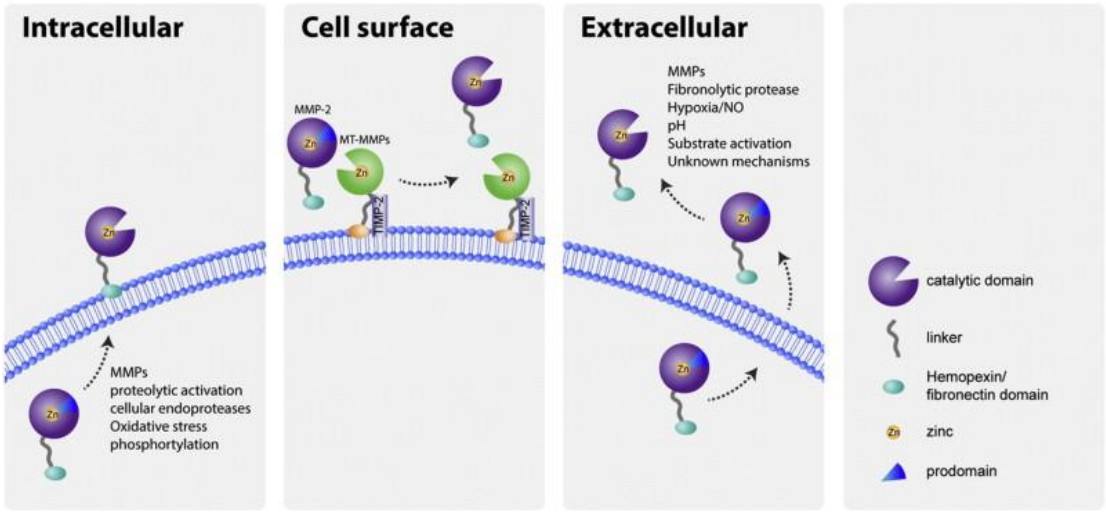

Figure 10 Schematic mechanism of activation for MMPs. The cysteine prodomain, obstructing the active Zn^{2+} catalytic centre, is cleaved off. The different activation possibilities, namely intracellular activation, activation on the cell surface with MT-MMPs or extracellular activation (left to right) [27]

The role of MMPs in different pathological manifestations, like cancer, has been known for the last 45 years. Different studies concluded, that MMPs are heavily involved in tumor metastasis, angiogenesis and growth by degrading foreign tissue types.[28,29,24] The expression of different MMPs is also used in medicine to diagnose or predict tumor formation and progression.[30] An example would be the expression levels of MMP2 in tumors of cervical epithelial cells, as elevated MMP2 expression stands in direct correlation with tumor size. The invasive potential of tumors is directly linked to the expression of MMPs as the malignant tissue needs to degrade the

stroma of the body as well as healthy tissue to create space. Angiogenesis, the formation of new blood vessels, is a necessary process to sustain the growing tumor with nutrients. MMP2 and 9, both gelatinases, have been found to play a specific role in the regulation of tumor invasion and are reported to be the most commonly overexpressed MMPs in different cancer types like lung, prostate and colon cancer[28].

5.5.1 Tissue inhibitors of matrix metalloproteinases (TIMPs)

To avoid damage to the host cell after formation of the MMPs, they can be inhibited by the so called TIMPs. There are four categories TIMP1-4 and these small proteins are structurally divided into two different domains. The *N*-terminal domain can bind to the active site of the MMPs and blocking it for substrates while the *C*-terminal domain can non-covalently bind to the hemopexin domain of the MMP and therefore inhibiting cell surface activation. [25] TIMP2 has also been reported to be involved in an unconventional activation mechanism for MMP2. As the presence of TIMP2 and MT-MMP1 are required to mature the MMP2 into its active form, as can be seen schematically in *Figure **10***. Therefore, the absence of TIMP2 leads to an inactivation of MMP2. This activation relies on the formation of the trimeric complex between TIMP2, MMP2 and MT-MMP1. A general rule of thumb for the role of TIMPs in tumor invasion and progression is, that the higher the expression level of MMPs and the lower the expression level of TIMPs, the worse the prognosis. As there are mechanisms, which require TIMPs for the activation of the MMPs, findings regarding TIMP1 and 2 suggest, that these TIMPs were highly overexpressed in different lymphomas.[29] TIMPs can be expressed by a variety of cells, which are involved in remodelling the ECM. TIMP1,2 and 4 are secreted from the cell in a soluble form and TIMP3 is mostly bound to different parts of the ECM.[31,32]

5.6 Chemoselective Ligations

The use of peptides and proteins in chemistry, biology and medicine has been facilitated by SPPS. Especially, the site and chemoselective functionalisation of these molecules is of interest. Drug design profits vastly from the ability to functionalise the biologically active macromolecules to fulfil or increase their designed purpose in the human body.[33] The length limitation of the peptides synthesized by SPPS also increased the need for coupling two or more peptide sequences by ligation methods. During the ideal ligation process no protection groups are required, the reaction preserves the stereochemistry and no additional enantiomerisation takes place during the reaction. Further the introduced linkage should be small in size, stable across a broad range of biological environments and the linker motif should not be common in the target organism. [33, 34]

One of the most commonly used and well known ligation techniques is the native chemical ligation (NCL), which was first described in 1994 by Dawson and Kent *et.al.* [35] The NCL takes place between in an *N*-terminal thioester and a *C*-terminal cysteine, after the first thiol-thioester exchange, the intramolecular shift takes place, preserving the natural stereochemistry of the peptide. In this work, two ligation techniques were applied to yield novel ISEr structures, the copper-catalysed azide-alkyne or “click” reaction and hydrazone formation.

5.6.1 CuAAc

The term “click” reaction was first defined in 2001 by Medal and Sharpless et al.[36], as they sought to define reactions mimicking natures ability to generate large molecules out of small building blocks. They defined a “click” reaction as a reaction that is stereospecific, does not produce side products in a relevant way, is fast, is easy to perform regarding the reaction conditions, should work in the presence of H_2O and under oxygenated conditions, produces high yields and is performable with a broad range of educt concentrations. Four main reaction categories were defined as click reactions in their first paper, 1,3-cycloadditions, nucleophilic substitutions, carbonyl chemistry with the formation of oximes, hydrazones etc. and addition reactions, like the Michael addition. Today the copper(I) catalysed azide alkyne cycloaddition is colloquially revered to as the “click” reaction, as it became the most commonly used one, but other reactions, like the sulfur (VI) fluoride exchange also fall under this umbrella term.[37]

The azide-alkyne cycloaddition yielding the 1,2,3-triazole disubstituted product has been known since 1893 as the Huisgen reaction. This reaction produces two diastereomers in form of 1,4 and 1,5-disubstituted products in equal amounts, requires heating and the products from slowly.[38] The introduction of a catalyst in form of

copper (I) reduced the high activation barrier and only yielded one diastereomer, the 1,4-substituted product. The [3+2] copper catalysed cycloaddition fulfils all criteria for a click reaction, as mentioned before. The three-dimensional triazole product has a distance of 5.4 Ä between both substituents, which is approximately the same as amide bonds. Therefore, the CuAAc is often used in peptide or protein conjugation, also because both reaction partners can be introduced by SPPS onto the molecules.

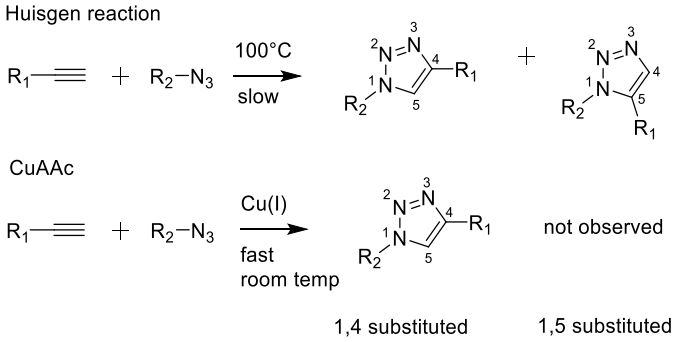

Figure 11 Comparison of the Huisgen reaction (top panel) and the CuAAc (bottom panel) regarding their reaction conditions and product formation. The 1,5 substituted product does not form with the use of the Cu(I) catalyst

For the CuAAc, the copper can either be introduced to the reaction as a pre-catalyst in form of copper(II) salt, as a copper(I) compound or in the form of Copper(0) with a wire. In addition, a reducing agent is used especially in the first two options, which is normally sodium ascorbate. The reducing agent reduces Cu(II) to Cu(I) but also inhibits the aerobic oxidation back from the desired Cu(I) to Cu(II). [38] Even with the use of a catalyst the CuAAc can progress slowly under atmospheric conditions, depending on the structure of the educts, as steric effects can have an effect here, as well as the concentration of Cu(I). To increase the reaction rate, different ligands, like polydentate nitrogen donors or amine containing molecules can be used. The most used ligands fall under the first category and examples would be TBTA, TBIA, or sulfonated bathophenanthrolines.

The mechanism of this reaction has been studied extensively and the best way to analyse this reaction is with density functional theory calculations (DFT). In the proposed mechanism the azide attacks the copper(I)-acetylide in the second step, as can be seen in *Figure **12***. For this attack Finn and Fokin et.al.[39] proposed a bimetallic transition state, with two involved copper species. This transition state decreases the electron density of the sp hybridized carbon atom of the alkyne to allow the electrophilic attack of the azide. Slightly different mechanism have been proposed but the basic steps, like the formation of the copper(I)-acetylide stay the same over all. [38,39]

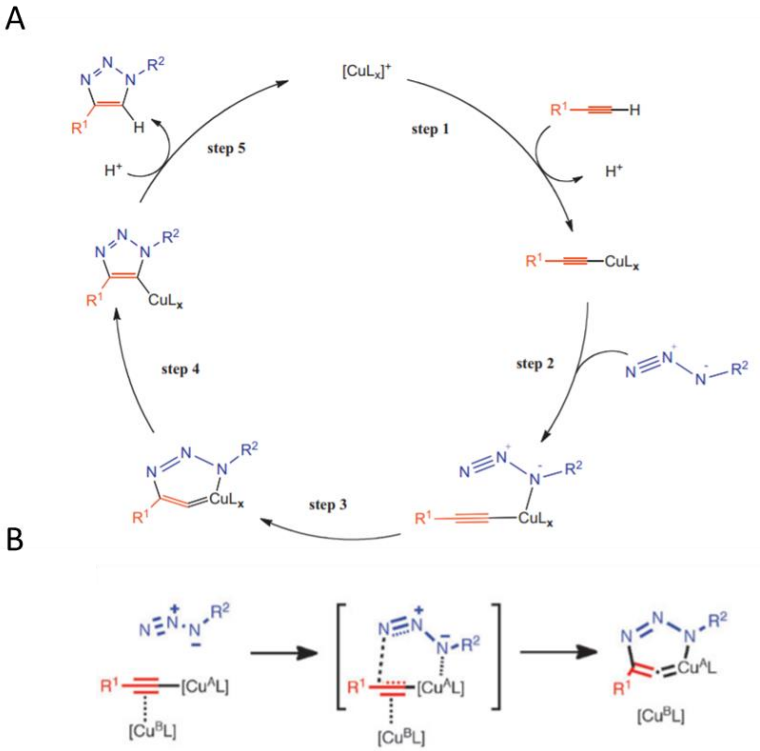

Figure 12 ***A)*** *Proposed reaction mechanism with five steps for the CuAAc by Finn and Fokin with the use of DFT calculations.*[38] ***B)*** *The proposed bimetallic transition state for the second and third step of the reaction, the attack of the azide*[39]

One of the most useful features of this reaction is the possibility to use a variety of different solvents from toluene or chloroform to DMF or even different alcohols. Even the addition of mixtures with water does not influence the reaction. The key step for the reaction is to solubilize the copper(I) catalyst, therefore, stock solutions with different solvents can be applied to ensure the best solubility of the reaction partners. This tolerance against a range of reaction conditions made the CuAAc a favourable reaction for drug development and modification of different large biomolecules.[38,40]

5.6.2 Hydrazone formation

The reaction between a carbonyl group, aldehyde or ketone, and amine nucleophile has been known since the late 19th century[34]. Since 1970 this reaction found its way in bioconjugation of peptides and proteins.[40] The amine has in its α-position an electron donating group which can either be oxygen, than the product of the reaction is called an oxime, or an nitrogen to yield a hydrazone product. In the product a new double bond is formed between the carbon of the carbonyl group and the nitrogen of the amine group. The formation of the hydrazone or oxime is a second order reaction and also an equilibrium reaction, which favours acidic conditions and proceeds quite slow at physiological pH. Another initial draw back for this reaction is that one of the educts needs to be added in a stoichiometric access over the other reaction partner.

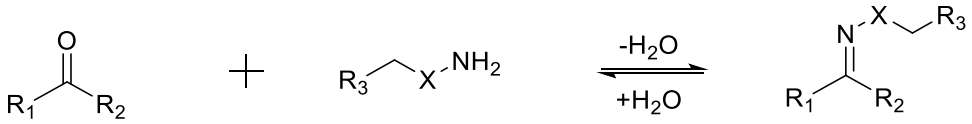

R_2= H (Aldehyde)
R_2= R (Ketone)

X= O (Alkoxylamine)
X= N (Hydrazide)

X= O (Oxime)
X= N (Hydrazone)

Figure 13 Reaction scheme of the condensation reaction to form oximes or hydrazones, based on the α-electron donating group from the amine

The introduction of nucleophilic catalysts, like aniline to increase the reaction rate allows to use lower concentrations of educts and also to perform the reaction at a higher pH. This has made it popular as a

bioconjugation tool.[40] Aniline was first introduced by Dawson et.al. to produce semicarbazones[33]. The catalyst reacts with the carbonyl group to form an imine intermediate namely a protonated Schiff-base, which is highly reactive[41]. The electrons from the nitrogen are delocalized into the ring, making aniline a good leaving group.[34] Other amine containing catalysts have been reported as well, for example the amino acid arginine or *N,N*-dimethylaminoethylamine.[42] The reaction mechanism for those bases always follow the same steps, with the tetrahedral intermediate, the release of water and the formation of the iminium intermediate, which is consequently substituted by the hydrazine or the hydroxylamine derivate to form the desired product. During the attack of the α-nucleophile, a second tetrahedral intermediate is formed, which is not shown in *Figure **14***. The catalytic mechanism requires more steps than the uncatalyzed reaction, but the highest energy barrier is still lower in the catalysed mechanism then in the uncatalyzed reaction. The reaction mechanism of a hydrazone bond formation in presence of aniline as a catalyst was also studied by the Dawson group. They proved the existence of the Schiff-base intermediate by adding $NaBH_3CN$ to the reaction, which preferably reacts with protonated imines, like the proposed intermediate.[41]

Other catalysts, like bimolecular molecules, to promote intramolecular proton transfer, have been reported.[34,43] An example for this catalysts would be derivates of anthranilates and they have an higher conversion rate than aniline. Even the use of amine buffers themselves as a catalyst at a physiological pH are known in literature. The amines as part of the buffer solution fulfil the function of a catalyst as well as keeping the pH at steady physiological conditions. An example of such a buffer is 2-(aminomethyl)(benz)imidazoles, but other buffer systems have been tested by Larsen et.al.[43] Without a catalyst, the α-nucleophile directly attacks the carbonyl carbon at acidic conditions.

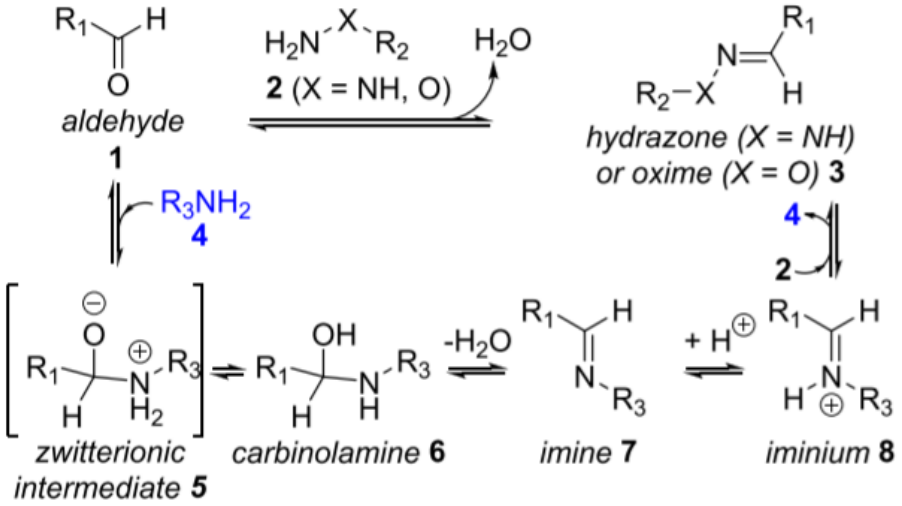

Figure 14 Reaction mechanism of hydrazone and oxime formation with the use of an amine containing molecule as a catalyst forming the protonated Schiff-base as intermediate, even under physiological conditions[42]

The high chemoselectivity, easily introducible functionalities and the use of an efficient catalyst made this reaction type a popular conjugation method. The hydrazone product is thermodynamically less stable than its oxime counterpart and more prone to reverse back to its educts. Educt concentrations higher than micromolar are reported to produce better yields than lower concentrations and the product is more stable during storage at higher concentrations. Oximes experience in general a higher stability than hydrazones due to the higher electronegativity of oxygen but both can be hydrolysed again depending on the structure, like the substituents at the α-nucleophile. The reverse reaction also needs acidic conditions but if there are electron withdrawing groups in close proximity of the hydrazone, the hydrolysis of the product even takes place at physiological pH value. In the presence of strong nucleophiles, the hydrazon bond formation can be challenged by competition between the strong nucleophile and the nucleophilic catalyst, the first step of the reaction seen in *Figure **14***.

When working with peptides, the aldehyde as well as the amine nucleophile can be introduced into the molecules at the desired place manually before the reaction. For the introduction of the aldehyde, sodium periodate can be used.[34] A *N*-terminal serine or threonine can be oxidized with periodate, yielding an *N*-terminal aldehyde.[34]

This reaction is only possible in the absence of other oxidizable functionalities and the periodate has to be quenched with a reducing agent after the completion of the reaction.[44]
The hydrazine group is most commonly introduced by using already functionalized building blocks. Depending on the desired place of the hydrazone bond, *C*-terminal hydrazone bonds can be added to the amino acid sequence, with the use of a special functionalized Wang resins and the use of hydrazine hydrate.[34]

6. Objective of the work

ISErs provide some advantages over normal antibodies. Compared to the latter, they provide better cell penetration, are more easily modified and can be synthesized faster[13,15]. A disadvantage of the ISErs can be for example fast dissociation upon entering the body. In this work four novel ISErs will be produced, purified and tested regarding their functionality. More specifically, the base structure of the ISEr Y9 should be modified to achieve one of two things. First, the Y9 core structure should be coupled with PEG chains of different lengths to increase the bioavailability and stability of the product and to form the so called tuneable-ISErs (t-ISEr), as seen in *Figure **15*** on the left-hand side. According to the reports present on Y9 in literature[13], the half-life in the guinea pig model was estimated to be about 2hours.

The second planned modification of Y9 is based on the introduction of a cleavage site between the effector and the two binder moieties to generate an activatable-ISEr (a-ISEr) as seen in *Figure **15*** on the right-hand side. It is already a known fact, that the attachment of the effector to the ISEr structure reduces its effectiveness to induce an immune system response[13]. By the introduction of a cleavage site, which should only be recognized upon entering the tumor tissue, the concentration of free effector should be increased, resulting in an enhanced immune response. For this method, two approaches will be tested, first the introduction of two novel amino acids in the scaffold of the Y9. Those amino acids should be recognized and subsequently cleaved by the MMPs, which are overexpressed in many cancers. The second attempt is the usage of a hydrazone linkage between the effector and the binders. As hydrazones are very pH sensitive, this linkage should in theory, be stable under physiological pH conditions but be cleaved off in the hypoxic, low pH environment of tumor tissue.

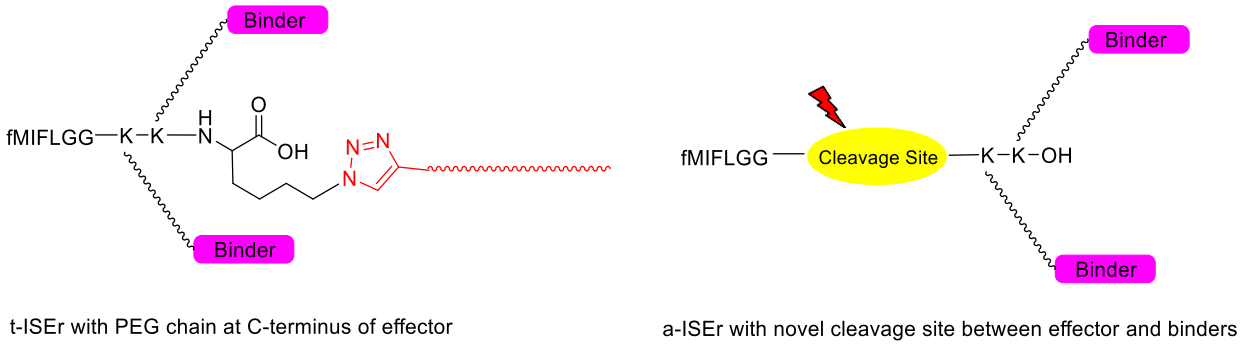

Figure 15 Schematic visualisation of t-ISEr with coupled PEG chain and a-ISEr with novel cleavage site

7. Materials and Methods

7.1 Materials

7.1.1 General

Chemicals, resins and solvents were obtained from commercial sources, used in high purity and were used without any purification steps needed. Fmoc-protected amino acid building blocks and resins were obtained from Novabiochem, Iris Biotech GmbH, CEM or GL Biochem (Shanghai) Ltd. The Fmoc protected PEG propionic acid was obtained from Polypure and the PEG-alkyne from Iris Biotech GmbH. DCM was purchased from Fischer Chemical and DMF from Supelco. The MMP2 human recombinant protease, anhydrous DMF, Dulbecco's Modiefied Eagle's Medium- high glucose, piperidine, Triisopropylsilane, N,N-Diisopropylethylamine, Hydrazine monohydrate as well as the 4-Nitrophenyl formate were purchased by Sigma Aldrich. For all working steps involving purified ISErs, endotoxin free sterile-filtered, BioReagent water from Sigma Aldrich was used. All other mentioned solvents or chemicals were obtained from one of the companies mentioned above.
All ISErs, if not stated otherwise, were purified using a Kromasil 300-10C4 column with 250 x 21.2 mm.

*Table 1 Used amino acids and their molecular weight**

Amino Acid	Molecular weight [g/mol]
Fmoc-Lys(N3)-OH	394.42
Fmoc-Lys(Mtt)-OH	624.79
Fmoc-Gly-OH	297.31
Fmoc-Leu-OH	353.41
Fmoc-Phe-OH	387.45
Fmoc-Ile-OH	353.51
Fmoc-Met-OH	371.45
Fmoc-D-Cys(Trt)-OH	585.7
Fmoc-L-Cit-OH	397.43
Fmoc-Val-OH	339.39
Fmoc-Asn(Trt)-OH	596.7
Fmoc-L-Hyp(tBu)-OH	409.46
Fmoc-Tyr(3-NO2)-OH	448.42
Fmoc-D-Asp(tBu)-OH	411.5

**All amino acids are in the L configuration, if not stated otherwise*

Table 2 Used chemicals and resins for the peptide synthesis

Resins	Reagents
Rink Amide AM resin LL	DMF
Pro Tide Rink Amide LL	HBTU
Wang Resin (100-200 mesh) Fmoc-Lys(Mtt)-preloaded	DIPEA
Cl(TCP)(Cl) Pro Tide	p-Nitrophenyl formate
	Oxyma
	HATU
	HOAT

All peptides in this work were synthesized using the classic Fmoc synthesis strategy on a solid phase in form of a resin. The first amino acid was coupled on a linker and for this work four different resins were used in the peptide

synthesis, which are summarised in *Table 2*. Depending on the resin in use, a different linker is applied from the manufacturer. During this work three different linkers were in use, as seen in *Figure **16***.

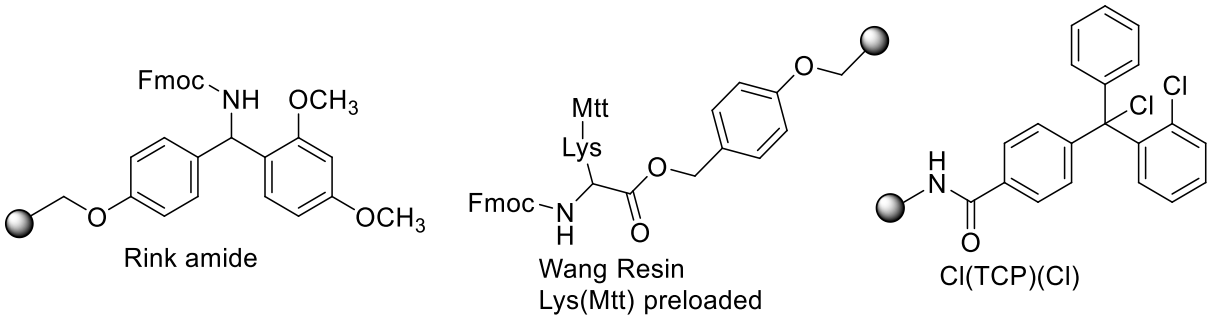

Figure 16 Linkers from different resins used during the synthesis

Table 3 Instruments in use during this work

Description	Name	Manufacturer
Centrifuge	3-16PK	Sigma
Centrifuge	Centrifuge 5418	Eppendorf
HPLC	Pro Star	Varian
Column Heater	Model 631	Alltech
Collector	Fraction collector	Waters
HPLC	Thermo Scientific	Vanquish
HPLC	Ultimate 3000 inkl. Fluoreszenz- and CAD-Detection	Dionex
HPLC- MS	Waters AutoPurification HPLC/MS (ESI) System	Waters
HPLC- MS	Thermo	Thermo
Ultrasound bath	Bandelin	Sonorex
Lyophilizer	Christ Alpha 2-4 LD plus	Christ
Incubator	/	Binder
Peptide synthesizer	Liberty Blue	CEM
Gel imaging	ChemiDocTM	BioRad

7.1.2 Solvent compositions

Table 4 Composition of the solvents used in this work

0.5 M HBTU in DMF	10 mL	1.8963 g HBTU 10 mL DMF
20% piperidine	500 mL	100 mL piperidine 400 mL DMF
Eluent A		Endotoxin free water + 1% TFA
Eluent B		ACN + 0.08% TFA
AB solution		H_2O:ACN (1:1) + 0.1% TFA
Testcleavage solution	1 mL	25 µL H_2O 50 µL TiS 925 µL TFA
Mtt deprotection solution	250 mL	5 mL TFA 2.5 mL TiPS 242.5 mL DCM

Final Cleavage solution	15 mL	750 µL DMS 375 µL H_2O 375 µL TiS 13.5 mL TFA
1x PBS buffer	1 L	8 g NaCl 0.2 g KCl 1.44 g Na_2HPO_4 0.24 g KH_2PO_4 pH 7.5 fill up to 1 L with endotoxin free H_2O
Phosphate buffer 50 mM	500 mL	2.77 g Na_2HPO_4 0.699 g NaH_2PO_4 endotoxin free H_2O

7.2 Experimental

7.2.1 Synthesis of Y9-N_3

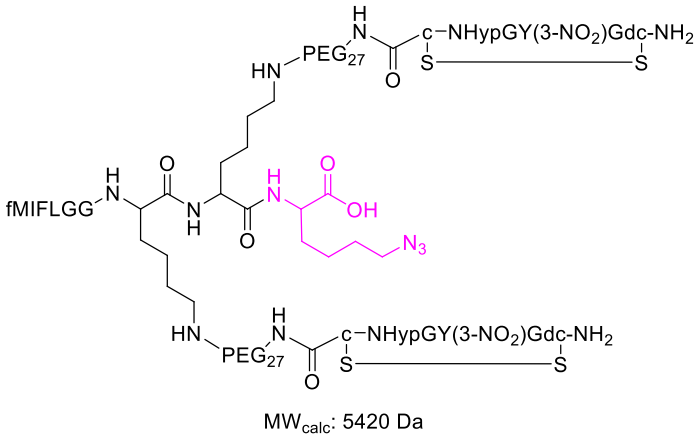

Figure 17 Structure and calculated molecular weight of Y9-N_3 with the azido-lysine marked in magenta

Core Structure Synthesis:

The base scaffold of this ISEr was synthesized with the Liberty Blue microwave peptide synthesizer, using two different resins. The scale of the synthesis for both resins was 0.1 mmol and the resins used were Rink Amide AM resin LL [365 mg] and Pro Tide Rink Amide LL [486 mg]. All other used chemicals for the synthesizer are summarised in *Table 5*. The volume, as well as the weight was calculated by the synthesizer itself. The resins were swelled beforehand and all amino acids were dissolved in DMF. The Fmoc deprotection as well as the coupling of the amino acids was performed at 90°C. The deprotection duration was 2 minutes and the coupling time for the AA 5 minutes. The amino acids were coupled at a 5-fold molar excess with a mixture of AA:Oxyma:DIC (1:1:1). These conditions were kept the same for all following synthesis on the Liberty Blue.

Table 5 Scale for chemicals used in the liberty blue synthesis for Y9-N_3 core structure

Reagent	Volume [mL]	Weighted portion [g]
Fmoc-Lys(N3)-OH	22	1.84
Fmoc-Lys(Mtt)-OH	22	2.86
Fmoc-Gly-OH	22	1.33
Fmoc-Leu-OH	11	0.80
Fmoc-Phe-OH	22	1.75
Fmoc-Ile-OH	22	1.68
Fmoc-Met-OH	22	1.71
DMF (washing solution)	1067	/
Piperidine (deprotection)*	252	/
DIC (activator)	60	9.30 mL
Oxyma (activator base)**	30	4.26

* + 0.1M Oxyma

** + 0.3M DIPEA → 1.6mL DIPEA

Formylation:

The methionine from both resins was formylated manually using *p*-Nitrophenylformat (3eq; 167.1g/mol; 50.13 mg) dissolved in 1 mL DMF and a reaction duration of three hours. Afterwards a testcleavage of both resins was performed, after washing subsamples of the resins with DCM and drying them in the desiccator. For the cleavage 1mL TFA:TiS:H_2O (92.5: 5: 2.5%) solution was incubated for two hours. The product was precipitated with cold Et_2O, centrifuged, dissolved in AB solution (50:50) and analysed with Waters HPLC-MS.

Mtt deprotection:

Only the Rink Amide AM resin LL was used for further synthesis, the Pro Tide resin was stored for later usage. The resin was swelled in DCM and 250 mL of the cleavage reagent DCM:TFA:TiPS (97: 2: 1%) were prepared. The resin was washed alternating with the cleavage solution and DCM till the washing solution has changed colour from yellow to transparent.

PEG-coupling:

The resin was washed with DMF and a solution of DMF:ACN (6:4) was prepared as well as HATU (2.4 eq; 380.3 g/mol; 183 mg) and Fmoc-PEG-COOH (2.75 eq; 1544.8 g/mol; 851 mg). The HATU was dissolved in 1mL of the DMF/ACN solution and the Fmoc-PEG-COOH was dissolved in the resulting solution. DIPEA (5 eq; 174 µL) was added and the resin was incubated with the solution on the rotator overnight. After a washing step with DMF another testcleavage was performed, using the same conditions as mentioned before.

Binder synthesis:

The binders were synthesised manually using the Fmoc strategy. The scale of the synthesis was now 0.2 mmol for both binders and all amino acids were used with 2.5 eq. First the Fmoc from the PEGylation was deprotected using 20% piperidine in DMF and afterwards Fmoc-D-Cys(Trt)-OH [299 mg] was dissolved over the time span of two minutes in 0.5 M HBTU solution (2.4 eq; 960 µL). Then DIPEA (5 eq; 176 µL) was added and the solution was shaken for another minute. The coupling time was 45 minutes and after the removal of the coupling solution and washing with DMF, the Fmoc group was again removed with 20% piperidine in DMF. This cycle of coupling, deprotection and washing was repeated for all following amino acids. The chronological order of the used amino acids as well as the amounts are summarised in *Table 6*. For the 7th amino acid, a double coupling was performed. The amount of activator used during manual synthesis was calculated using the following formula:

$$v = \frac{n}{c}$$

V... Volume of activator [mL]

n… calculates from synthesis scale*equivalent used [mmol]

c… concentration of the HBTU solution [0.5M]

The activator base for manual synthesis was calculated as follows:

$$m = n * M$$

$$v = \frac{m}{\rho}$$

m… mass of the base

n… calculates from synthesis scale*equivalent used [mmol]

M… molar mass of DIPEA [129.25 g/mol]

V… volume of the basis [mL]

ρ… density of DIPEA [0.742 g/mL]

Table 6 Amount of amino acid used for the scaffold synthesis of Y9-N_3

1. Fmoc-D-Cys(Trt)-OH	299mg	2. Fmoc-Asn(Trt)-OH	300mg
3. Fmoc-L-Hyp(tBu)-OH	212mg	4. Fmoc-Gly-OH	152mg
5. Fmoc-Tyr(3-NO_2)-OH	231mg	6. Fmoc-Gly-OH	153mg
7. Fmoc-D-Asp(tBu)-OH	212mg 214mg	8. Fmoc-D-Cys(Trt)-OH	307mg

Final Cleavage:

The dry resin was suspended in 15mL of the final cleavage solution with the composition TFA:TiS:H_2O:DMS (90: 2.5: 2.5: 5%) for three hours. The product was precipitated with cold Et_2O and centrifuged at 4500 rpm for 5 min. The pellet was again dispersed in cold Et_2O and centrifuged. This was repeated three times and the pellet was afterwards dissolved in 15 mL AB solution and lyophilised producing a crude product with a yield of 339.5 mg.

Binder oxidation:

217.5 mg of the crude product were dissolved in 27 mL 1x PBS buffer and openly stirred overnight under room temperature. The next day an HPLC-MS was performed on the Waters device to confirm the complete oxidation.

Purification:

The product was purified in three different runs via HPLC directly in the PBS buffer using a solvent gradient with eluent A and B with 30-70% eluent B in 45 minutes. The fractions were collected using an auto sampler and pooled using direct injections on the Waters HPLC-MS. From each run one main pool (MP) and one side pool (SP) was collected. The combined weight of the main pools was 24.7 mg (11% yield) and of the side pools 20.9 mg (10% yield).

Final analysis:

The final analysis of the product was performed with an HPLC run on the Vanquish device with 5-65% eluent B in 30 min followed by direct injections on Waters HPLC-MS. As final analyses from three different runs were performed, one main pool and one side pool are showed exemplarily in *Figure **25*** and *Figure **26***. The other final analysis can be found in the Supplementary Information.

The synthesis steps from the formylation up to the final analysis were repeated similar, as described above, for all following products. Therefore, further in this work, only significant changes to these protocols are mentioned in synthesis steps of the different products.

7.2.2 Synthesis of t-ISEr Y9-N_3

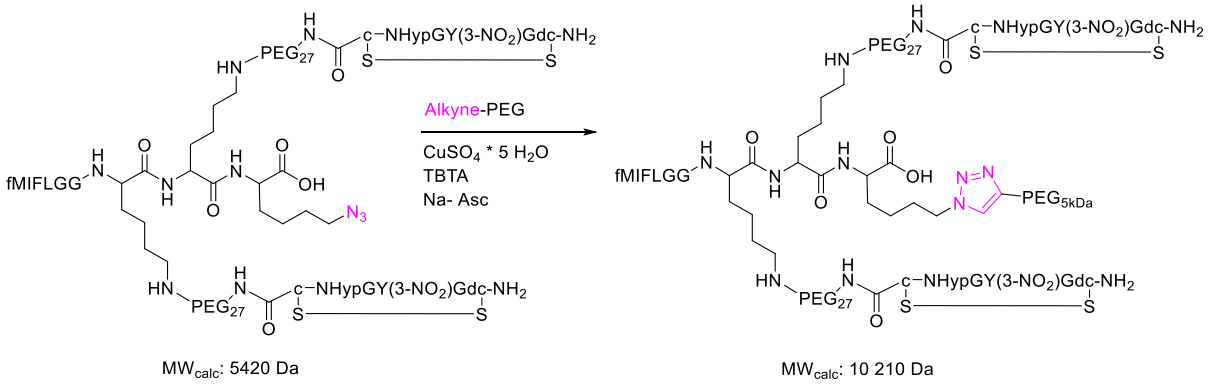

Figure 18 Reaction scheme of the CuAAc and calculated masses, where the reaction partners and the 1,2,3-triazole are shown in magenta

t-ISEr Y9-N_3 5kDa PEG:

The protocol for the click reactions performed in this work was adapted from a previously existing protocol written by Dr. Anne C. Conibear. Two different click reactions were performed to couple different PEG sizes with the Y9-N_3. For the coupling with the smaller alkyne-PEG (~5kDa) all reagents were prepared as stock solutions as seen in *Table 7*.

Table 7 Stoichiometric conditions of the CuAAc with 5kDa PEG- alkyne

Compound	Mass [mg]	Molar Mass [g/mol]	n [µmol]	Equivalent	Volume [µL]
Y9-N_3	2.1	5420	0.369	1	50
PEG- alkyne	2.8	4790	0.554	1.5	/
$CuSO_4$ * $5H_2O$	5.1	249.7	1.661	4.5	100
TBTA	10.8	530.6	1.808	4.9	100
Na- Asc	10	198.1	2.768	7.5	100
Endotoxin free water	/				200
Anhydrous DMF	/				150

As a first step, the endotoxin free water, used for the reaction, was degassed for 5 min using the Argon line and all later used Eppendorf tubes were also flushed with argon. Copper(II) sulfate pentahydrate as well as sodium ascorbate were dissolved in the prepared water and TBTA as well as Y9-N_3 were dissolved in DMF. The PEG-alkyne was dissolved in the Y9-N_3 solution. 9 µL of the TBTA solution were mixed with 8.3 µL of the copper solution resulting in a turquoise mixture. To this solution 5.5 µL Na-Asc were added, inducing a colour change to yellow. To start the reaction the prepared 22.8 µL of the yellow solution were added to the mixture of Y9-N_3 and PEG- alkyne. During the reaction time of 60 min subsamples were collected to monitor the reaction progress. The samples were analysed on the Dionex HPLC at 60°C with a solvent gradient of 5-65% eluent B in 55 min. To stop the reaction, it was quenched with 300 µL endotoxin free H_2O.

Final purification:

The final product was also purified on Dionex C_4 HPLC at 60°C with the same gradient and time as during the reaction monitoring. The product was collected manually and lyophilized producing a yield of 3.1 mg (95%).

Final analysis:

For the final analysis a subsample of the product was dissolved in AB solution and analysed at 60°C with the same gradient as mentioned beforehand. The mass of the product was confirmed with an LC- MS maXis from Bruker in the mass centre.

t-ISEr Y9-N_3 20kDa PEG:

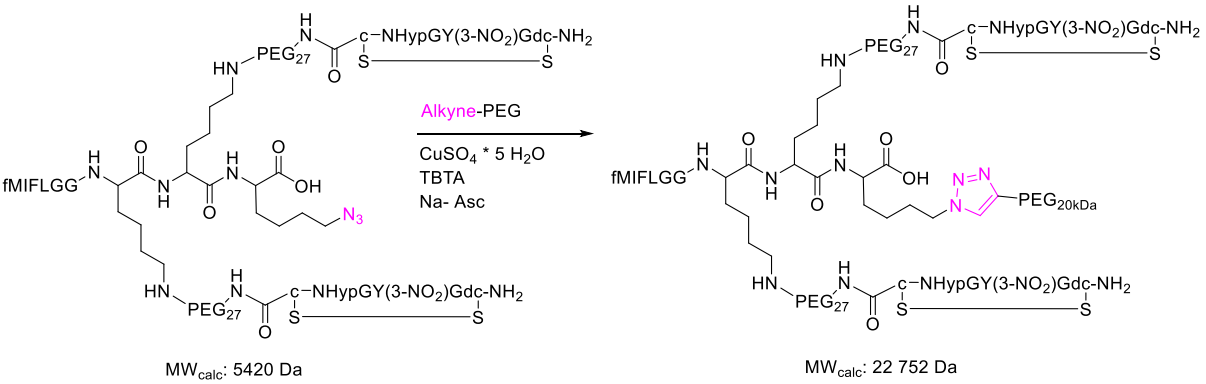

Figure 19 Schematic structure of t- ISEr Y9-N_3 20 kDa PEG with calculated masses and reaction partners and the 1,2,3-triazole marked in magenta

For the coupling of the larger PEG-alkyne the stochiometric relations have been changed a bit, because of the smaller size differences between the PEG- alkyne and the final product. The separation between the product and educt proved to be not efficient enough, therefore PEG-alkyne was used at a smaller scale as seen in *Table **8***.

Table 8 Stochiometric conditions of the CuAAc with 20kDa PEG-alkyne

Compound	Mass [mg]	Molar Mass [g/mol]	n [µmol]	Equivalent	Volume [µL]
Y9-N_3	1.7	5420	0.277	1	50
PEG- alkyne	4.2	17 332	0.249	0.9	/
$CuSO_4$ * $5H_2O$	5.2	249.7	1.245	4.5	100
TBTA	10.8	530.6	1.356	4.9	100
Na- Asc	10.2	198.1	2.076	7.5	100
Endotoxin free water	/				200
Anhydrous DMF	/				150

The Eppendorf tubes and the endotoxin free water were prepared as described in the synthesis for the 5kDa PEG coupling. Copper (II) sulfate pentahydrate and sodium ascorbate were dissolved in water while TBTA and Y9-N_3 were again dissolved in anhydrous DMF. PEG-alkyne was added to the Y9-N_3 solution. In a separate tube 6.2 µL of the copper solution were mixed with 6.8 µL of TBTA resulting in a turquoise solution. To this solution 4.2 µL Na-Asc were added resulting in a colour change to yellow. The reaction was started by adding the mixture of Y9-N_3 and PEG-alkyne to the stock mixture. After a reaction time of one hour the reaction was quenched with 300 µL H_2O. The reaction was monitored using Dionex HPLC with a solvent gradient of 5-65% eluent B in 55 min at 60°C and a C_4 column.

Final purification:

The product was purified with the same HPLC and gradient as the reaction monitoring, the product peak was collected manually and lyophilized producing a yield of 4.6 mg (81%).

Final analysis:

For the final analysis the same HPLC and solvent gradient, as mentioned beforehand was used as well as a gel to compare the product with the 5kDa PEG product.

7.2.3 SDS Page

The 5kDa t-ISEr as well as the 20kDa t-ISEr, the reaction control subsamples, and the educts were compared on an SDS gel. The SDS Page protocol was performed after Laemmli et al.[45] All compositions of the used reagents are summarised in *Table 9*. To measure solid samples, a small amount of sample was dissolved in endotoxin free water. 10 µL of this solution was diluted (1:1) with SDS sample buffer before loading the sample on the gel. For liquid samples, like the reaction control subsamples, a 10 µL aliquot was taken and dissolved (1:1) with SDS buffer. The used gels were prepared according to the composition summarised in *Table 10*. After the separating gel was poured between the prepared glass spaces it was suspended in 70% isopropanol during the polymerisation process. Afterwards the isopropanol was drained and the stacking gel was poured on top of the separation gel. In the still liquid gel the combs were introduced as space holders. The combs were removed from the hardened gel and all prepared gels were stored in a moist tissue in the fridge at 4°C for later usage.

Table 9 composition of the buffers used for SDS Page

Separating gel buffer	1.5 M TrisHCl, 0.4% (w/v) SDS, pH 8.8
Stacking gel buffer	0.5 M TrisHCl, 0.4% (w/v) SDS, pH 6.8
2x SDS sample buffer	500 mM Tris, 6% (w/v) SDS, pH 6.8, 35% (v/v) glycine, 3.55% β-mercaptoethanol, 0.05% (w/v) bromphenolblue
10x Laemmli buffer	250 mM Tris, 2 M glycine, 1% (w/v) SDS
Coomassie blue staining solution	0.1% (w/v) Coomassie R250, 10% (v/v) Acetic acid, 45% (v/v) methanol in water

Table 10 Composition of the gels for the SDS Page (12 gels)

Separating gel	ddH_2O	12.5 mL
	Separating gel buffer	13.5 mL
	30% Acrylamid	26 mL
	10% SDS	550 µL
	10% APS	550 µL
	TMED	18 µL
Stacking gel	ddH2O	12.5 mL
	Stacking gel buffer	2.5 mL
	30% Acrylamid	3.5 mL
	10% SDS	185 µL
	10% APS	185 µL
	TMED	18 µL

The solutions, diluted with the SDS buffer, were vortexed and centrifuged before being loaded on the gels. First 7.5 µL of an LMW marker aliquot was loaded into the first gel pocked. From the prepared mixture of sample and SDS buffer 10 µL were loaded in the pockets of the finished gel, the gel chamber was filled with 1x Laemmli buffer (diluted from 10x Laemmli buffer) and the gels were developed at 250 V for 38 minutes. All gels were stained with Coomassie blue for one hour and destained with ddH_2O overnight. During the destaining process the water was changed every 30 minutes at first and after one hour it was changed every 1.5 hours before the night. The gels were documented using a gel imaging system (ChemiDocTM, BioRad).

7.2.4 Synthesis of a-ISEr Val-Cit

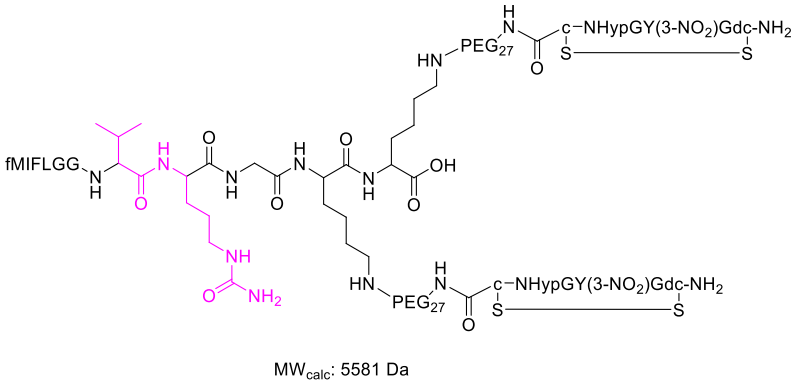

MW_{calc}: 5581 Da

Figure 20 Structure of Val-Cit modified Y9-N_3 with the calculated mass and the two novel amino acids marked in magenta

Synthesis of the scaffold:

Here a Wang resin (100-200 mesh; 0.33 mmol/g; 249 mg and 255 mg) with preloaded Fmoc-Lys(Mtt)-OH was used in an automated synthesis on the Liberty Blue peptide synthesizer with a reaction scale of 0.1 mmol. Two different batches with the same scale were synthesized, the exact amounts used for the liberty blue synthesis are summarised in *Table 11.*

Table 11 Scale of the synthesis used by liberty blue for a-ISEr Val-Cit

Reagent	Volume [mL]	Weighted portion [g]
Fmoc-Lys(Mtt)-OH	6	0.77
Fmoc-Gly-OH	17	1.07
Fmoc-Leu-OH	6	0.45
Fmoc-Phe-OH	11	0.88
Fmoc-Ile-OH	11	0.80
Fmoc-Met-OH	11	0.89
Fmoc-Val-OH	11	0.90
Fmoc-L-Cit-OH	6	0.77
DMF (washing solution)	580	/
Piperidine (deprotection)*	137	/
DIC (activator)	35	5.5 mL
Oxyma (activator base)**	20	2.84

* + 0.1M Oxyma

** + 0.3M DIPEA→ 1mL DIPEA

The formylation, Mtt deprotection and PEG coupling for both resins was performed as described in 7.2.1 Synthesis of Y9-N. For the formylation *p*-Nitrophenyl formate (3 eq; 167.1 g/mol; 54 mg and 51 mg) was used and for the PEG coupling Fmoc-PEG-COOH (2.75 eq; 1544.8 g/mol; 2x 851 mg) with the activator HATU (2.4 eq; 380.3 g/mol; 2x 183 mg) and DIPEA (5eq), as described before.

Binder synthesis:

The binders were only synthesized in one batch, the other one was stored for later usage. The synthesis was performed on Liberty Blue and the reagents are summarised in *Table **12***.

Table 12 Scale for chemicals used in the liberty blue synthesis for binders of a-ISEr Val-Cit

Reagent	Volume [mL]	Weighted portion [g]
Fmoc-Asn-OH	11	1.35
Fmoc-Gly-OH	11	0.68
Fmoc-D-Cys-OH	17	2.10
Fmoc-Hyp(tBu)-OH	6	0.53
Fmoc-Tyr(3-NO_2)-OH	6	0.57
Fmoc-D-Asp-OH	6	0.52
DMF (washing solution)	467	/
Piperidine (deprotection)*	105	/
DIC (activator)	30	4.7 mL
Oxyma (activator base)**	20	2.84

* + 0.1M Oxyma

** + 0.3M DIPEA→ 1mL DIPEA

The final cleavage was performed as again described in 7.2.1 Synthesis of Y9-N producing a crude product of 229.6 mg. The binders were oxidized on 113.4 mg of the crude product and the final purification was performed on the Varian Pro Star system with 5-30% eluent B in 5min 30-70% B in 40 min. Two main pools with a combined weight of 6.2 mg (6%) and two side pools with a combined weight of 6.4 mg (6%) were collected.

Final analysis:

A subsample of the pools was dissolved in AB solution and the final analysis was performed on Vanquish HPLC-MS with a solvent gradient of 5-65% eluent B on a C_4 column. One main and one side pool are displayed below, the other analysis can be found in the supplementary information.

7.2.5 Cell culture studies

To test the cleavage site of the Val-Cit sequence, a cell culture experiment with HT29 cells was carried out. All working steps involving living cells were performed in the Laminar air flow, which was disinfected with 70% EtOH before and after usage. All solutions coming into contact with living cells were previously heated in the water bath to 37°C. The cells were grown in a tissue culture flask from Merck and as a growth medium DMEM with 10% FBS was used. To grow the cells an incubator was used, under the conditions of 37°C and 5% CO_2. To keep the growing cells healthy, every few days, the medium of the cells was changed by pipetting the old one away and adding 10 mL of fresh medium. The growth rate of the cells was checked using a microscope, and when the cells occupied about 90% of the flask they were split. For the splitting of the cells the old medium was drained from the flask and the cells were incubated with 2 mL Trypsin for 5 minutes. Afterwards the Trypsin was used to wash the rest of the cells from the flask walls by pipetting. The solution was diluted with 2 mL medium, transferred to a falcon tube and centrifuged by 300rpm for 3 minutes. The supernatant was taken away and the resulting pellet was dissolved in 5 mL fresh medium. 1 mL was pipetted back into the flask and resuspended with 10 mL medium resulting in a 1:5 dilution of the cells, giving them enough space to grow. After the cells looked healthy enough under the microscope, the cells were peeled of the flask wall with Trypsin. After centrifugation the pellet was dissolved in 5 mL medium and from this solution 100 µL were put in pockets of a 96- well plate. The cells were allowed to grow inside the wells before the sample was added.

For another approach, the cells were counted from a defined 1 mL volume and calculated how many cells were seeded into the wells of the 96-well plate. The cells were calculated using the following approach:

$$\frac{119}{4} * 2 * 10^4 = \sim 575\,000\ cells/mL$$

119… Cells counted
4… division factor from the manufacturer
2… dilution factor
10^4… multiplication factor from the manufacturer

The calculated cell concentration was divided with the amount of the cells wanted per well to obtain the dilution factor necessary to calculate de volume per well.

A solution of 1 mg/mL in medium was prepared from a-ISEr Val-Cit and the precursor Y9-N_3 as a control sample. From both solutions 100 µL each were incubated with the cells. Several samples were prepared as well as control groups without cells. For the controls the sample solution was filled in an empty well. Also wells with just medium and without cells were prepared as a blank measure.

After the desired incubation time, the supernatant was transferred in Eppendorf tubes. To get rid of all remaining cells before measurement all samples were treated as follows:

- Eppis were centrifuged for 10 minutes at 14 000 rpm
- Supernatant was transferred in fresh eppis
- EtOH was added to precipitate all peptides
- The eppis were cooled for 10 min at 4°C in the refrigerator
- Eppis were centrifuged for 10 minutes at 14 000 rpm
- Supernatant taken off
- Pellet dried with argon
- Pellet dissolved in 50 µL AB solution

The analysis was done on Thermo HPLC- MS, where 40 µL were injected and for analysis a C18 column with a gradient of 1-61% eluent B in 11 minutes was used. All cell culture experiments were performed following this procedure.

7.2.6 Matrix metalloproteinase experiment

In addition to the cell culture experiments a human MMP2 proteinase was purchased from Sigma-Aldrich. The MMP2 was lyophilized from 10 mM sodium phosphate at a pH of 7.5 with addition of 0.1 mM calcium chloride, according to the manufacturer.

Prior to opening, the vial was centrifuged at 1000rpm for one minute and the MMP2 was dissolved in 10 µL endotoxin free water to achieve a final concentration of 1 mg/mL, as recommended by the manufacturer. Before usage, this solution stayed 30 minutes at room temperature.

To test the cleavage site with MMP2, 0.5 mL solution with a concentration of 2 mg/mL of a-ISEr Val-Cit in endotoxin free water was prepared. To this solution 1.25 µL of MMP2 was added to achieve a final concentration of 2.5 µg/mL of the proteinase. After 30 minutes the pH was adjusted with 0.1 M NaOH from 3.39 to 6.80. The experiment was controlled by RP- HPLC-MS.

The same experiment was repeated by dissolving the a-ISEr Val-Cit in 50 mM phosphate buffer at pH 7.4 where the concentrations of the a-ISEr as well as the MMP2 were kept the same. Additionally, a 100 mM $ZnCl_2$ solution in endotoxin free water was prepared. After three hours 5 µL of the $ZnCl_2$ solution were added to the mixture, to obtain a final concentration of 1 mM $ZnCl_2$. The cleavage was again monitored with RP-HPLC- MS.

7.2.7 Synthesis of hydrazide precursor

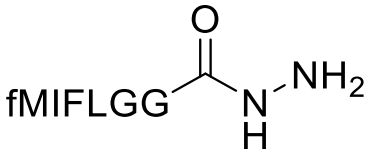

MW= 678.9 Da

Figure 21 Structure of hydrazide precursor

Functionalising the resin:

For the synthesis of this compound the resin Cl(TCP)(Cl) Pro Tide (0.47 mmol/g; 853 mg) was used with a reaction scale of 0.4 mmol. The resin was washed with DMF, DCM and DMF consecutively and swelled in DMF:DCM (50:50) for 30 min. Meanwhile 15 mL of a 10% hydrazine monohydrate solution in DMF was prepared and the resin was incubated with the solution twice for 30 min each and washed with DMF in between and in the end. The remaining unreacted functional groups were capped with 5 mL of a 5% MeOH solution in DMF, which was incubated with the resin for 20 min. The first amino acid Fmoc-Gly-OH (4 eq; 477 mg and 491 mg) was double coupled using HATU (2.38 eq; 380.23 g/mol; 359 mg and 366 mg) and HOAT (2.5 eq; 136.1 g/mol; 138 mg and 137 mg) as activators and DIPEA (8 eq; 557 µL) as base. HATU and HOAT were dissolved in 1.6 mL DMF and Fmoc-Gly-OH was added. In the end DIPEA was added and both coupling steps were performed in 45 min with a washing step in between.

Afterwards all unreacted amines were capped with acetic anhydride (3 eq; 102.1 g/mol; ρ 1.08 g/mL; 113.4 µL) in DIPEA (3 eq; 209 µL). The capping solution was diluted 1:1 with DMF and incubated for 20 min with the resin.

Loading level:

To control the final loading level of the resin 13.2 mg of the dried resin were suspended in 10 mL 20% piperidine for 30 min to deprotect the remaining Fmoc protection group. Afterwards 200 µL of the supernatant were 10-fold diluted with 1.8 mL of DMF and the UV absorption at 301 nm was measured against a 20% piperidine blank. The loading level calculates as described in the following formula.

$$Loading\left[\frac{mmol}{g}\right] = \frac{A * d}{\varepsilon * l * m} * v * 10^3$$

A… UV absorbance at 301 nm

ε… extinction coefficient for dibenzofluvene adduct [7731.9 mol^{-1} L cm^{-1}]

m… mass of resin used [mg]

d… dilution factor [10]

l… length of cuvette [1 cm]

V… Volume of 20% piperidine used [10 mL]

10^3… change of units→ mmol; L→ mL; mg→ g

With a measured absorbance of 0.133 the new loading level calculated at 0.169 mmol/g.

Fmoc- Strategy:

All remaining amino acids were coupled manually with a new synthesis scale of 0.2 mmol and 759 mg of the previously functionalised Cl(TCP)(Cl) Pro Tide resin. All amino acids were coupled following the same procedure. First HATU (2.38 eq; 380.2 g/mol; 182 mg) and HOAT (2.5eq; 136.1 g/mol; 68 mg) were dissolved in 1.5 mL DMF and the amino acid (4 eq) was dissolved in the resulting solution. In the end DIPEA (8 eq; 278.7 µL) was added to the mixture and the coupling time for each amino acid was 45 min. Between the coupling steps various washing steps were performed.

Table 13 Used amino acids for hydrazide precursor

1. Fmoc-Gly-OH	240 mg	2. Fmoc-Leu-OH	287 mg
3. Fmoc-Phe-OH	311 mg	4. Fmoc-Ile-OH	285 mg
5. Fmoc-Met-OH	298 mg		

The formylation was performed, using *p*-Nitrophenyl formate (3 eq; 167.1 g/mol; 102 mg) and after the final cleavage, under the same conditions mentioned before, 62.1 mg of crude product was obtained. Due to the high hydrophobicity of the product, a bad solubility of the pellet in AB solution was observed.

Final purification:

30.95 mg of the small peptide were purified using Varian HPLC. Because of the bad solubility of the product, it was dispersed in AB solution and diluted with endotoxin free water up to 25% ACN and filtered before the separation on the column. This was done to ensure an adequate separation of the product on the column. The high ACN percentage would hinder the interaction of the solid phase and the product, as it would rush through the column. The product was purified using a solvent gradient of 5-65% eluent B in 30 min, at a temperature of 60°C and an automated sample collector. The fractions were pooled using Thermo LC- MS and one main and one side pool were collected. The total yield of the main pool was 7.8 mg (25%) and 1 mg for the side pool (3%).

Final analysis:

The product was analysed using Vanquish HPLC with a C4 column and a solvent gradient of 5- 65% eluent B in 30 min at 60°C. The mass was analysed using Waters HPLC-MS.

7.2.8 Synthesis of the Serin scaffold

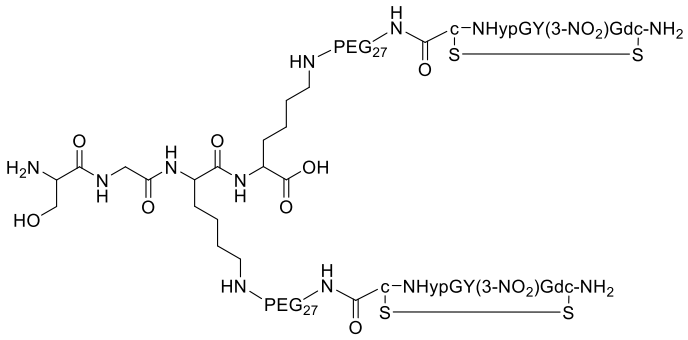

Figure 22 Structure of the Serin scaffold

The serin scaffold was synthesised manually with an Fmoc-Lys(Mtt) Wang resin (100-200 mesh; 0.33 mmol/g; 306 mg) with a reaction scale of 0.1 mmol. After the resin was swelled in DMF, the peptide was synthesised using the classic Fmoc strategy with the deprotection, activation, coupling and washing steps. For Fmoc deprotection 20% piperidine in DMF was used, the activation reagents for the amino acids (2.5 eq) were HBTU (2.4 eq; 0.5 M; 480 µL) and the base DIPEA (5 eq; 87.1 µL). The used amounts of amino acids are summarised in *Table 14* and all amino acids in the base scaffold were double coupled.

Table 14 Amounts of amino acids used for the synthesis of the Serin scaffold

1. Fmoc-Lys(Mtt)-OH	158 mg	2. Fmoc-Gly-OH	77 mg
	158 mg		79 mg
3. Boc-Ser(tBu)-OH	2x 68 mg		

For the last amino acid, a Boc protected Serine was used to ensure the orthogonality of the protecting groups as the *N*-terminal amide needs to be protected during the PEGylation. After the coupling a testcleavage was performed.

The Mtt deprotection and following PEG coupling were performed following the established protocol. For the PEGylation HATU (2.4 eq; 380.3 g/mol; 183 mg) and Fmoc-PEG-COOH (2.75 eq; 1544 g/mol; 850 mg) dissolved in DIPEA (5 eq; 174 µL) was used.

Binder synthesis:

The binders were synthesized manually using the classic Fmoc strategy. First the Fmoc-PEG was deprotected with 20% piperidine and then the classic Fmoc cycle of coupling, washing, deprotection, washing and coupling was performed. The amino acids were used with 2.5 eq, HBTU with 2.4 eq (0.5 M; 960 µL) and DIPEA with 5 eq (176 µL).

Table 15 Amounts of amino acid used for the serin binders

1. Fmoc-D-Cys(Trt)-OH	297 mg	2. Fmoc-Asn(Trt)-OH	303 mg
3. Fmoc-L-Hyp(tBu)-OH	213 mg	4. Fmoc-Gly-OH	150 mg
5. Fmoc-Tyr(3-NO_2)-OH	227 mg	6. Fmoc-Gly-OH	150 mg
7. Fmoc-D-Asp(tBu)-OH	208 mg	8. Fmoc-D-Cys(Trt)-OH	305 mg
	208 mg		306 mg

After the final cleavage 283 mg of crude product were obtained. The binders were oxidized in 100 mg of the crude. Additionally, the pH of the solution was adjusted from 4.28 to 7.22 with 0.1 M NaOH (endotoxin free) and air was directly bubbled through the solution overnight as the oxidation was not complete after one night. After final purification with a solvent gradient of 5-65% eluent B in 60min, 15min desalt, a main pool with 11.7 mg (12%) and a side pool with 29.2 mg (29%) were obtained.

Final analysis

A subsample of each pool was dissolved in AB solution and analysed on Vanquish HPLC with a solvent gradient of 5- 65% eluent B in 30min followed by direct injections on Waters HPLC-MS.

7.2.9 Periodate Oxidation

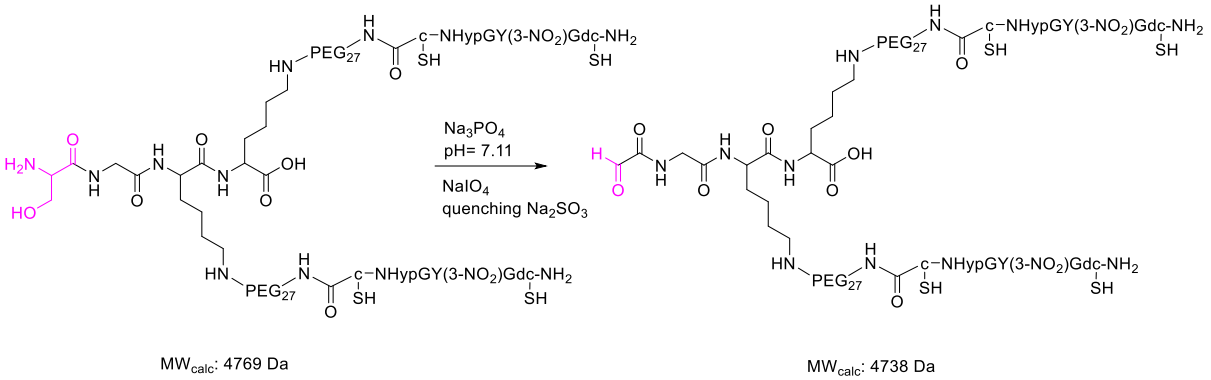

Figure 23 Reaction scheme of the serin periodate oxidation and calculated masses. Serin, as well as the resulting aldehyde are marked in magenta

For the *N*-terminal serin oxidation the reaction protocol of Bioconjugate techniques [44] based on the methods of Geoghegan and Stroh (1992) and Stolowitz et al. (2001) was followed.
Stock solutions were prepared for every reagent. First 100 mL of a 0.04 M Na_3PO_4 solution pH 7 was prepared by dissolving Na_3PO_4 (654 mg; 163.48 g/mol) in endotoxin free water and adjusting the pH with 3 M HCl. For $NaIO_4$ a 20 mM stock solution was prepared by dissolving $NaIO_4$ (8.8 mg; 213.89 g/mol) in 2 mL Na_3PO_4 solution. For the oxidation the crude product, with open disulfide bridges, as can be seen in *Figure 23,* was used because the periodate re-opens the cysteine bonds. 22 mg of the serin scaffold were dissolved in 5 mL sodium phosphate resulting in a final concentration of 4.4 mg/mL. For quenching of the reaction, a stock solution of 2 mL Na_2SO_3 (30 mM; 126.09 g/mol) was prepared by dissolving 7.7 mg in 2mL endotoxin free water. All reaction vessels containing $NaIO_4$ were encased in tinfoil to protect the reaction from UV light.
To start the reaction 714.3 µL of the $NaIO_4$ stock solution was added to the dissolved serin scaffold to obtain a final concentration of 2.5 mM periodate in the reaction vessel. The whole duration of the reaction was 6 min and the reaction was quenched by adding Na_2SO_3 in 10- fold molar excess over the periodate, with a final concentration of 10 mM in the reaction vessel, and stirring for 10 minutes. The reaction was monitored with Waters HPLC-MS.

Final purification:
The reaction was purified with Varian HPLC at a flow rate of 3 mL and a solvent gradient of 5-65% eluent B in 60 min and a desalt time of 10 min. The fractions were collected automatically and pooled with Waters LC- MS. Two main pools were collected from two different runs producing a total yield of 5.1 mg (23%).

No final analysis in form of an HPLC was performed for this product, just a mass analysis after purification.
This reaction was performed more than once, but the general scheme and used stock solution concentration didn't change.

7.2.10 Synthesis of a-ISEr Hydrazon

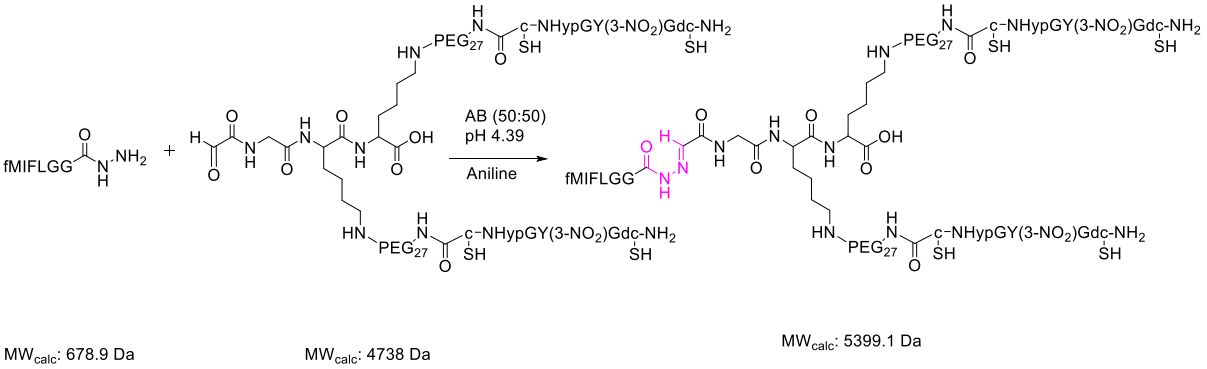

Figure 24 Reaction scheme of the hydrazone formation. The hydrazone linkage is marked in magenta

The stoichiometric relations and workflow steps followed in this reaction were adapted from the book Bioconjugation Techniques[44] as well as *A. Dirksen et. al* (2006)[41].
Other than recommended by the authors, the reaction was not carried out in a buffer solution rather than in AB solution and the pH was adjusted with 0.1 M NaOH. This decision was based on the poor solubility of the hydrazide precursor, making AB solution the best solvent option for the reaction at the time.
First, the aldehyde containing scaffold (1 eq; 0.91 µmol; 4.29 mg; 4737 g/mol; 2.2 mL) was dissolved in AB solution to a final concentration of 2 mg/mL. The hydrazide effector (4 eq; 3.62 µmol; 678.9 g/mol; 2.2 mg) was predissolved in 200 µL AB solution with the help of the ultrasonic bath and vortex. Afterwards the two solutions were mixed and to start the reaction Aniline (24 µmol; 93.13 g/mol; ρ= 1.022 g/mL; 2.2 µL;) was added as a catalyst to obtain a final concentration of 10 mM Aniline in the solution. After the addition of Aniline, the pH of the solution was adjusted from 3.11 to 4.39 with 0.1 M NaOH. The reaction was monitored with Waters HPLC-MS and the total reaction time was 4 hours and 30 minutes.

Final purification:
The reaction solution was frozen over night before the final purification on Varian. To accommodate the instability of the formed hydrazone against low pH, for the purification the solutions A and B were freshly prepared with only half the TFA concentration (solution A: H_2O + 0.05% TFA; solution B: ACN + 0.04% TFA). The reaction solution was diluted with endotoxin free water to a total volume of 7 mL. The solution was centrifuged at 4000rpm for 5 min and analysed with a solvent gradient of 10 min desalt time, 5- 20% eluent B in 2 min and 20- 65% eluent B in 11 min on a C_4 column. The fractions were collected automatically, pooled with Waters HPLC-MS and lyophilized. A yield of 0.8 mg (17%) was collected.

Final analysis:
Due to the instability of the product in the conventional AB solution no final analysis was performed.

7.2.11 Cell based Assays

For the testing of the novel synthesized ISErs regarding their binder and effector activity, samples were sent to Syntab Therapeutics GmbH in Aachen (Germany). For the binder testing, three different cell lines were obtained from LGC/ATCC or DSMZ and cultured according to the provider's guidelines. The cell line MDA-MB231, a human breast adenocarcinoma, 4T1, a breast carcinoma from immunodeficient BALB/c mice and E0771, a breast/ mammary gland carcinoma from C57BL/6 mice. Different sample concentrations were incubated against 50 nM biotin-marked ISEr Y9lc and measured with Streptavidin-PerCP-Cy5.5 in flow cytometry.

For the DHR assay to test the effectors, crude human leucocytes were isolated at room temperature from healthy volunteers using dextran sedimentation and hypotonic lysis to remove erythrocytes. The gated leucocytes were incubated with different sample concentrations and the oxidative burst was measured with the oxidation from DHR to rhodamine.

The exact step by step description as well as the different parameters used for the DHR assay as well as the biotin- streptavidin assay are summarized in the work of AndréJ. G. Pötgens et. al. [16] as well as Manuel Brehs et. al.[13] All working steps were performed in accordance with the previously established protocols.

8. Results and Discussion

8.1 t-ISEr Y9-N_3 coupled with 5kDa PEG

8.1.1 Y9-N_3 starting material

The educt for the t-ISEr was synthesized with the classic Fmoc-strategy on two different resins and consequently purified using an RP-HPLC. After the synthesis of the scaffold on the Liberty Blue peptide synthesizer the *N*-terminal methionine was formylated with *p*-Nitrophenyl formate. During this formylation process the cap of the syringe had to be secured with parafilm to compensate for the gas release during formylation.

With the selective removal of the Mtt protection group from the coupled lysine, a branched peptide could be synthesized. Mtt was removed with DCM/TFA/TiPS, where the acid TFA in an amount of 1% was used. TiPS was added to prevent the reattachment of the cleaved Mtt to the free amines and quench the trityl-cations[46]. The reaction was monitored by the bright yellow colour from the cleavage product, the Mtt-carbocation. The absence of yellow cleavage product, and therefore the completeness of the Mtt cleavage, was visually confirmed. During the following PEG coupling, the resin was closely monitored, due to the higher viscosity after coupling resulting from the PEG chains. If the solution became too viscous a small amount of DMF was added to allow proper mixture during the coupling process.

After manual synthesis of the binders, the peptide was cleaved from the two resins resulting in the product Y9-N_3 with two reduced cysteines on each binder. To dissolve the product in PBS for lyophilisation, it was necessary to vortex the sample. The process of vortexing introduces air into the peptide solution and the peptide can assist with the reduction of the surface tension and simultaneously make the solution more viscous, which in turn increases the possibility of foam formation. The protective layer, which forms the bubble in the foam can be plastered with peptides while they orient their hydrophilic side chains toward the water solution and the hydrophobic chains towards the air, increasing the stability of the foam bubble. This effect is often used in food chemistry.[47] This foam formation could not be prevented but it did not have an impact on the following lyophilisation.

After the final purification, three pure main pools (MP) and three side pools (SP) could be obtained, MP3 is shown exemplary in *Figure **25***. One of the main detectable side products, with the mass of 5377 Da, was the structure without the azide group, as can be seen in the SP shown in *Figure **26***. The exact reasons behind the cleavage of the azide could not be determined, but the conditions during the final cleavage are most likely responsible for the reduction of the azide to the amine[48]. As the reduced azide was not produced in a significant amount, it did not influence the CuAAc later on, therefore no adaptations are necessary for future synthesis.

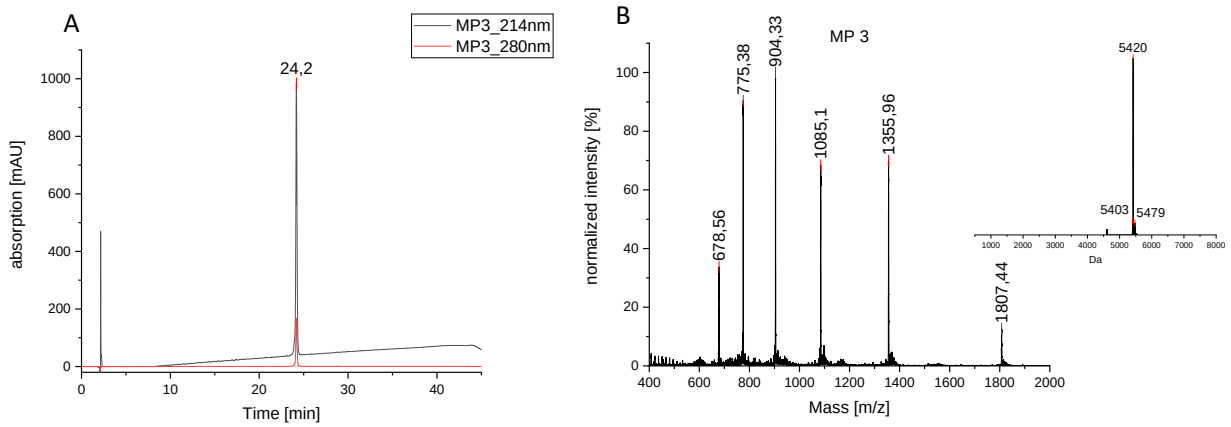

*Figure 25 **A)** RP- HPLC final analysis of Y9-N3 MP3 at 214 and 280 nm **B)** Mass spectrogram of Y9-N3 MP3 and the deconvoluted spectrum. MW_{calc}: 5420 Da*

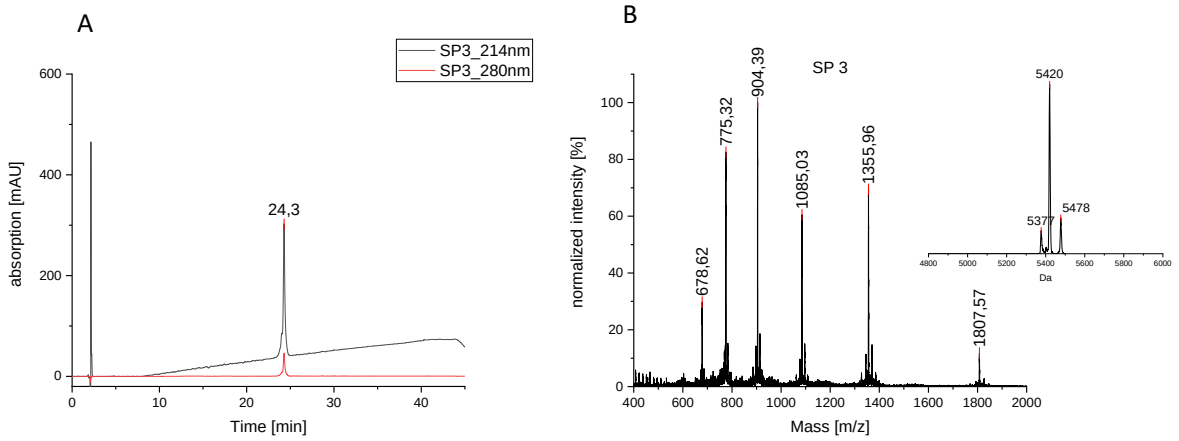

Figure 26 ***A)*** *RP-HPLC final analysis of Y9-N_3 SP3 at 214 and 280 nm.* ***B)*** *Mass spectrogram of Y9-N_3 SP3 with the deconvoluted spectrum. MW_{calc}: 5420 Da*

8.1.2 Click Reaction with 5kDa PEG-alkyne

The coupling of Y9-N_3 with PEG-alkyne was optimized in several reactions, starting with coupling experiments on the side pool. Reaction controls were performed on a Dionex/CAD system with a C4 column and a solvent gradient of 5-65% eluent B in 30 minutes at room temperature. These first analysis were monitored with HPLC-MS analysis from Waters, to determine the mass of the product. During this, two peaks could be detected, but mass analysis revealed, that the first peak correlates with the mass of the TBTA added to the reaction and the second peak corresponds to a side product of Y9-N_3, where the azide was cleaved from the scaffold and therefore no CuAAc could have taken place. No desired product was observable in the 214nm HPLC trace, as seen in *Figure **27***. The cleavage of the azide is most likely a reduction process from the azide to the amine from the conditions during the final cleavage of the peptide from the resin.[48] The mass of the product was also not detectable in direct injections with the ESI-MS detector from Waters. Therefore, we assumed, that the t-ISEr Y9-N_3 5kDa PEG could not be detected with Waters ESI-MS. During reaction monitoring in the Dionex system a reduction in the educt peak of Y9-N_3 was observed over time and we concluded that the product was formed but undetectable. The remaining educt showed a mass of 5377 Da, corresponding with the previously mentioned reduced azide, which would not participate in the click reaction.

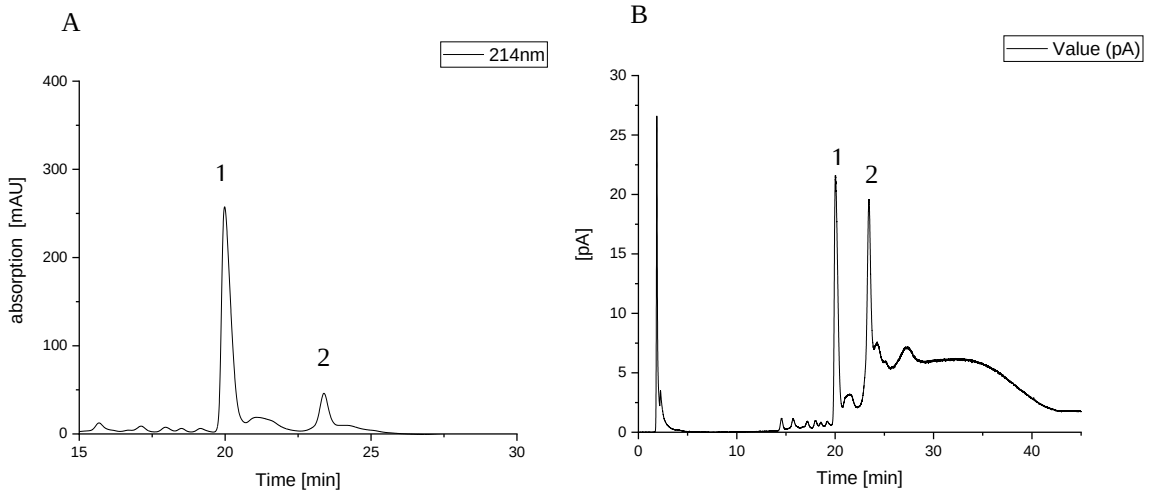

Figure 27 Zoomed in chromatogram of the first CuAAc with two detectable peaks marked as 1, with the mass of TBTA and 2, with the mass of Y9-N_3 and its side products. ***A****) at 214nm in the RP-HPLC and* ***B****) in the CAD detector.*

As seen in *Figure **27 B***, in addition to the described two sharp peaks, a third smaller and broader peak was detected in the CAD trace. To avoid the possibility of product accumulating on the column during the different runs, a wash run with Guanidine*HCl buffer was performed at 60°C. Here, a previously undetected peak with a high absorbance at 214 nm as well as at 280 nm was visible. The next CuAAc was performed under the same conditions, but the reaction control was analysed at 60°C. The new peak was detected in the UV trace and subsequently collected per hand. The fact, that the peak increased in intensity during the reaction monitoring was a strong indication of product formation. Peak 3, as displayed in *Figure **28 A***, was measured in the mass centre with a maXis ESI-Qq-TOF from Bruker. In the upper panel of *Figure **28 B*** the deconvoluted mass spectrum is displayed. The numerous peaks are due to the fact that the 5 kDa PEG-alkyne used during the click reaction is polydisperse, meaning that during the manufacturing process different PEG lengths were obtained. The mass differences between the peaks are 44 Da, which correlates with the mass of the ethylenoxide monomer. The observed masses were in the expected range of the product with a calculated approximate mass of 10210 Da. The peaks in the UV trace, labelled as 1-3 appear at different time points than before because of the use of the column oven. The reason, why the mass spectrometer from Bruker was able to detect the t-ISEr while the ESI-MS system from Waters was not can be that the former one has a higher sensitivity or the usage of different additives like formic acid. FA is generally the more preferred additive during mass analysis as it possesses a lower pKa and offers a higher degree of protonation than TFA.[49]

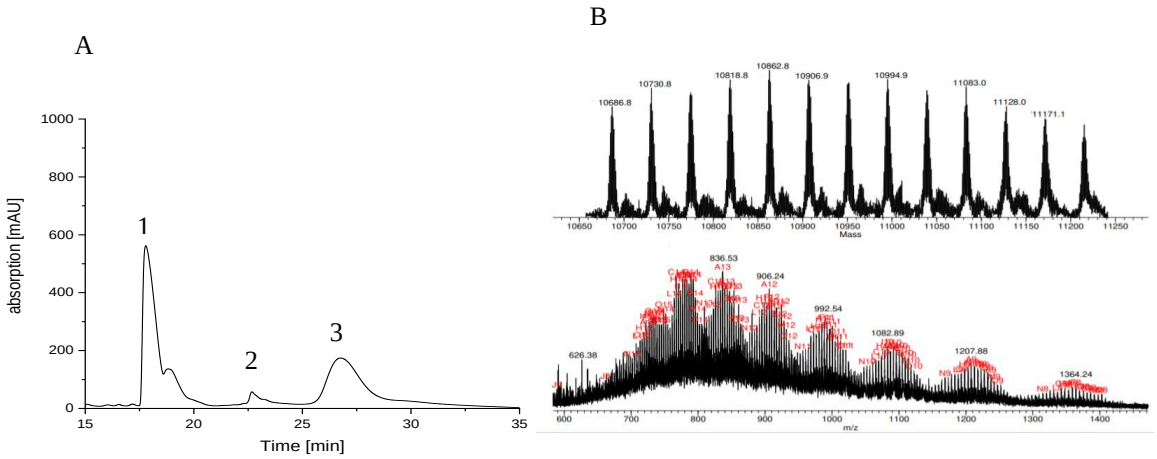

*Figure 28 **A**) RP-HPLC zoomed in chromatogram at 214 nm of the last timepoint (1 hour) from the CuAAc with 5 kDa PEG-alkyne and Y9-N_3. Peak labelled as 1 corresponds with TBTA, 2 with the educt Y9-N_3 and 3 with the desired t-ISEr product **B**) Mass spectrum analysis from t-ISEr Y9-N_3 5 kDa PEG, displayed in MagTran*

To confirm product formation, an SDS PAGE was performed, where the reaction control sub-samples as well as both educts were analysed. As seen in *Figure **29*** , the CuAAc reaction proceeds very fast, as the product stain could already be detected in the crude mixture (t= 0) and did not increase significantly in the following 30 minutes. The product spot appears to possess a larger apparent mass than expected as it is found above the 14.4 kDa mark from the marker. This phenomenon was attributed to the coupled PEG chain, as the polydisperse PEG chain slows the movement of the product through the gel due to its large hydrodynamic radius. Therefore, the product does not move as fast as expected. Both adducts did not stain in the gel, most likely because due to their small size, they travelled too fast and exited the gel before completion of the set time for the SDS PAGE. This problem was corrected in the second gel, as the runtime was shortened to visualize Y9-N_3 on the gel (see *Figure **32***).

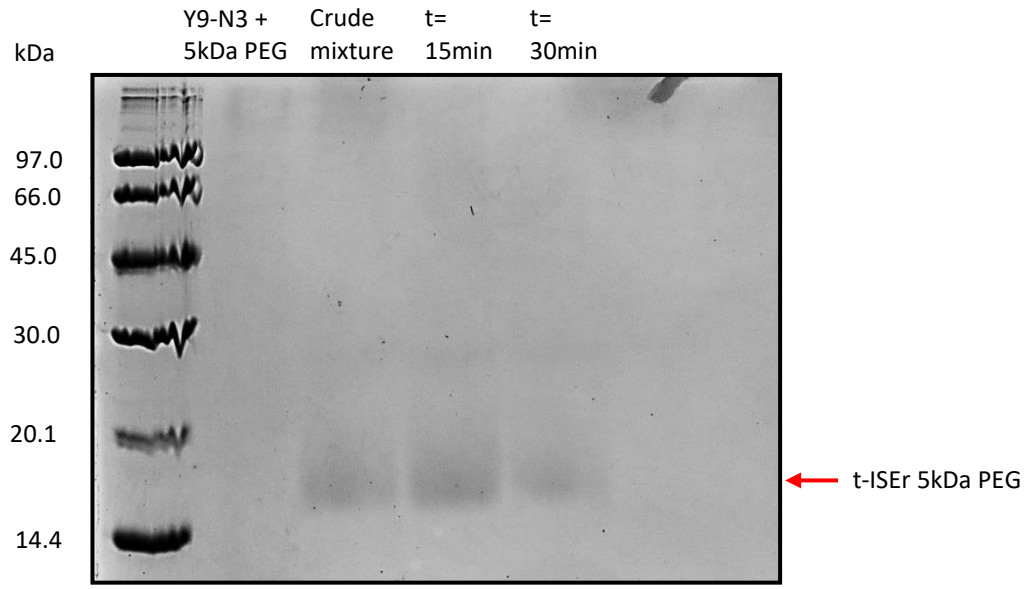

Figure 29 SDS PAGE of different time points (crude mixture= t 0; t=15 min and t=30 min) during the reaction control for the synthesis of t-ISEr Y9-N3 5 kDa PEG

The final analysis of the product showed one singe peak, as can be seen in *Figure **30*** **A**. The product was not perfectly pure, which is indicated by the small shoulder after the product peak. This is due to the fact, that the product peak was collected manually during purification.

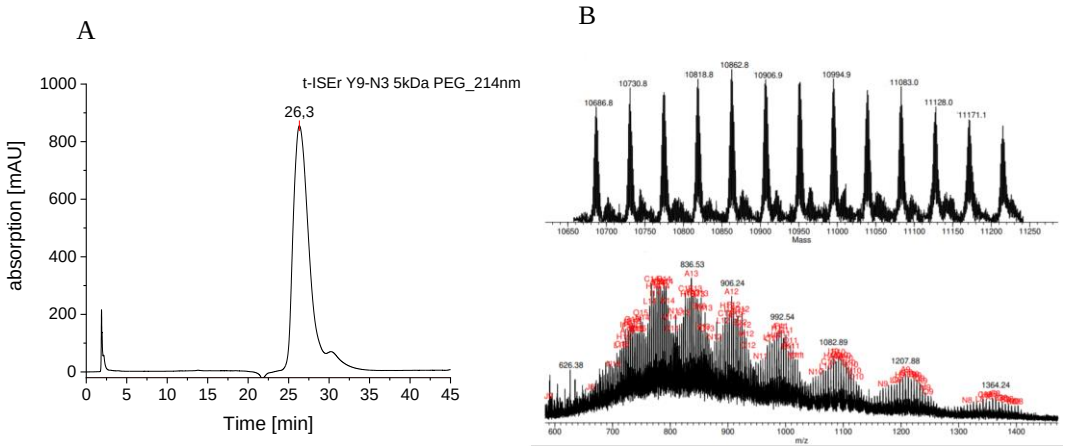

*Figure 30 **A)** RP- HPLC final analysis of t-ISEr Y9-N3 5 kDa PEG. **B)** Top panel: deconvoluted mass spectrum. Calculated mass: 10210 Da. Bottom panel: Mass spectrum of t-ISEr Y9-N3 5 kDa PEG*

8.1.3 Click Reaction with 20kDa PEG- alkyne

During the first test reaction with a Y9-N_3 side pool, the same equivalents as in the CuAAc with 5 kDa PEG-alkyne were used. For the reaction control at 60°C the same gradient as mentioned for the 5 kDa PEG coupling was used. It was apparent, that the separation from the product and the 20 kDa PEG-alkyne would not be sufficient, as the peak of the product overlapped with the larger PEG related peak, visible in the CAD spectrum as the PEG-alkyne does not possess an UV line at 214 nm. This can be seen in *Figure **31**,* where the third peak in the UV trace correlates with the desired product while the third peak in the CAD trace stems from PEG. As can be seen in the figure below, the detected PEG peak in the CAD trace overlaps with the product peak in the UV trace. This overlap was most likely due to excess of PEG in the reaction compared to the product. This overlap would interfere with the purity of the product during the peak collection.

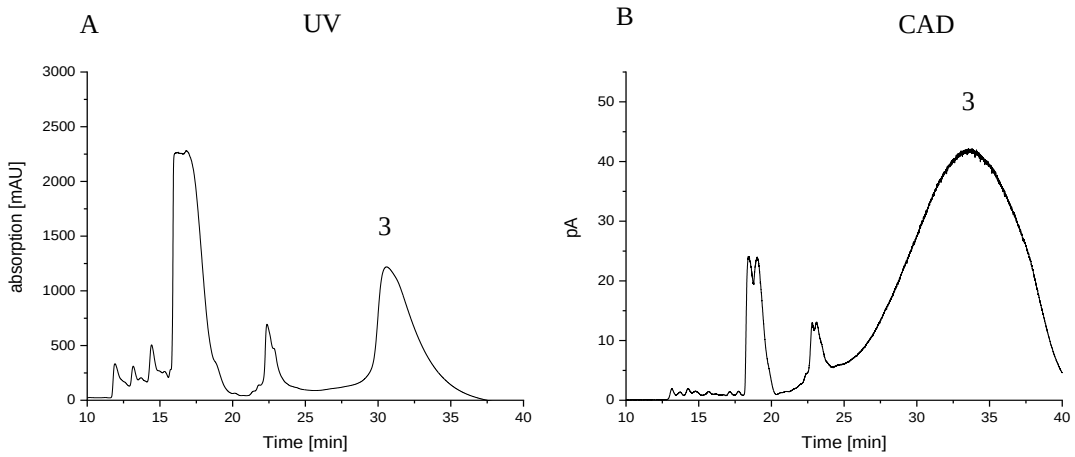

*Figure 31 **A)** UV trace at 214 nm after the reaction was quenched with H_2O, the product peak is marked as "3" **B)** CAD trace of the same sample with the broad PEG peak visible, also marked as "3", already starting at 25 minutes*

An SDS PAGE analysis confirmed the excess of remaining PEG, this can be seen in *Figure **32***. In this SDS page, the runtime was shortened to visualize the Y9-N_3 in the gel. The t-ISEr Y9-N_3 20 kDa PEG formation could already be observed in the crude mixture (t= 0) and only a small increase in the intensity could be observed during the remaining time stamps. This leads to the conclusion that the CuAAc reaction with the larger PEG-alkyne proceeds as fast as with the 5kDa PEG. In this gel, the t-ISEr Y9-N_3 5 kDa PEG was also analysed to compare the sizes of both products. Between both products a definite size increase could be observed, adding another evidence to the success of the formation of the t-ISEr Y9-N_3 20 kDa PEG. With the larger product the same phenomenon, of the spot appearing at a larger size than expected, was noticeable. The reason for this is the same as mentioned before, that the long polydisperse PEG chains possess a large hydrodynamic radius, henceforth hindering the movement of the compound in the gel.

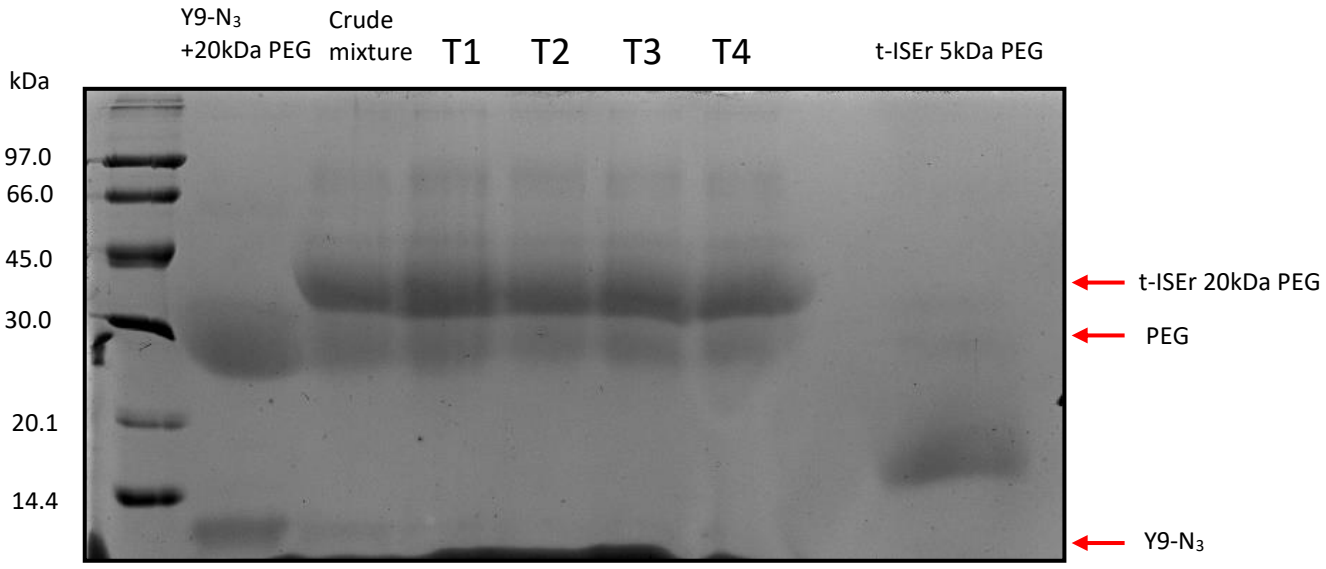

Figure 32 SDS PAGE of different time points during the formation of t- ISEr Y9-N_3 20 kDa PEG (t1-4; Crude Mixture and both educts) as well as t-ISEr Y9-N_3 5 kDa PEG (far left) for comparison

To avoid the access of 20 kDa PEG-alkyne educt in the final product, the equivalents were adjusted, using PEG as the limiting factor. Therefore, the reaction was performed with 0.8 as well as 0.9eq PEG. To confirm the absence of excess PEG, the products were analysed by SDS PAGE after purification, as seen in *Figure **33***. On this gel the PEG line was no longer visible in the product for both equivalents and 0.9eq was chosen for further synthesis. Analysis of the product by mass spectrometry was attempted, but the large size of the product prevented accurate analysation, as the mass centre had technical problems analysing large molecules at the time of the thesis.

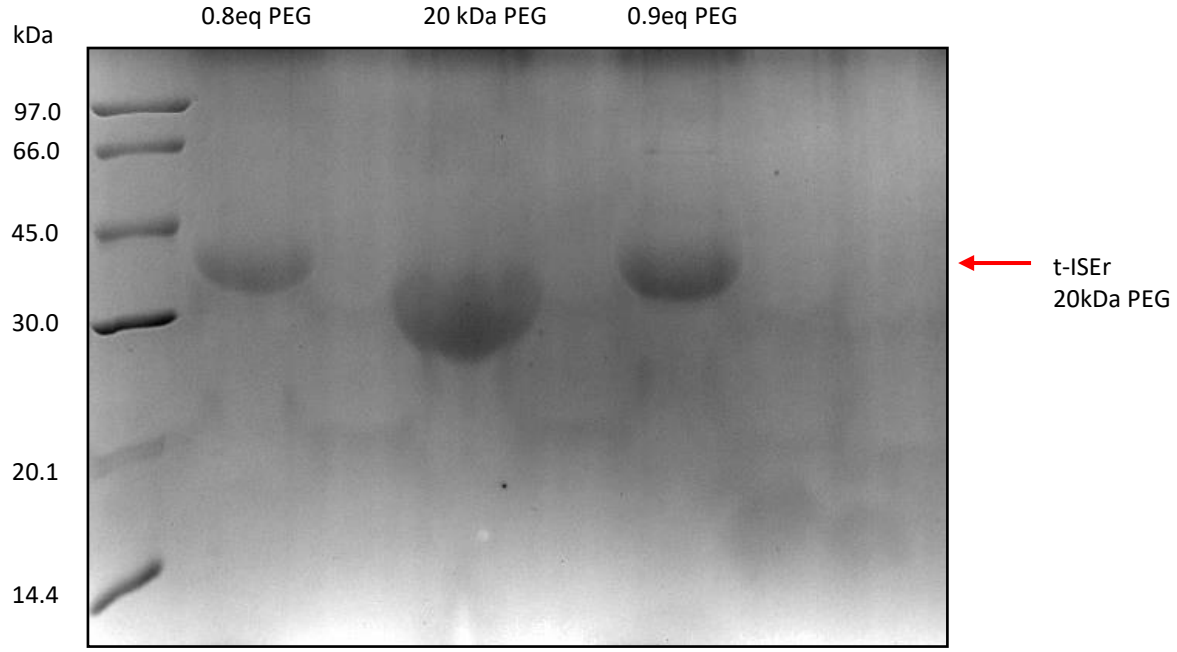

Figure 33 SDS PAGE of two t-ISErs synthesized with different equivalents of 20 kDa PEG. Left: 0.8eq PEG/ Right: 0.9eq PEG/ Middle: pure 20kDa PEG for comparison

The final analysis of the product with HPLC revealed one single, broad peak. As the product was collected per hand, a small shoulder can be seen in *Figure **34*** before the product peak, indicating small impurities. The broadness of the peak is a result of the coupled PEG chains.

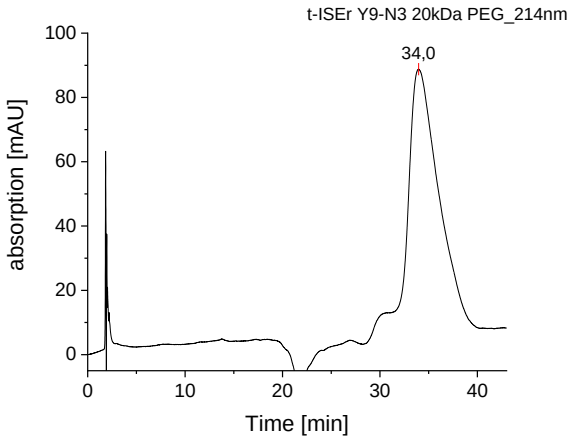

Figure 34 RP- HPLC final analysis from t-ISEr Y9-N_3 20kDa PEG

8.2 a-ISEr with Val-Cit cleavage site

This compound was synthesized using Fmoc SPPS, following the protocols described in chapter **7.2** . After the final cleavage, part of the product was oxidized in 1x PBS buffer overnight to form disulfide bonds in the B9 binder peptides. Afterwards the product was filtrated and centrifuged before purification on the Varian RP-HPLC, to remove remaining insoluble material. During the final analysis, the product peak appeared in some runs as a double peak and in others as one single peak, as shown in *Figure **35***. Mass analysis indicated the same mass, of the desired product, in both peaks. A reason for the observed double peaks could be a misalignment of the disulfide bridges between the cysteines in the binders. Instead of disulfide bridges forming between one B9 binder peptide, it is possible, that the disulfide brides formed between two B9 arms. Such a misalignment could lead to the same mass but different elution times on a RP-HPLC. To test this theory a subsample of the product was reduced by dissolving it in AB solution and adding a catalytic amount of TCEP. After 15 minutes of reduction the sample was analysed again and only one peak could be detected with a mass corresponding to the reduced product. No further analysis was performed, as this was already a strong indication to why the double peak was observed. To avoid this problem in the future, it would be recommended to perform the oxidation at lower concentration in PBS buffer.

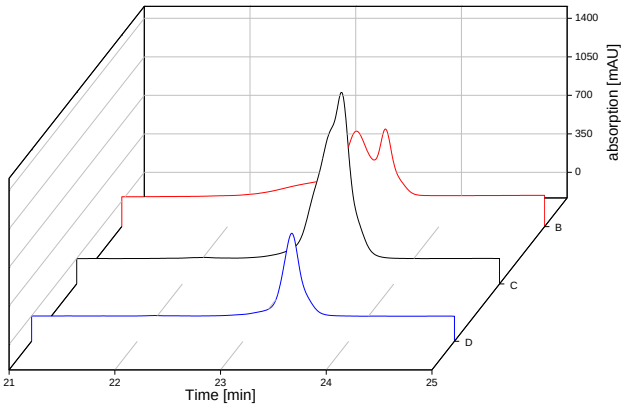

Figure 35 Zoomed in chromatograms at 214 nm of measurements from a-ISEr Val-Cit MP2. The exact concentrations vary, as can be seen in the heights of the peaks, but the double peak in the red trace and the shoulder in the green trace are observable compared to the peak in the blue trace. All measurements were performed from the same product.

The final analysis of the product revealed no significant side products. In the deconvoluted mass spectrum of the main pool (MP), shown in *Figure **36*** **B**, a peak with the mass of 5639 can be seen. This is a salt adduct of the product with sodium and potassium. This salt adduct formed in the mass spectrometer due to residue from a previous measurement, it can not be seen in the side pool (SP) in *Figure **37***.

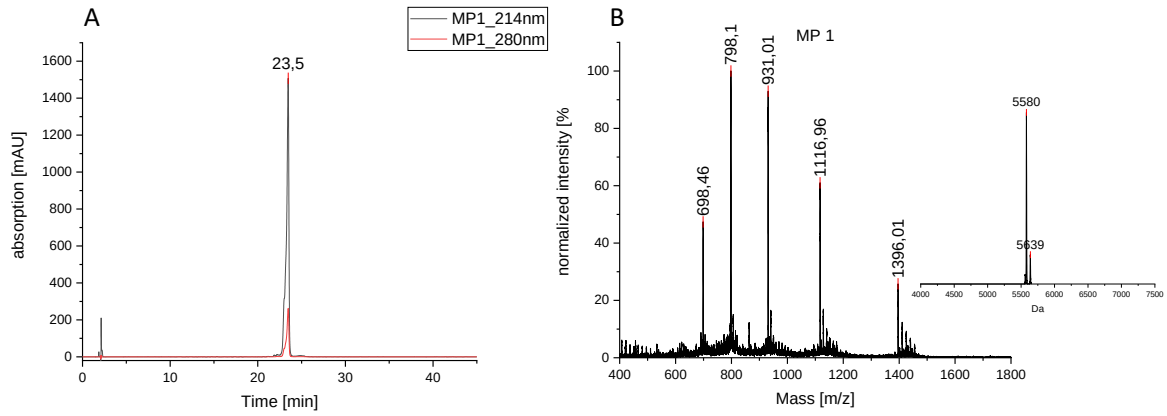

*Figure 36 **A)** RP- HPLC of a-ISEr Val-Cit from MP1. **B)** Mass spectrum and deconvoluted spectrum of a-ISEr Val-Cit MP1. Calculated mass: 5581 Da*

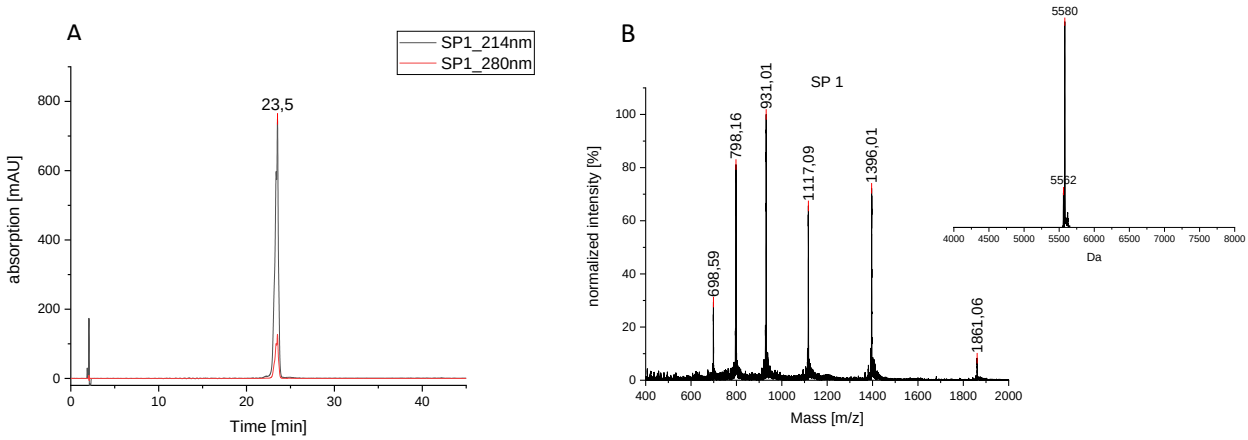

*Figure 37 **A)** RP-HPLC final analysis of a-ISEr Val-Cit SP1. **B)** Mass spectrum and deconvoluted spectrum of a-ISEr Val-Cit SP1. Calculated Mass: 5581 Da*

8.2.1 Cleavage studies on HT29 cells with a-ISEr Val-Cit

To test the ability of matrix metalloproteinases to cleave at Val-Cit, the HT29 human colon cancer cell line was chosen. First, because HT29 are easy to cultivate and were available on site. Second, according to the online database ARCHS4[50] HT29 were documented to express MMP2. To test the Val-Cit cleavage site MMP2 was chosen, because it is one of the most frequently expressed MMPs, can be found in most cancers and cleaves Val-Cit.[29]

The testing of the cleavage site was performed with two different stocks of cells, as in the first one, the cells did not grow well. No initial cause for this problem could be identified, as the tissue culture flask as well as the medium were changed without improvement in cell growth. The second stock was obtained from another working group but contained the same cell line. With this stock the cells proceeded to grow at the expected rate. The first experiment was set up, as described in chapter 7.2.5 Cell culture studies. The proposed cleavage reaction is described in *Figure **38***. For the first two cell experiments, the cells were grown directly in the wells of the 96-

well plate to reach the desired confluency of approximately 80%. For the last experiment the cells were seeded dense to begin with, by introducing 200 000 cells per well, to reach a confluency of 100% and the cells were just grown for one night in the wells.

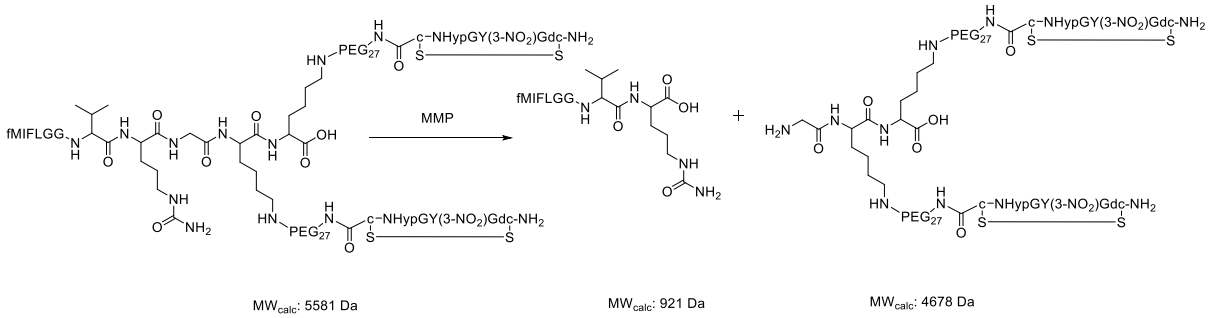

Figure 38 proposed cleavage scheme of a-ISEr Val-Cit with an MMP and the calculated masses of the cleavage products

The a-ISEr Val-Cit was incubated with cells and the supernatant was analysed after 24h and after 6 days to monitor the cleavage with RP-HPLC. In addition to the supernatant with a-ISEr Val-Cit, samples from untreated cells, just medium without cells as well as pure Y9-N_3, as a control, were taken and analysed as well. The Y9-N_3 educt was chosen as a control group, as it possesses a similar structure of the effector (fMIFL) and the binders as the a-ISEr Val-Cit. This control was set in place, to check for unspecific cleavages, related with the structure, other than the Val-Cit cleaving site. Neither after 24 hours, nor after 6 days could the mass of the desired cleavage product of the a-ISEr be observed, as can be seen in *Figure **39***. The sample, incubated with the cells express the same peaks as the pure a-ISEr after the different timepoints. No unrelated cleavage of the structure in the Y9-N_3 control could be observed, the related UV traces can be found in the Supplementary Information.

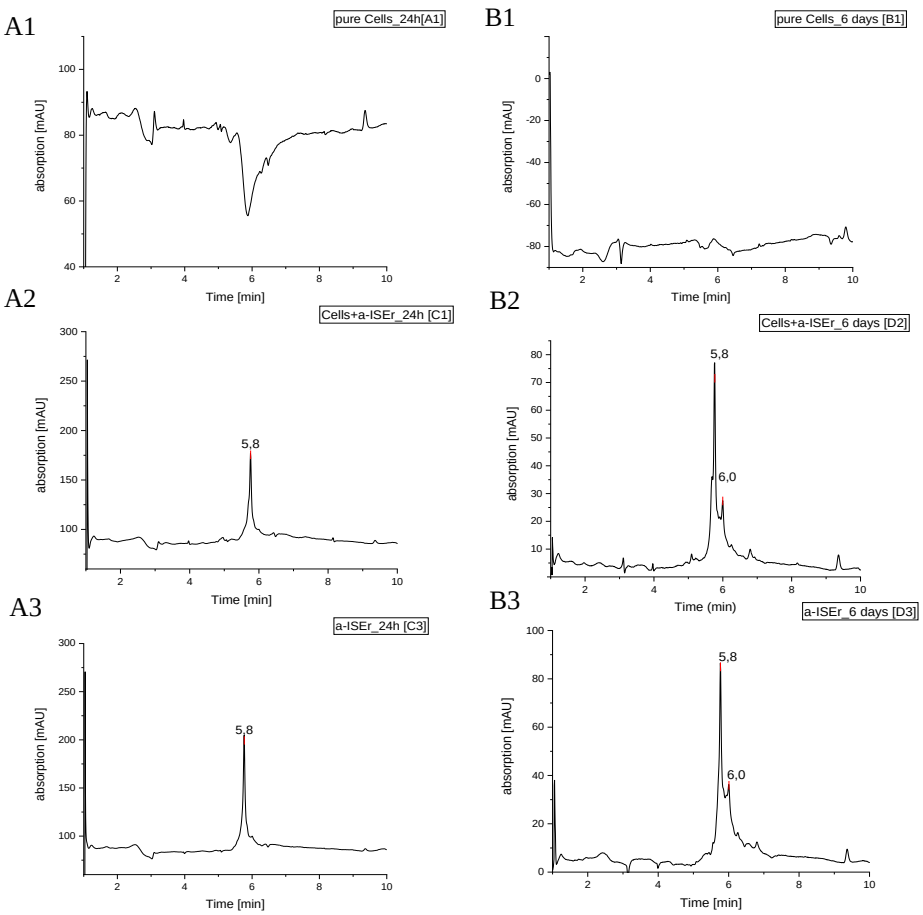

*Figure 39 Comparison between UV traces at 214 nm of a-ISEr Val-Cit after 24h and 6 days. On the left side **(A1-3)**, the three chromatograms after 24h and on the right side **(B1-3)** after 6 days. The top two panels (**A1** and **B1**) show untreated cells. The middle panels (**A2** and **B2**), cells incubated with the a-ISEr and the bottom panels (**A3** and **B3**) display the supernatants of pure a-ISEr in the wells*

The lack of observable cleavage can be explained by a variety of reasons. There are 24 different mammalian MMPs, which are divided into different categories. The chosen MMP2 belongs to the subfamily of gelatinases and is responsible for the degradation of the extra cellular matrix (ECM). Therefore, like many other MMPs, the cells excrete the MMP2 in the extracellular space, where it is activated. MMP2 was chosen because of its frequent occurrence in tumour cells as well as its established involvement in metastasis and tumour growth. It is possible, that the MMP2 could not recognize the cleavage site but another MMP from another subfamily can cleave the Val-Cit site but is not expressed by the HT29 cell line. An example for this is MMP3 from the subfamily of the stromelysins, which is not frequently expressed in the HT29 cells[50].

Another explanation for the absence of cleavage is, that the expressed MMP2 was not properly activated. Cells release MMPs as a pro peptide, where the active site is obstructed and therefore inactive[51]. Activation can occur through different proteinases in the ECM or through pericellular activation on the cell surface itself. The activation on the cell surface takes place by MT-MMPs and HT29 cells especially are reported to express the MT-MMP5, which is known to activate the pro MMP2[52]. It is a possibility, that the activation on the cell surface did not take place properly, although is highly unlikely, as the cells were grown in the wells beforehand to reach a confluency of 70-80%. In later experiments nearly 100% confluence was reached, without observing any cleavage product.

Another possibility for the absence of cleavage would be inhibition of the MMP2. Naturally the MMPs are inhibited by specific inhibitors like TIMPs (= tissue inhibitors of metalloproteinases) and unspecific occurring proteinase inhibitors like α1-proteinase inhibitor and α2-macroglobulin[30]. The TIMPs are divided into 4 groups,

TIMP 1-4, and the HT29 cells express three of the 4 groups. The inhibition of MMP2 can be a reason behind the lack of cleavage.

To eliminate the possibility of a lack of co-factor, for the next experiment, a zinc solution was added to the cells during incubation, as all MMPs are zinc and calcium dependent proteinases. For this attempt, the cells were not grown in the wells but seeded very confluent to begin with. Calcium was already present in the DMEM medium, so the experiment was performed with the addition of Zn^{2+}. For this a 200 mM $ZnCl_2$ solution was prepared in endotoxin free water, and from this solution 2 µL were added in the wells. Each well was prepared with 200 000 cells and the same samples as mentioned in the previous experimental setup, with just DMEM, a-ISEr Val-Cit and Y9-N_3 were prepared. For comparison, in some of the wells the zinc solution was added and the supernatant was analysed after 24 hours with RP-HPLC. As there was again no observable cleavage, it was concluded, that the lack of co-factors was most likely not the reason. It can be seen in *Figure **40***, that during the analysis of the cell culture experiments, the former mentioned double peaks of the a-ISEr Val-Cit could again be observed. Both compounds appear to have the same mass in the mass spectrum, as these are most likely the result of falsely closed disulfide bridges. No mass fitting to the expected cleavage products could be observed after 24 hours incubation in neither the wells with just a-ISEr Val-Cit, nor in wells, where additionally Zn^{2+} solution was added. The data from the Y9-N_3 control incubation is summarised in the Supplementary Information.

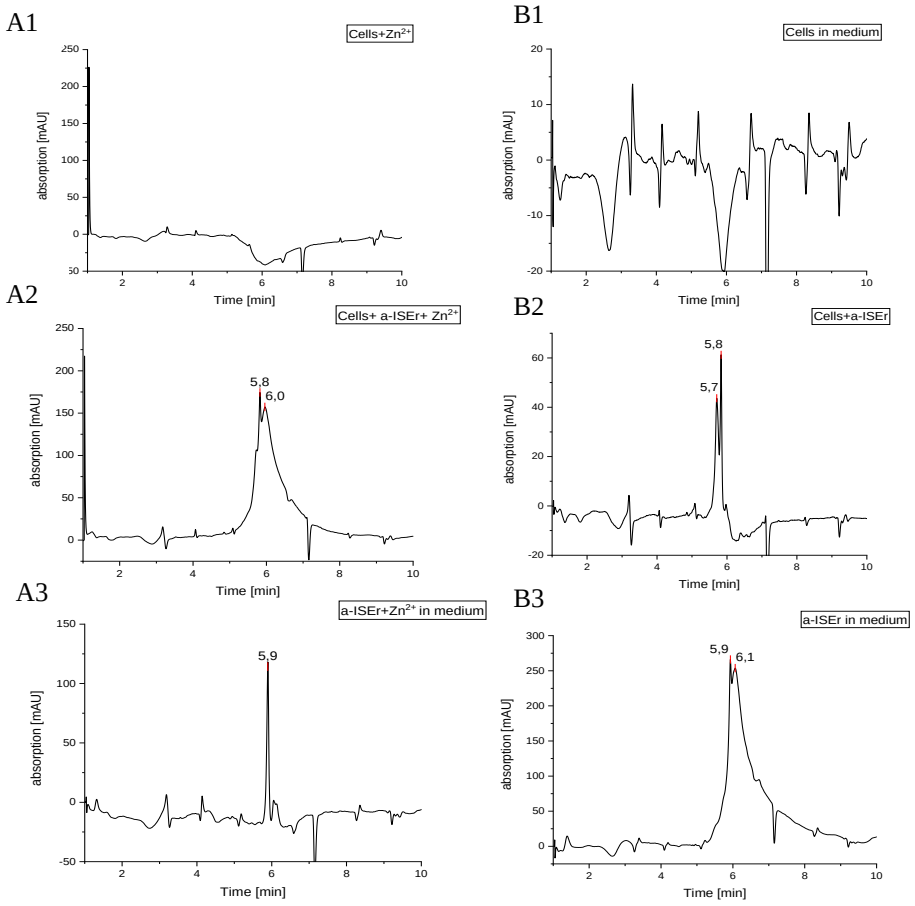

*Figure 40 Comparison between UV traces at 214 nm of a-ISEr Val-Cit cell incubation experiment with and without the addition of Zn^{2+}. All samples were taken after 24h. On the left side(**A1-3**), Zn^{2+} solution was added into the wells. On the right (**B1-3**) the wells were treated under the same conditions as in the previous experiment without Zn^{2+}. The top two panels (**A1** and **B1**) show untreated cells. The middle panels (**A2** and **B2**) cells incubated with a-ISEr and the bottom panels (**A3** and **B3**) display the supernatants of pure a-ISEr in the wells*

Therefore, after the cell culture experiments, it could be concluded that the HT29 cell line did not cleave the a-ISEr Val-Cit cleavage site but as there are several reasons for this phenomenon further experiments need to be performed. Furthermore, other cancer cell lines expressing other MMPs could be tested. The lack of cleavage can also be related to the structure of the a-ISEr. The binders can sterically obstruct the cleavage site making it

inaccessible for MMP2. Further cleavage experiments with a short amino acid sequence, containing the Val-Cit cleavage site must be performed.

8.2.2 MMP2 direct incubation

To exclude the possibility that complex activation or inhibition cascades were responsible for the inactivity of MMP2 during the cell studies with HT29 cells, the matrix metalloproteinase was purchased from Sigma Aldrich in its active state, recombinant expressed in *E. coli*. After the proteinase was prepared according to the manufacturer (described in 7.2.6 Matrix metalloproteinase experiment), it was incubated with a-ISEr Val-Cit twice, one time in endotoxin free water and the other time in phosphate buffer. Additionally, the co-factor zinc was added in form of a $ZnCl_2$ solution during the second experiment. No additional calcium was added, because the proteinase was lyophilized from 10 mM sodium phosphate and 0.1 mM calcium chloride according to the manufacturer.

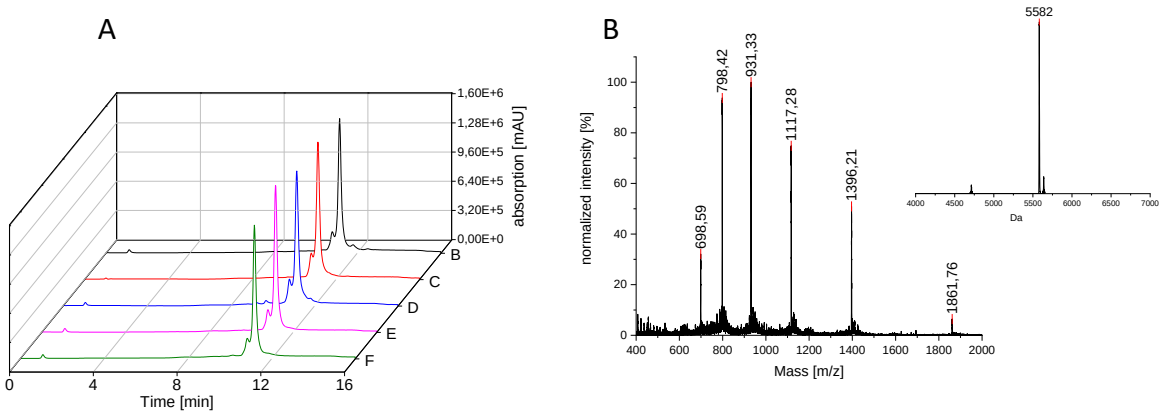

Figure 41 ***A)*** *UV trace at 214 nm with the different time points after the incubation of MMP2 with a-ISEr Val-Cit in endotoxin free water. B= a-ISEr Val-Cit; C= 25 min; D= 1 hour; E= 2h 20 min F= overnight* ***B)*** *mass spectrum and deconvoluted spectrum of the peak. Calculated mass of a-ISEr Val-Cit: 5581 Da*

In panel A of *Figure* ***41*** the waterfall diagram of all different time stamps is visualized, making it clear that no cleavage took place as neither a reduction of the peak was observed nor was a cleavage related new peak detectable. This experiment was started, using the recommended amount of MMP2 from the manufacturer, with 2 µg/mL. After 2 hours, the MMP2 amount was doubled to 5 µg/mL without an effect on the experiment.

The cleavage experiment was repeated in 50 mM phosphate buffer with addition of 1 mM $ZnCl_2$ solution as co-factor. The chromatograms of the different time stamps, summarised in panel A of *Figure* ***42***, show again no sign of the desired cleavage products or even reduction of the a-ISEr Val-Cit peak, indicating, that no reaction took place. During the analysis a slight baseline shift occurred, as can be seen in the same figure, which could not be corrected because no blank was measured beforehand. This result strengthens the theory, that the MMP2 does not recognize the Val-Cit cleavage site in the tested conditions. During the testing of the pure MMP2 the possibilities of insufficient activation of the pro MMP as well as the inhabitation of the proteinase could be excluded. These findings would also be in accord with the results of the cell culture studies. Other members of the MMP family could be tested in the future, but the cheaper and more sufficient way would be repeating the cleavage experiment in cancer tissue, expressing different MMPs. Another possibility would be to change the cleavage sequence Val-Cit, to target specifically the MMP2. There are many reports on the different cleavage sites recognised by different MMPs[53], but within the timeframe of this work no other cleavage sites could be tested. The last possible reason for the lack of cleavage could be a problem with the Val-Cit cleavage site itself. This is highly unlikely but for the sake of completeness worth mentioning. If the used valine or citrulline amino acid building blocks were not pure L-enantiomers, it would be possible that this could hinder the recognition of the cleavage site by MMP2. It is also possible, that the cleavage site could not be accessed by MMP2 after

incorporation in the ISEr. This could be tested by designing a smaller, less steric demanding peptide with a Val-Cit site. During the timeframe of this thesis, no such experiment was performed.

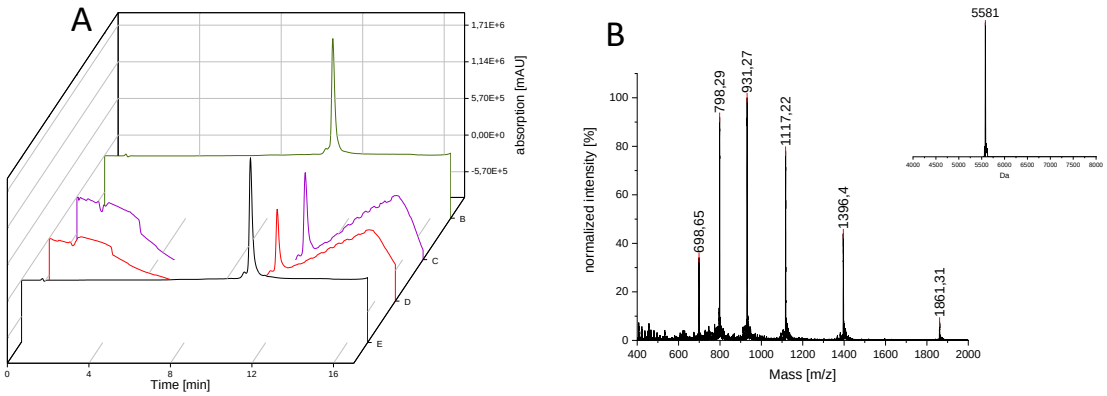

Figure 42 ***A)*** *UV trace at 214 nm with the different time points after the incubation of MMP2 with a-ISEr Val-Cit in endotoxin free water. B= pure a-ISEr Val-Cit; C= 25 min; D= 1 hour; E=overnight* ***B)*** *mass spectrum and deconvoluted spectrum of the peak. Calculated mass of a-ISEr Val-Cit: 5581 Da*

8.3 a-ISEr Hydrazone

8.3.1 Hydrazide precursor

To obtain the hydrazide as a functional group on the effector, a resin was modified with a 10% hydrazine solution. The remaining free chlorides on the resin, which did not react with the hydrazine, were capped with 5% MeOH, to avoid side products, not containing the hydrazide. The first amino acid was coupled with different activation reagents as usual, namely HOAt and HATU. HATU was preferred in this reaction over HBTU, as it reacts faster and less epimerisation occurs during the coupling of the amino acid, according to literature[54]. HOAt was used, as it reduces the racemisation of the product. This might have been unnecessary for the short effector sequence synthesized on the resin, but no deviation from the established protocol was made. After the coupling of the first amino acid, glycine, all remaining, unreacted amin groups were capped with acetic anhydride, to avoid undesired side products of different lengths.

The remaining amino acids were coupled and after the *N*-terminal formylation of methionine, the peptide was cleaved from the resin. The resulting white pellet of the product proved to be difficult to dissolve in the standard AB solution. The bad solubility was a result of the short, apolar sequence of the product. The solubility could be enhanced by vortexing and the use of the ultrasonic bath, but precipitation of the effector sequence could not be completely avoided. The suspension of product in AB solution was lyophilized, resulting in two distinguishable textures of the product. A white fuzzy like product, presumably resulting from the part of the product, dissolved in AB solution, and a harder more pellet like product, resulting from the undissolved precipitate. The differences in appearance were solely based on the solubility during lyophilization. Both fractions were analysed on Thermo HPLC-MS revealing, that both fractions contained the desired product. For the analysis a very small sub sample was taken and with the help of the ultrasonic bath, vortex, centrifugation and filtration clear solutions were obtained for analysis, which can be seen in *Figure* ***43***.

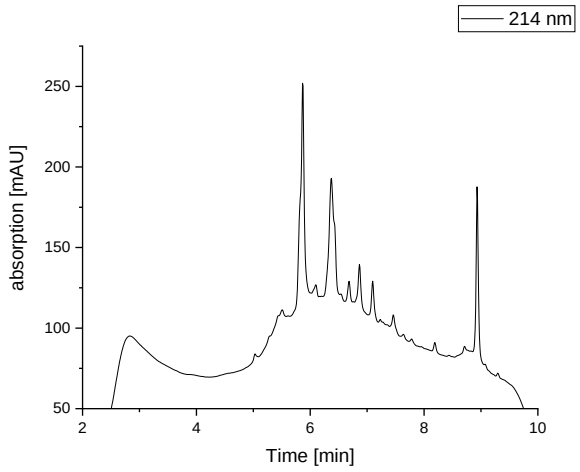

Figure 43 UV trace at 214 nm of crude hydrazide precursor on Thermo HPLC-MS. Different peaks all show the mass of the precursor, according to mass analysis

After analysis on the Thermo system, more peaks than expected were detected. The mass analysis of the peaks revealed that the mass of the effector was present in all the peaks. The product proved to be persistent on the C18 Kromasil column installed in the Thermo system and after the analysis a wash run at 60°C was performed. The detection of the mass of the product in the different peaks can be an indication, that this apolar small molecule ionizes better than other components and remains on the capillaries of the mass spectrum. With this information, the purification on Varian system as well as the final analysis were all performed at 60°C. At the higher temperature the multiple peaks were avoidable, as can be seen in the final analysis in *Figure **45*** hinting at a residue of the product remaining in the mass spectrometer. Before purification the product was suspended in AB solution and was diluted with endotoxin free water to 25% solvent B. This was necessary to ensure suitable separation on the column with the applied eluent gradient. The solution was centrifuged for 20 min at 4700rpm and filtered before it was loaded on a column. This procedure had to be established due to the bad solubility of the product in water.
After the final analysis, the most abundant side product with a mass of 533 Da, was the sequence, missing the phenylalanine the second mass with 420 Da was the sequence minus the phenylalanine and the isoleucine.

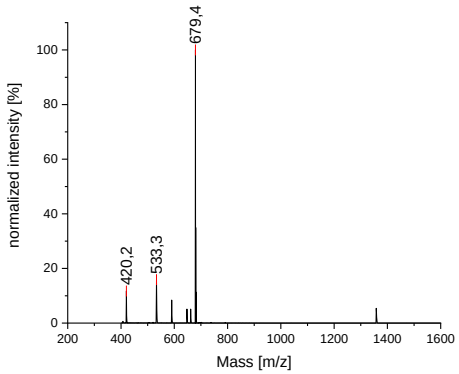

Figure 44 Mass spectrum of the MP from hydrazide effector with the main product as well as both side products

The reason behind the absence of these two particular amino acids in the sequence is unclear, as the coupling was performed the same way as for the other amino acids without any complications. The coupling time for all amino acids, with 45 minutes, was also already longer than for the other products synthesized in this work. In future synthesis, double couplings for these amino acids, would be recommendable. No other noteworthy side products were detected and the final analysis of MP and SP can be seen in *Figure **45*** and *Figure **46*** respectively.

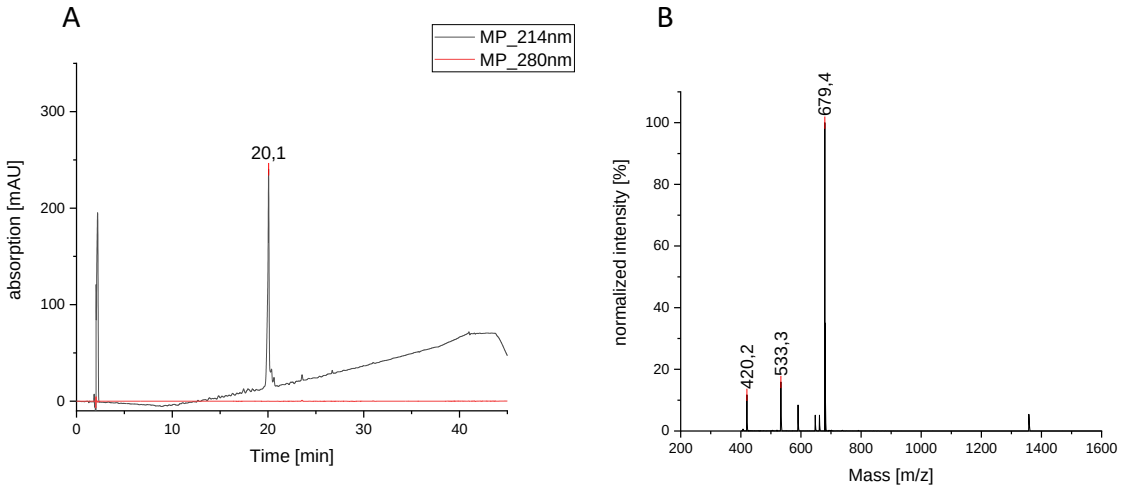

Figure 45 ***A)*** *RP- HPLC final analysis hydrazide precursor MP.* ***B)*** *Mass spectrum of hydrazide precursor MP. Calculated mass: 678.9 Da*

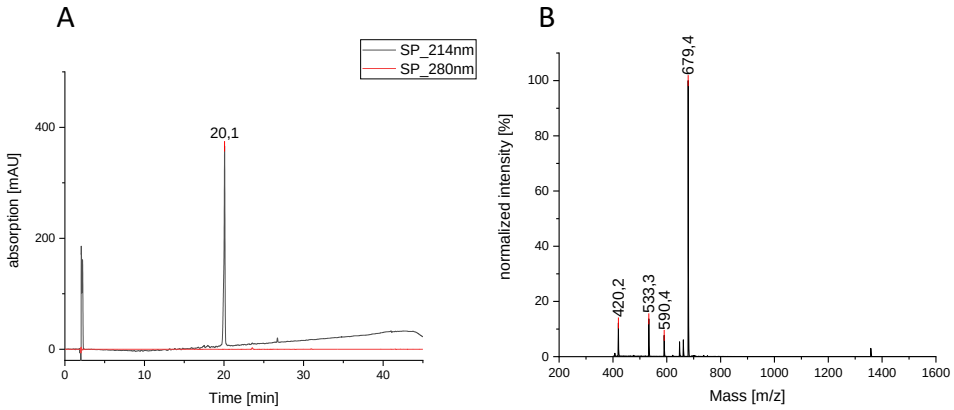

Figure 46 ***A)*** *RP- HPLC final analysis hydrazide precursor SP.* ***B)*** *Mass spectrum of hydrazide precursor SP. Calculated mass: 678.9 Da*

8.3.2 Serine scaffold

The core scaffold was synthesized in accordance with the classic Fmoc-strategy up to the last amino acid serine. During the binder synthesis of the other products, the *N*-terminal amine was formylated and therefore no side reactions could take place. For this scaffold, the use of an Fmoc protected serine was not possible, as the Fmoc group would be cleaved during the binder synthesis, leaving the amino group open for coupling. To avoid this problem, a *N*-Boc protected Serin was used during the synthesis, as the Boc protection group is stable under the coupling conditions of the Fmoc synthesis and would be cleaved during the final cleavage of the product with TFA. After the final cleavage 100 mg of the crude product were oxidized by passing air directly through the solution. Compared to the former oxidations, where simple stirring was sufficient to close the disulfide bridges, this new method was adapted, because after overnight stirring, no clear oxidation product could be observed in mass analysis on the Waters HPLC-MS. Additionally, the pH of the solution was adjusted with 0.1 M NaOH from 4.28 to 7.22. The low pH in the beginning was probably due to remaining TFA in the product, which lowered the pH after dissolving the product in PBS buffer. During the reaction the oxygen serves as a catalyst for the oxidation and a lower pH is in general reducing the reactivity of the cysteines whereas a higher pH, close to physiological level, is more favourable. After purification, the product as well as the mass of the dimer were observable in the SP, as seen in *Figure* ***48***. This side product can be avoided by reducing the concentration during the oxidation. For

the following periodate reaction, the dimer was not a problem, as the disulfide bridges reopen during the oxidation reaction.

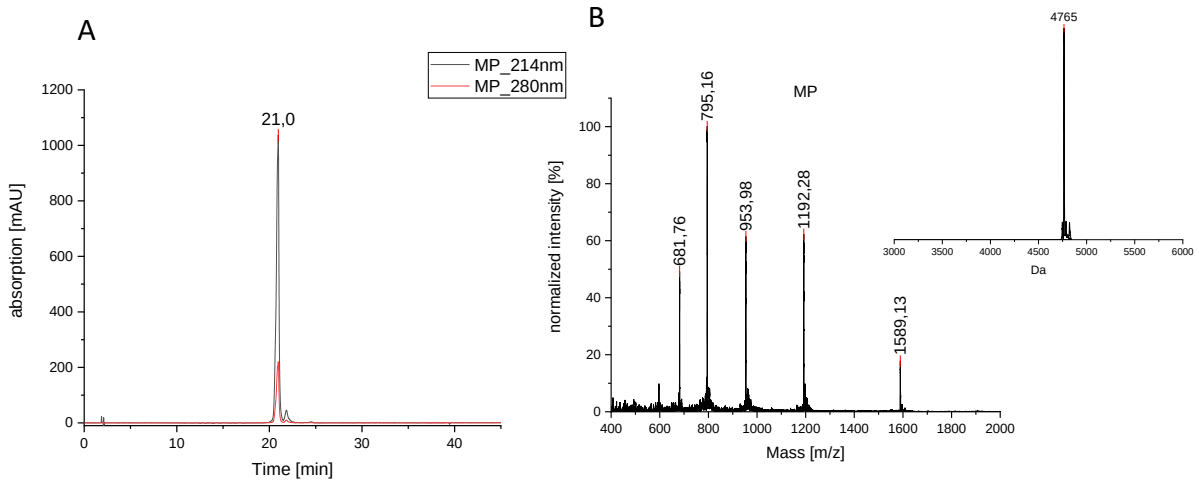

Figure 47 ***A)*** *RP- HPLC final analysis from serin scaffold MP.* ***B)*** *mass spectrum and deconvoluted data from serin scaffold MP. Calculated mass: 4765 Da*

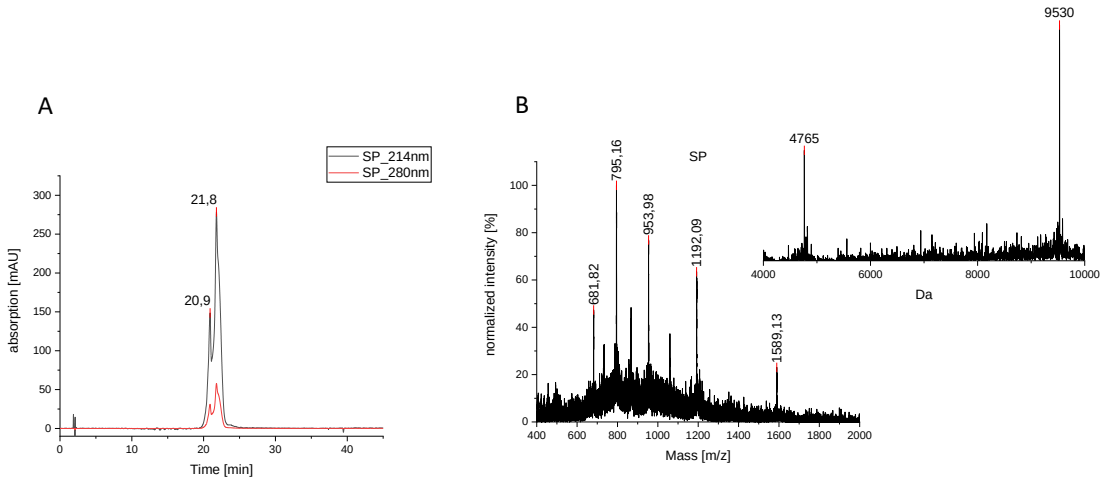

Figure 48 ***A)*** *RP- HPLC final analysis of serin scaffold SP.* ***B)*** *Mass spectrum of serin scaffold SP with deconvoluted spectrum. Calculated Mass: 4765 Da*

8.3.3 Periodate oxidation of serine

The goal of this reaction was to oxidize the *N*-terminal serine to the aldehyde, for the later hydrazone formation. The oxidation protocol was taken from the book Bioconjugate techniques[44] and as oxidizing agent sodium periodate was used. The reaction was performed with the crude product of non-oxidized serine scaffold as well as with the purified oxidized product with closed disulfide bridges. All reagents were prepared as stock solutions and added to the reaction as described in 7.2.9 Periodate Oxidation. During the reaction sub samples were taken at different time points, to monitor the progress. The monitoring revealed that the reaction was complete after just 5 minutes as no further change in the peaks and corresponding masses was observable after this point. All subsamples as well as the finished reactions were quenched with Na_2SO_3 to neutralize the remaining periodate. During analysis, the desired mass peak as well as three or four mass peaks with a difference of 81 Da could be detected in the oxidized as well as the reduced starting material, as seen in *Figure* ***49 C***. The number of peaks in

the deconvoluted spectrum, as well as the mass difference between them, were indications of the sulfite attaching itself to the open cysteines. It appears that during the periodate oxidation the disulfide bridges of the oxidized product reopen and during the quenching of the reaction, the sulfite binds to the free SH groups. The intensity of the de-convoluted peaks suggests that the most frequent side product was one sulfite group attached and the intensities declined with two, three or four sulfite adducts. The oxidation of the cysteines before the periodate oxidation was redundant, as the conditions during the oxidation reopened the disulfid bonds.
To reduce the number of side products, TCEP was added to the crude reaction mix after quenching, to eliminate the sulfites from the cysteines. After 10 minutes incubation with TCEP the following HPLC-MS revealed that just the 3 and 4 adducts with the sulfite were reduced. A reason for this might be, that even if TCEP cleaves the sulfite from the cysteine, it can reattach as it is still present in the solution.

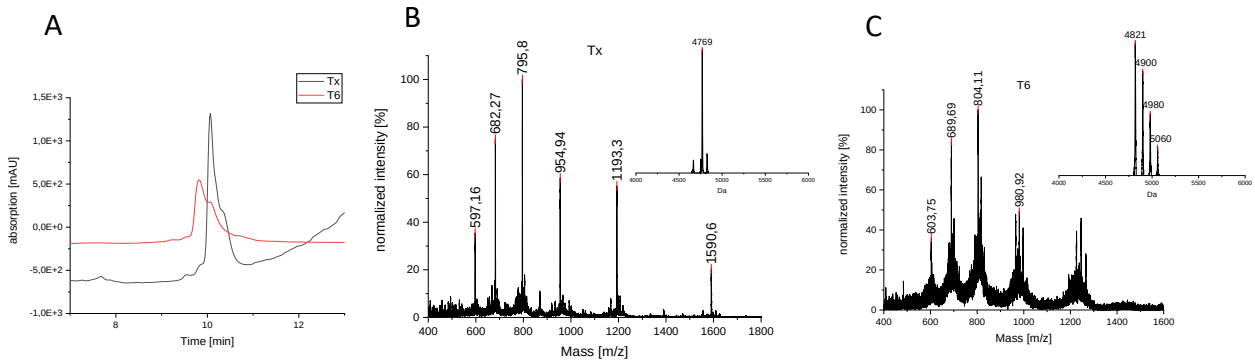

Figure 49 ***A)*** *Zoomed in overlay of the RP-HPLC UV line of the unoxidized serin educt (Tx; black) and the time point after 6 minutes (T6; red) after the reaction was quenched* ***B)*** *Mass spectrum and deconvoluted Mass from Tx* ***C)*** *Mass spectrum and deconvoluted Mass from T6. Calculated mass serine educt (unoxidized cysteines): 4769 Da; aldehyde product: 4738 Da*

The mass spectrum of the time point 6 revealed, that the crude product was not very pure. After purification, the mass spectrum was cleaner, as can be seen in *Figure* ***50***, but still all four peaks were detectable in the solution. To avoid these products it would be possible to quench the reaction with *N*-acetylmethionine instead of sodium sulfite[44]. This approach was not tested in this thesis, due to lack of time, but is worth considering for future experiments.

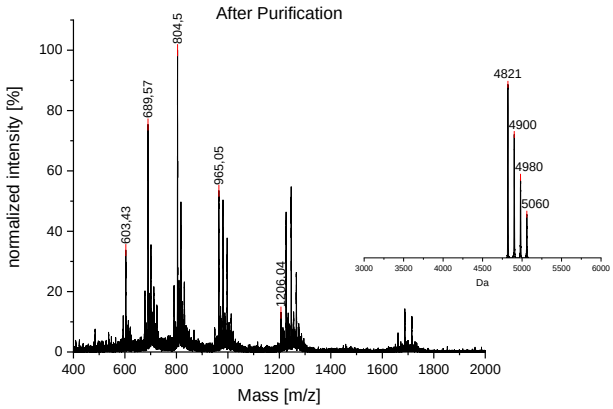

Figure 50 Mass spectrum and deconvoluted spectrum of the oxidized serin scaffold. Calculated mass of the aldehyde product: 4738 Da

8.3.4 Hydrazone formation

The a-ISEr with hydrazone linkage was synthesized from the aldehyde scaffold and the hydrazide precursor. The basic protocol for the workflow was taken from Bioconjugation Techniques[44], but three modifications were made for this reaction. First, the authors of this section in the book claim, the reaction can be performed without a catalyst in two hours. Second, they recommend a 10-fold molar excess of the hydrazide containing molecule over the aldehyde to avoid protein conjugation. And third, they recommend a buffered solution at either pH 6 or pH 7-8.5. It was attempted to dissolve the hydrazide precursor in 0.04 M Na_3PO_4 pH 7 but due to the bad solubility of this educt in water, this was not possible. Therefore, for further reactions, the hydrazide effector was pre-dissolved in AB solution to avoid loss of product. For the first test reaction the aldehyde was also dissolved in Na_3PO_4 and mixed with the pre-dissolved hydrazide and afterwards the two solutions were mixed resulting in a pH of 6.99 and an HPLC-MS was performed. Before analysis the solution was centrifuged at 14000rpm for 5 minutes and just the clear supernatant was loaded on the column. Neither after two hours of reaction time at room temperature nor after stirring overnight, could the desired product be observed.

For further reactions, the protocol was adapted and a catalyst was added to increase the reaction time[41]. To adapt to the poor solubility of the hydrazide effector, both educts were dissolved in AB solution and after addition of the catalyst, the pH was adjusted with 0.1 M NaOH. Different pH levels ranging from 3.5 to 4.5 were tested and the reaction was fastest with a pH level between 4.3 and 4.5. As reported in literature, Aniline proved to be a good nucleophilic catalyst for the hydrazone formation and it was added to a final concentration of 10 mM in the reaction solution[41]. The molecular excess of the effector was also lowered from 10 to just 4 times excess over the aldehyde to avoid precipitation of the effector during the reaction. With these new adaptations, the desired product formed in about 4 hours and 30 minutes, although the hydrazide as well as the aldehyde educts were still detectable, as can be seen in *Figure **51***. The observable baseline shift in *Figure **51*** **A** could not be corrected as the measurements were performed on Waters HPLC without a blank measurement beforehand. To test if the amount of product could be increased, one batch was stirred overnight but HPLC-MS analysis during the next day revealed, that the acidic reaction conditions lead to the reopening of the hydrazone bond. Just the hydrazide and aldehyde educts could be detected and therefore no longer reaction times were adapted.

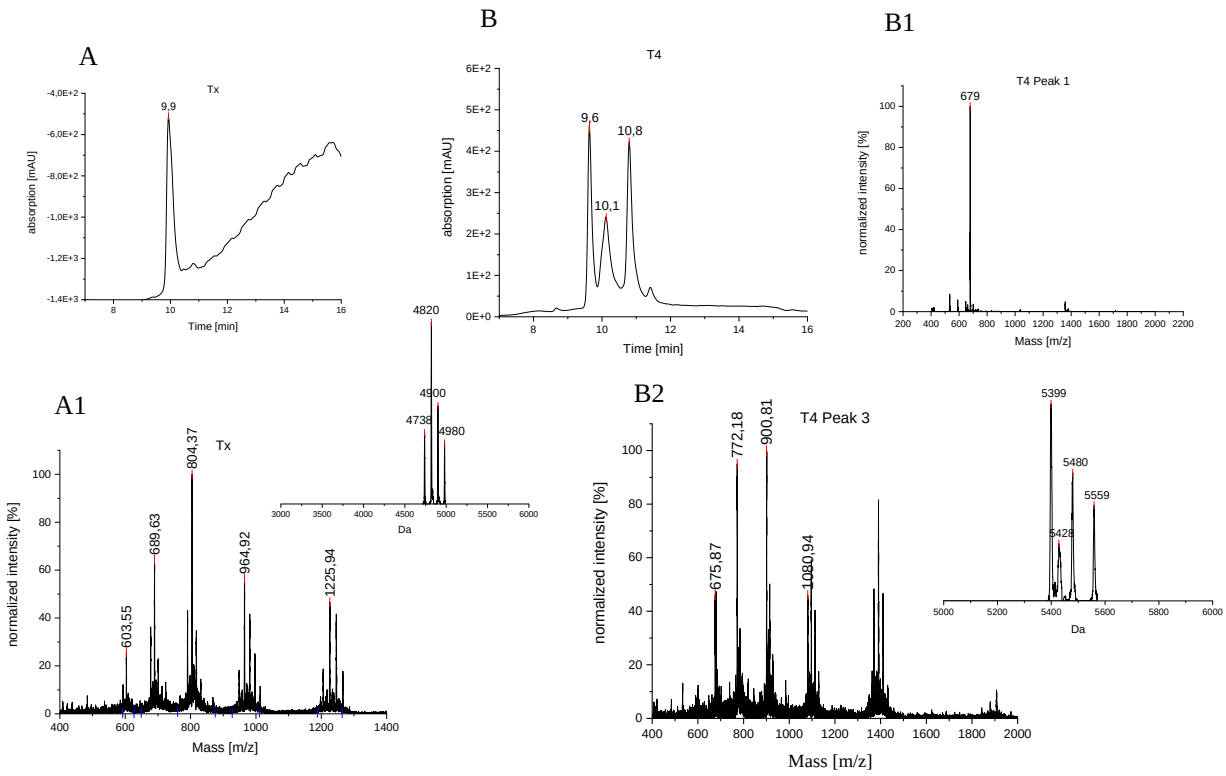

Figure 51 ***A)*** *UV trace at 214 nm of the aldehyde educt* ***A1)*** *Mass spectrum and deconvoluted spectrum of the aldehyde educt peak. Calculated mass: 4738 Da* ***B)*** *UV trace at 214 nm after 4h and 30min reaction time with three visible peaks.* ***B1)*** *Mass spectrum of the first peak, which belongs to the hydrazide precursor* ***B2)*** *Mass spectrum and deconvoluted spectrum from the third peak. The middle peak correlated with the aldehyde educt. Calculated mass a-ISEr Hydrazone: 5399 Da*

As the reaction was performed in AB solution, it had to be diluted with water up to 20% eluent B before purification to ensure a sufficient separation on the column with the chosen gradient. After centrifugation a small pellet formed, which was the result of undissolved hydrazide residues precipitated by the addition of water. The first purification was performed with normal A and B solution with a gradient of 5-56% eluent B in 60 minutes on a C4 semi preparative column with an automated sample collector. During the pooling of the fractions, no product could be detected anymore, just the hydrazide and the aldehyde containing educt molecules. This is a consequence of the instability of the hydrazone at a low pH level, which is present in the A and B solutions, because of TFA. The most likely scenario was, that the hydrazone was cleaved on the column and as a result just the educts eluted, in form of the hydrazide and aldehyde molecules. To avoid this outcome a steeper gradient was used and the pooling of the fractions accelerated. The new gradient was 10 min desalt time, 5-20% eluent B in 2 min and 20- 65% B in 11 min on a C4 column. Additionally, only half of the TFA concentration was used to prepare solution A and B (*Table 4*), to increase the pH level during purification. Even with these measures, the recovery rate after purification was quite low and cleavage products were detectable in the HPLC-MS. As the hydrazine proved to be unstable in the normal HPLC-MS buffer conditions, no final analysis was performed but instead a subsample of the collected main pool was dissolved in water and analysed on Waters HPLC-MS in just 10 minutes, as displayed in *Figure* ***52***. The product as well as both educt peaks were observable in the UV trace. With this data alone, it cannot be determined whether the cleaved compounds are present in the product itself due to poor separation or form on the column during analysis and purification. To further analyse the a-ISEr with hydrazone linkage, the use of other buffers with a higher pH level for purification would be interesting to test. Due to lack of time no other buffers were tested for purification in this thesis.

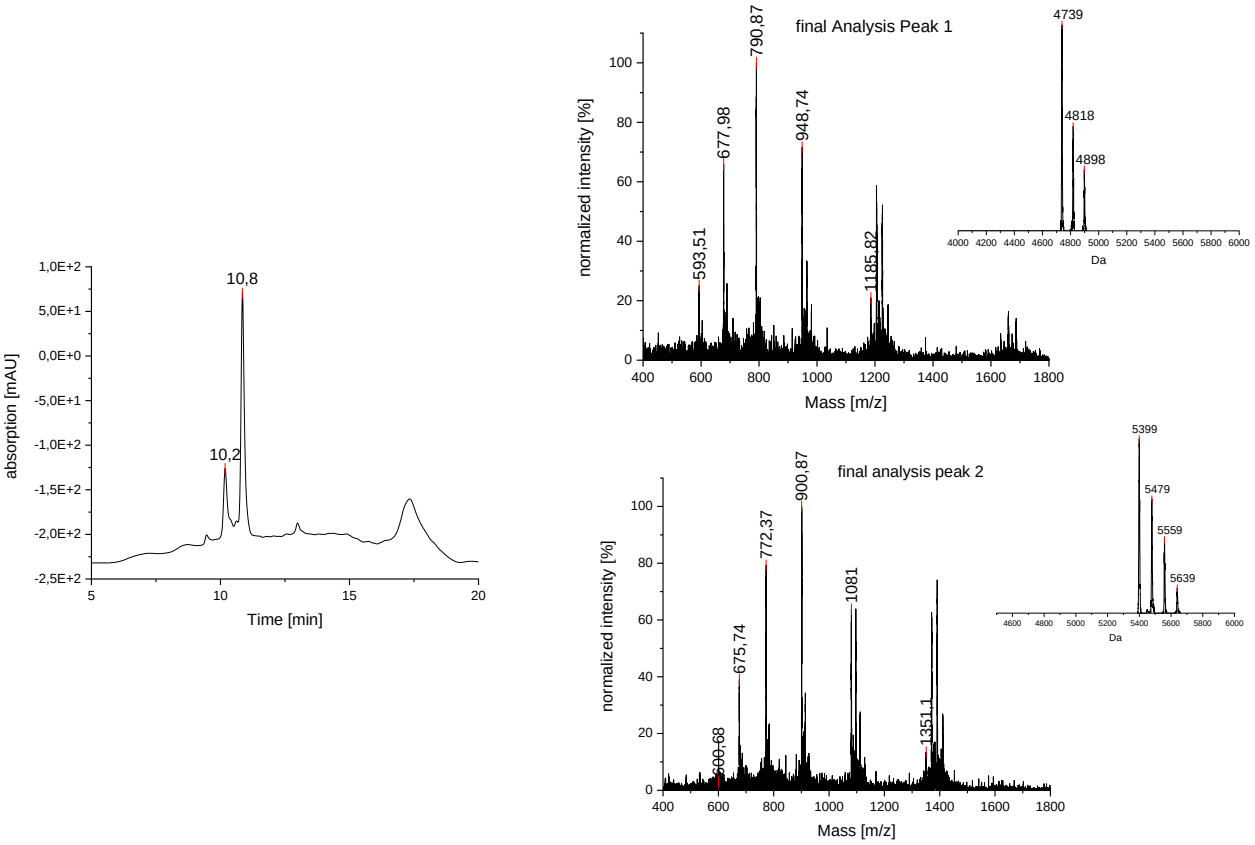

Figure 52 Analysis of a-ISEr Hydrazone dissolved in water. Left hand side: UV trace at 214 nm with two detectable peaks. Right hand side mass spectrum and deconvoluted spectrum of both peaks

8.4 Comparison studies between two t-and one a-ISEr

Three of the four synthesized ISErs were sent to Syntab Therapeutics GmbH in Aachen (Germany), to test the effectors and binders of the new ISErs and compare them to the unmodified Y9. These three products where two t-ISErs with different PEG lengths and one a-ISEr with Val-Cit. The a-ISEr with the hydrazone linkage was not sent because at that time, the product was ned yet obtained in a purified form.

8.4.1 Binder studies

The binder studies were performed with three different cell lines, which all express the integrin α3 on their surface. These cell lines were MDA-MB231, 4T1 and E0771. The MDA-MB231 cells belong to a human breast adenocarcinoma, the 4T1 cells to a breast cancer line from BALB/c laboratory mice and the last line, E0771, belongs to a breast cancer line from C57BL/6 laboratory mice. As an example the representative results from the human cell line are shown down below, the results from the other two can be found in the Supplementary Information.

To test the binders, the cells were first incubated with 50 nM biotinylated-ISEr-Y9lc and afterwards the competitor ISErs as well as the reference were added in different concentrations to compete against the available integrin binding sites. The biotin is attached at the C-terminus of the Y9 structure, as can be seen schematically in *Figure **53***.

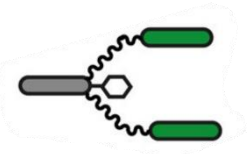

Figure 53 Schematic structure of C-terminal biotinylated Y9. In the colour scheme grey represents the effector, green the binders and the white hexagon the biotin label[14]

Afterwards, the fluorescence marker Streptavidin-PerCP-Cy5.5 was added to visualize how much of the biotin marked ISEr had been replaced by the competitors. The lower the fluorescence signal, the more competitor ISEr had bound to the integrin binding sites and the higher the affinity of the binders towards the integrin. Both t-ISErs with different PEG lengths competed against the binding site, as can be seen in the lowering fluorescence signal in *Figure **54***. As expected, the ISEr with the larger PEG chain performed worse than the ISEr with the shorter PEG chain. This is because of the steric hindrance the 20 kDa PEG chain poses compared to the 5 kDa chain. According to the IC50 values, the difference between the binding affinity of both PEG chains was about two-fold. Both t-ISErs with different molecular weight PEG linkers, expressed generally lower IC50 values than the reference. It is visible, in the panel A) that the detected fluorescence of the t-ISErs was consistently lower than the reference.

A

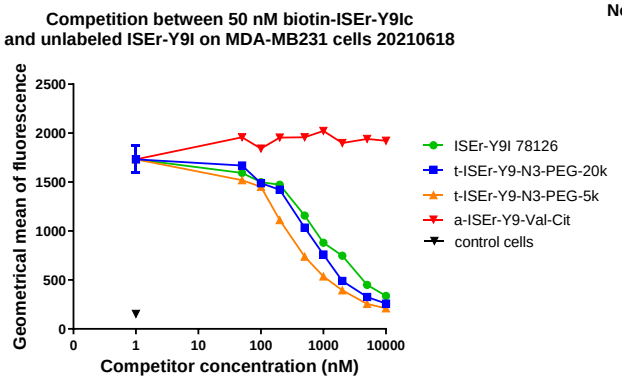

B

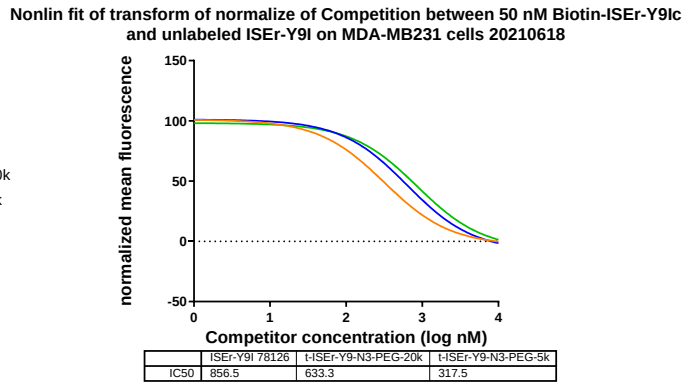

	ISEr-Y9l 78126	t-ISEr-Y9-N3-PEG-20k	t-ISEr-Y9-N3-PEG-5k
IC50	856.5	633.3	317.5

*Figure 54 **A)** measured fluorescence of MDA-MB231 cell line after staining with 50 nm Biotin-ISEr-Y9lc against the competitor concentration. Measured fluorescence on the cells not incubated with peptide (background signal) is visible as a black triangle. **B)** Normalized fit of the data and the calculated IC50 values in nM. ISEr-Y9l 78126 (green), t-ISEr-Y9-N3-20k-PEG (blue), t-ISEr Y9-N3 5kPEG (orange)*

As the PEG chains should not influence the binder function per se, it is possible that the PEG had an influence on the dwell time of the ISEr on the cell surface. If the product can stay on the surface for an extended period of time, the interaction of binder and integrin can be elevated. For the 20 kDa PEG product, the steric effect outweighed the benefit. Further data needs to be acquired to test this phenomenon.

Surprisingly, no binder competition could be detected in the a-ISEr Val-Cit, despite no change in the binder sequence, compared to the established Y9. This could be because, the former discussed, disulfide bridge mismatch in the a-ISEr Val-Cit, but this would most likely not lead to a complete loss of binding affinity to the integrin except when all bridges were a mismatch. Another explanation might be, a manual error during the Liberty Blue synthesis, as maybe the wrong conformation for one of the amino acids was used by accident. Or a technical error during the Liberty Blue synthesis, that the synthesizer mixed up the sequence of the amino acids, which would lead to the same mass but a loss in function. This could explain the complete lack of binding, for

final determination of the cause, a re-synthesis of the a-ISEr Val-Cit would be the best choice. On panel B in *Figure **54***, the a-ISEr Val-Cit was not included in the calculation of the different IC50 values, because of its lack of binding. Another way to visualize the data is by plotting the fluorescence in an overlay histogram, as seen in *Figure **55***. As an example, the histograms of the MDA-MB231 cells are displayed for the reference ISEr as well as the three competitors.

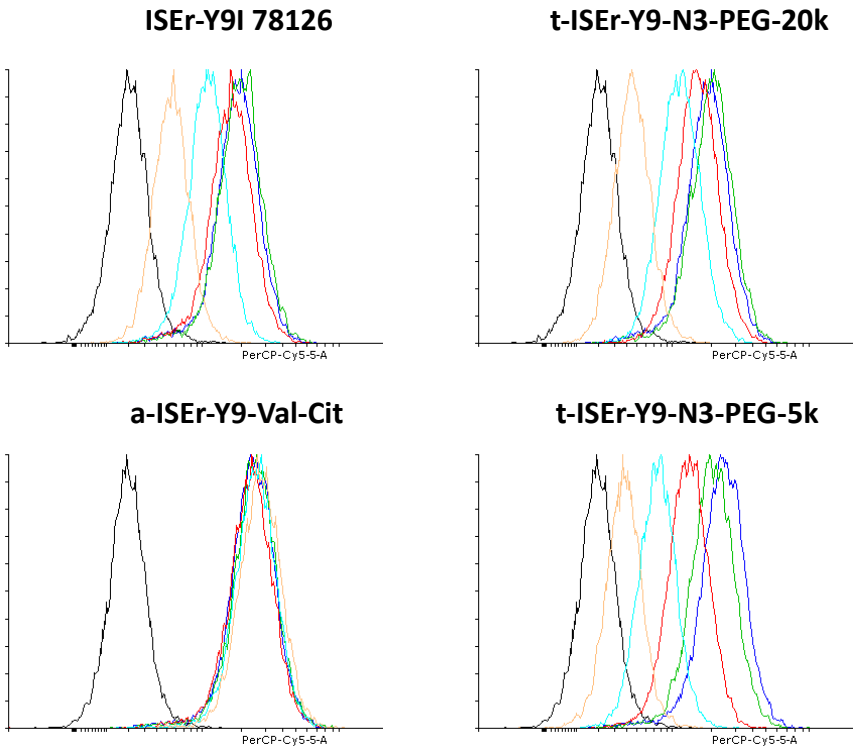

Figure 55 Overlay histograms of MDA-MB231 cells incubated with 50 nM biotin-ISEr-Y9Ic along with 0 (blue), 100 nM (green), 500 nM (red), 2 µM (turquoise) or 10 µM (orange) of the different ISEr-Y9I variants, stained with Streptavidin-PerCP-Cy5.5; black: no biotin-ISEr-Y9Ic

The black histogram on the left end of the graphs represents the cells without any bound biotin and the dark blue on the right represents the biotin marked ISEr without any competitor. The further the histograms of the different concentrations move towards the black histogram the higher the affinity to the integrin. It is again visible, that the a-ISEr Val-Cit did not express any binding competition towards the integrin. The t-ISEr with the 5 kDa PEG performed best compared to all the other competitors. All other histograms of the different cell lines can be found in the Supplementary Information.

8.4.2 Effector studies

To test the functionality of the effector, a DHR assay was performed with human leukocytes. For this experiment the cells were incubated with buffer, as a negative control and PMA as a positive control, as well as the three manufactured ISErs and the reference ISEr. Additionally, in this experiment a scrambled version of the reference ISEr, called sscY9l, was used, to exclude random effects of different amino acids present in the sequence on the DHR assay.The effector induces a neutrophil respiratory burst in the leukocytes and the generation of reactive oxygen species as the *N*-formylated effector activates the defence mechanism of the leukocytes. This leads to the oxidation of DHR to rhodamine. Rhodamine is fluorescent and can be detected using a flow cytometer. The percentage of rhodamine positive cells can then be plotted against the concentration of the different samples to generate dose-effect curves. For this analysis, the cells were gated from an FSC/Hoechst plot to just include live cells for the final analysis. The Hoechst neg. cells are alive whereas the Hoechst pos. cells are dead and not included in the assay. An example for a gating assay can be found in the Supplementary Information. The already gated cells can be seen in *Figure **56*** below, where the rhodamine negative cells are marked green and the positive cells pink.

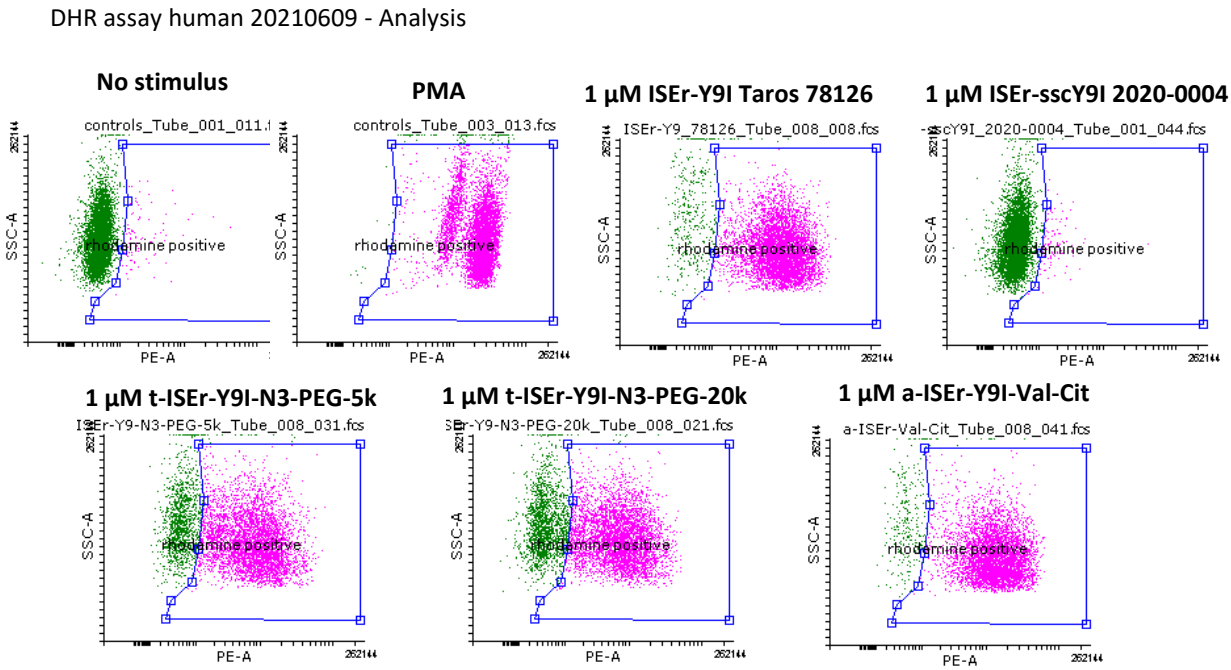

Figure 56 Rhodamin-positive leukocytes shown in the pink region in the SSC/PE plot with buffer only, PMA, 1µM ISEr-Y9l (78126), 1µM t-ISErs, 1µM a- ISErs or 1µM ISEr-ssc Y9l 2020-0004. Gated cells displayed against the fluorescence channel PE-A and the scatter plot SSC-A

The cells incubated with only buffer show no significant signal in the rhodamine positive section, whereas the PMA incubated cells are set as a reference of 100% rhodamine positive cells. For the scrambled ISEr, no unrelated activation of the leucocytes could be observed, indicating that the stimulation of the leukocytes is specific and solely related to the effector sequence of the ISEr. In *Figure **56***, the rhodamine positive cells are shown for 1 µM concentration of the different ISErs, but different concentrations were tested to generate the dose-effect curve.

The black inverse triangle, seen in *Figure **57***, represents the maximal measured signal achieved by PMA incubation and the black circles represent the signal achieved by the Y9 with scrambled effector sequence. Both compounds performed as expected, with the scrambled version generating no significant response from the leukocytes. The Y9 performed as expected from previous experiments with an EC50 value of 100 nm. The EC50 value is the half maximal effective concentration and is defined as the concentration halfway between the baseline and the expected maximum of the dose-effect curve.

According to the dose-effect curves both t-ISErs performed worse than the reference ISEr Y9 in stimulating the leucocytes. This can be seen in the delayed increase in rhodamine positive cells as well as the EC50 values, which can be extracted from the graph in *Figure **57***. For the 20 kDa product, the measure point for 3 µM shows a much higher value than expected. Since the rest of the curve appears to run parallel to the 5 kDa product, this was

deemed to be an outlier and was therefore not considered for further interpretations. The worse performance of both t-ISErs can be related to the PEG chains, as the 20 kDa product performed worse than the 5 kDa product. This would be in accordance with the expected steric hindrance, which has a higher impact with the larger PEG chain attached. The 5 kDa PEG product had an EC50 of 400 nM and the 20 kDa product had an EC50 of 500 nM, making both variants about 10-fold less effective than the reference.

Interestingly, the a-ISEr Val-Cit performed significantly better than the reference ISEr in activating the leucocytes. With an EC50 value of 20 to 30 nM the a-ISEr performed similar to how the free effector would perform in such an assay. The higher efficacy of the free effector had already be proven in former assays[13]. With this data alone, it is not possible to determine if the effector is still attached to the rest of the scaffold during measurement or if cleavage of the valine-citrulline cleavage site was recognized by the leucocytes. The EC50 values, similar to free effector is a strong indication for cleavage taking place. It is already reported in literature, that natural killer cells and T-cells express different MMPs, like MMP2 or MMP9.[55,56] The MMP2 production of T-cells is generally upregulated after contact with an antigen or cytokine. Therefore it is possible, that the cleavage site was recognized. Further investigation of this phenomenon is necessary, like incubation of the a-ISEr with leukocytes, similar to the experiments with HT29 cells. RP-HPLC measurements of the supernatant can then determine if a cleavage of the ISEr by leukocytes takes place.

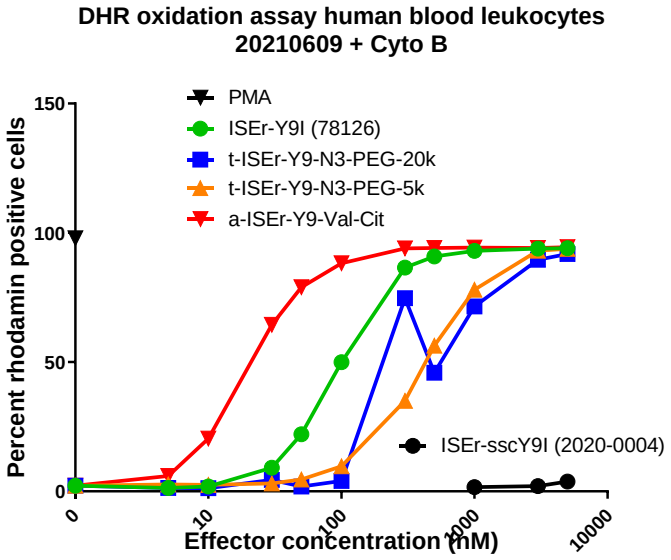

Figure 57 Dose-effect curves of ISEr-Y9I 78126 (green), t-ISEr Y9-N_3 20kDa PEG (blue), t-ISEr Y9-N_3 5kDa PEG (orange), a-ISEr Val-Cit (red) and ISEr-ssc Y9I 2020-0004 (black) in the DHR oxidation assay, on human blood-derived leukocytes measured in the presence of cytochalasin B. The black inversed triangle on the y-axis shows the maximal signal achieved with PMA

9. Conclusion and Outlook

In this thesis four novel ISErs were synthesised, two t-ISErs and two a-ISErs, as summarised in *Figure **58***. For the synthesis of these molecules, the base structure of Y9 was modified to improve bioavailability and to increase the immune system response. The structure consists of the effector, which activates the innate immune system, and two binders, which are reported to bind on the integrin α3, a receptor overexpressed on several cancer cells. For the first modification two polydisperse PEG polymer chains with different molecular weights at 5 and 20 kDa were coupled to the core structure via CuAAc ligation. To perform this reaction, an azido-lysine was added at the C-terminus of Y9.

Both a-ISErs were synthesised with cleavable effectors to increase the effector concentration in the target tissue. Once with the introduction of a novel amino acid sequence, which should be recognized by MMPs and the second a-ISEr was synthesized with a pH sensitive hydrazone linkage. Three out of the four products were tested in a biotin-streptavidin competitive study to determine the binding capability compared to the core structure Y9. The functionality of the effector was tested in a DHR assay with human leucocytes with the same three compounds.

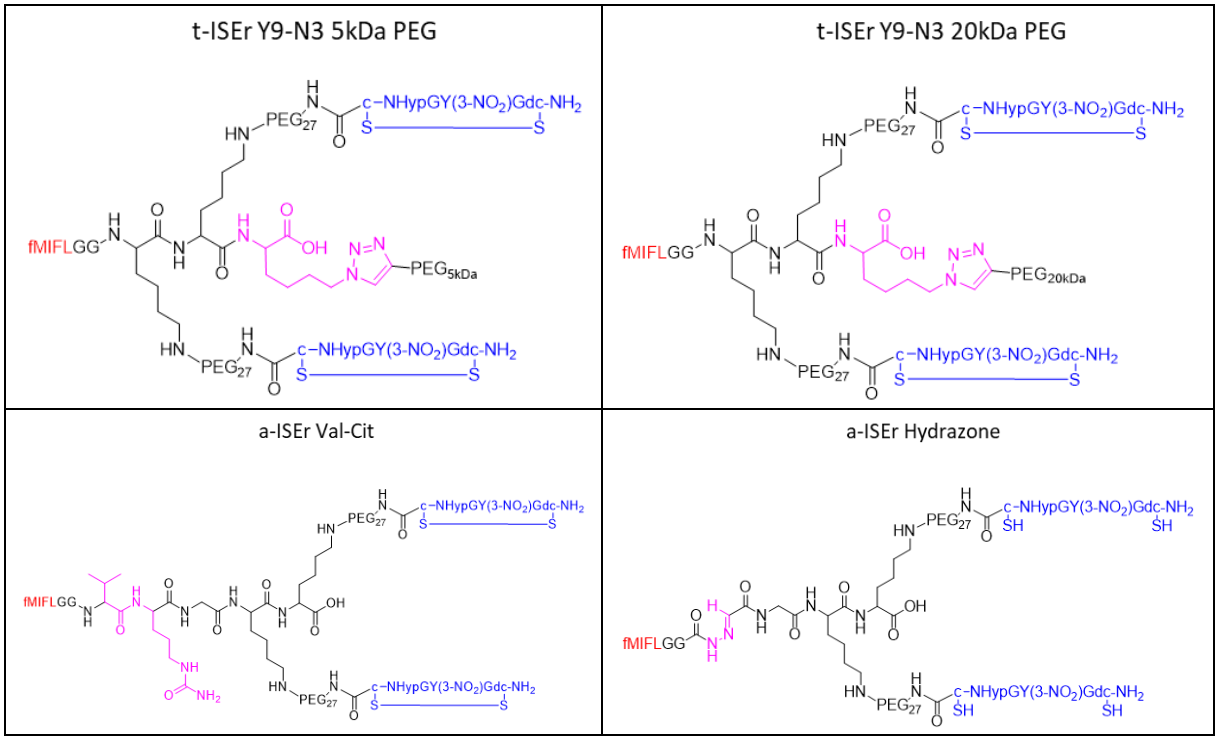

Figure 58 Summary of all for synthesized ISErs in this thesis. In the top panels both t-ISErs with different PEG lengths and in the bottom panels both a-ISErs with Val-Cit cleavage site and hydrazone. The effector sequence is marked red, the binder sequence is marked blue and the novel introduced structure is marked in violet.

Three out of the four compounds were successfully synthesised with a yield of 95% and 81% for the 5 and 20 kDa PEG t-ISEr respectively after the CuAAc and 6% yield for the a-ISEr Val-Cit after Liberty Blue synthesis. Only the a-ISEr Hydrazone was not fully synthesized. Due to the stability problems of the hydrazone linkage during analysis and purification as well as the coupling of the cysteines with sulfite during periodate oxidation, the cysteines of the binders remained in their reduced state at the end of this thesis. The small yield of the a-ISEr with hydrazone linkage was another reason, no further oxidation attempts were made to form the disulfide bridges to avoid additional product loss. For the a-ISEr with Val-Cit, the idea was to use MMPs to cleave the Val-Cit site and to release the small effector sequence from the structure. It was attempted to cleave the site with HT29 cells in cell culture studies as well as with isolated MMP2 protease, but no cleavage could be observed. The reasons behind the absence of cleavage are: An inaccessible cleavage site after the Val-Cit amino acids are incorporated in the structure of an ISEr, or, in case of the cell culture studies, a lack of proper activation of MMP2 as well as a lack of

co-factor. The last possibility was ruled out by the addition of Zn^{2+} during incubation time. It is also a possibility that another member of the MMP family is better suited for cleavage but no tests with other MMPs were performed during the course of this thesis.

The direct comparison between t-ISEr with 5 and with 20 kDa PEG in the biotin-streptavidin comparison study to test the binder effectiveness, revealed a general higher affinity for both t-ISErs to the integrin factor compared to the Y9. The compound with the larger PEG chain had a reduced binding capacity to the integrin receptor, with a 2-fold difference, compared to its smaller counterpart. This can be explained by the larger polymer chain, where the steric hindrance outweighs the benefits of the PEG chain.
For a-ISEr with Val-Cit, the biotin-streptavidin studies revealed weak to no binding to the integrin α3 compared to the Y9. One of the reasons behind this result might be the incorrect disulfide formation within the binders. For a complete inhibition of affinity to the integrin α3, all disulfide bridges must be falsely closed. A resynthesis or reduction and re-oxidation at a reduced concentration of the compound would be necessary to draw a conclusion regarding this phenomenon.
The DHR oxidation assay of human blood leukocytes, to test the ability of the effector to induce a respiratory burst, revealed a higher effectivity of the a-ISEr Val-Cit effector, compared to the Y9. This might be an indication of cleavage from the Val-Cit site and therefore presence of free effector, but no final assumption can be made based on this study alone. And indication for the cleavage is the reported expression of different MMPs by T-cells, which are able to recognize the novel amino acids. Both t-ISErs performed worse than the reference Y9 in their ability to induce a respiratory burst reaction in the leukocytes, as both needed higher concentrations to achieve similar effects to the Y9. This reduced function can be attributed to the steric hindrance posed by the attached PEG chains, which is accordance with the observed greater loss of function in the larger compound.

Small proteins like ISErs are well suited to overcome a variety of problems in drug development due to their capacity to carry different modifications, easy handling and fast synthesis potential. With their mass range between conventional antibodies and small molecule drugs, the immune system engagers offer an exciting alternative to the established drugs in use. The different ISErs covered in this thesis alone, can be further analysed, especially the a-ISEr with Val-Cit showed potential worth further research as it has increased effector activity in the DHR oxidation assay compared to the established Y9. It has to be established if the cleavage site is recognized by MMPs expressed by the leucocytes. Another possibility worth exploring is the combination between cleavable effectors and a PEGylated scaffold to take advantage of both approaches, as the PEGylated ISErs displayed a stronger affinity to the integrin α3, compared to Y9. Instead of a PEG chain, a lipide could also be coupled with the same ligation technique as described in this thesis.

10. References

1. Berg, J. M., Stryer, L. & Tymoczko, J. L. *Stryer Biochemie*. (Springer Spektrum, 2013). doi:10.1007/978-3-8274-2989-6.
2. Peptides: Chemistry and Biology, 2nd Edition
3. Pauling, L. & Corey, R. B. A Proposed Structure For The Nucleic Acids. *Proc. Natl. Acad. Sci.* **39**, 84–97 (1953).
4. Góngora-Benítez, M., Tulla-Puche, J. & Albericio, F. Handles for Fmoc Solid-Phase Synthesis of Protected Peptides. *ACS Comb. Sci.* **15**, 217–228 (2013).
5. Behrendt, R., White, P. & Offer, J. Advances in Fmoc solid-phase peptide synthesis. *J. Pept. Sci.* **22**, 4–27 (2016).
6. How the Immune System Works | Lauren M. Sompayrac.
7. citation, A. R. and M. H., M. D.-Author info-Reusing images-Conflicts of interest: NoneMikael HäggströmExample. *Simplified hematopoiesis*. (2009).
8. Medzhitov, R. & Janeway, CharleS. J. Innate immune recognition: mechanisms and pathways: Innate immune recognition. *Immunol. Rev.* **173**, 89–97 (2000).
9. Tonegawa, S., Brack, C., Hozumi, N., Matthyssens, G. & Schuller, R. Dynamics of Immunoglobulin Genes. *Immunol. Rev.* **36**, 73–94 (1977).
10. Zander, H. *et al.* Checkpointinhibitoren in der Tumortherapie. *Bundesgesundheitsblatt - Gesundheitsforschung - Gesundheitsschutz* **63**, 1322–1330 (2020).
11. Scott, A. M., Wolchok, J. D. & Old, L. J. Antibody therapy of cancer. *Nat. Rev. Cancer* **12**, 278–287 (2012).
12. Monoclonal Antibodies for the Treatment of Cancer. *Anticancer Res.* **37**, (2017).
13. Brehs, M. *et al.* Synthetic integrin-binding immune stimulators target cancer cells and prevent tumor formation. *Sci. Rep.* **7**, 17592 (2017).
14. Lu, R.-M. *et al.* Development of therapeutic antibodies for the treatment of diseases. *J. Biomed. Sci.* **27**, 1 (2020).
15. Conibear, A. C. *et al.* Synthetic Cancer-Targeting Innate Immune Stimulators Give Insights into Avidity Effects. *Chembiochem Eur. J. Chem. Biol.* **19**, 459–469 (2018).
16. Pötgens, A. J. G., Conibear, A. C., Altdorf, C., Hilzendeger, C. & Becker, C. F. W. Tumor-Targeting Immune System Engagers (ISErs) Activate Human Neutrophils after Binding to Cancer Cells. *Biochemistry* **58**, 2642–2652 (2019).

17. He, H.-Q. & Ye, R. D. The Formyl Peptide Receptors: Diversity of Ligands and Mechanism for Recognition. *Mol. J. Synth. Chem. Nat. Prod. Chem.* **22**, 455 (2017).
18. Sliwkowski, M. X. & Mellman, I. Antibody therapeutics in cancer. *Science* **341**, 1192–1198 (2013).
19. Rudnick, S. I. & Adams, G. P. Affinity and Avidity in Antibody-Based Tumor Targeting. *Cancer Biother. Radiopharm.* **24**, 155–161 (2009).
20. Yao, N. *et al.* Structure −Activity Relationship Studies of Targeting Ligands against Breast Cancer Cells. *J. Med. Chem.* **52**, 6744–6751 (2009).
21. Sheldrake, H. M. & Patterson, L. H. Strategies To Inhibit Tumor Associated Integrin Receptors: Rationale for Dual and Multi-Antagonists: Miniperspective. *J. Med. Chem.* **57**, 6301–6315 (2014).
22. Meyer, A., van Golen, C. M., Kim, B., van Golen, K. L. & Feldman, E. L. Integrin Expression Regulates Neuroblastoma Attachment and Migration. *Neoplasia* **6**, 332–342 (2004).
23. Obrist, R., Schmidli, J., Müller, R., Gallati, H. & Obrecht, J. P. Acute and subacute toxicity of chemotactic conjugates between monoclonal antibody and fMet-Leu-Phe in humans: A phase I clinical trial. *Cancer Immunol. Immunother.* **32**, 406–408 (1991).
24. Page-McCaw, A., Ewald, A. J. & Werb, Z. Matrix metalloproteinases and the regulation of tissue remodelling. *Nat. Rev. Mol. Cell Biol.* **8**, 221–233 (2007).
25. Cieplak, P. & Strongin, A. Y. Matrix metalloproteinases – from the cleavage data to the prediction tools and beyond. *Biochim. Biophys. Acta* **1864**, 1952–1963 (2017).
26. Cathcart, J., Pulkoski-Gross, A. & Cao, J. Targeting matrix metalloproteinases in cancer: Bringing new life to old ideas. *Genes Dis.* **2**, 26–34 (2015).
27. Gaffney, J., Solomonov, I., Zehorai, E. & Sagi, I. Multilevel regulation of matrix metalloproteinases in tissue homeostasis indicates their molecular specificity in vivo. *Matrix Biol. J. Int. Soc. Matrix Biol.* **44–46**, 191–199 (2015).
28. Quintero-Fabián, S. *et al.* Role of Matrix Metalloproteinases in Angiogenesis and Cancer. *Front. Oncol.* **9**, (2019).
29. Roeb, E. & Matern, S. Matrixmetalloproteinasen als Promotoren der Tumorinvasion und Metastasierung. *Z. Für Gastroenterol.* **39**, 807–813 (2001).
30. Stamenkovic, I. Matrix metalloproteinases in tumor invasion and metastasis. *Semin. Cancer Biol.* **10**, 415–433 (2000).
31. Johansson, N., Ahonen, M. & Kähäri*, V.-M. Matrix metalloproteinases in tumor invasion. *Cell. Mol. Life Sci. CMLS* **57**, 5–15 (2000).

32. TIMPs. https://www.spektrum.de/lexikon/biologie/timps/66762.

33. Hackenberger, C. P. R. & Schwarzer, D. Chemoselective Ligation and Modification Strategies for Peptides and Proteins. *Angew. Chem. Int. Ed.* **47**, 10030–10074 (2008).

34. Kölmel, D. K. & Kool, E. T. Oximes and Hydrazones in Bioconjugation: Mechanism and Catalysis. *Chem. Rev.* **117**, 10358–10376 (2017).

35. Dawson, P. E., Muir, T. W., Clark-Lewis, I. & Kent, S. B. H. Synthesis of Proteins by Native Chemical Ligation. *Science* **266**, 776–779 (1994).

36. Kolb, H. C., Finn, M. G. & Sharpless, K. B. Click Chemistry: Diverse Chemical Function from a Few Good Reactions. *Angew. Chem. Int. Ed.* **40**, 2004–2021 (2001).

37. Dong, J., Krasnova, L., Finn, M. G. & Sharpless, K. B. Sulfur(VI) Fluoride Exchange (SuFEx): Another Good Reaction for Click Chemistry. *Angew. Chem. Int. Ed.* **53**, 9430–9448 (2014).

38. Liang, L. & Astruc, D. The copper(I)-catalyzed alkyne-azide cycloaddition (CuAAC) "click" reaction and its applications. An overview. *Coord. Chem. Rev. - COORD CHEM REV* **255**, 2933–2945 (2011).

39. Hein, J. E. & Fokin, V. V. Copper-catalyzed azide–alkyne cycloaddition (CuAAC) and beyond: new reactivity of copper(I) acetylides. *Chem. Soc. Rev.* **39**, 1302–1315 (2010).

40. Tiefenbrunn, T. K. & Dawson, P. E. Chemoselective ligation techniques: Modern applications of time-honored chemistry. *Pept. Sci.* **94**, 95–106 (2010).

41. Dirksen, A., Dirksen, S., Hackeng, T. M. & Dawson, P. E. Nucleophilic Catalysis of Hydrazone Formation and Transimination: Implications for Dynamic Covalent Chemistry. *J. Am. Chem. Soc.* **128**, 15602–15603 (2006).

42. Ollivier, N. *et al.* Catalysis of Hydrazone and Oxime Peptide Ligation by Arginine. *Org. Lett.* **22**, 8608–8612 (2020).

43. Larsen, D. *et al.* Exceptionally rapid oxime and hydrazone formation promoted by catalytic amine buffers with low toxicity. *Chem. Sci.* **9**, 5252–5259 (2018).

44. Hermanson, G. T. Chapter 2 - Functional Targets for Bioconjugation. in *Bioconjugate Techniques (Third Edition)* (ed. Hermanson, G. T.) 127–228 (Academic Press, 2013). doi:10.1016/B978-0-12-382239-0.00002-9.

45. Laemmli, U. K. Cleavage of Structural Proteins during the Assembly of the Head of Bacteriophage T4. *Nature* **227**, 680–685 (1970).

46. Li, D. & Elbert, D. L. The kinetics of the removal of the N-methyltrityl (Mtt) group during the synthesis of branched peptides. *J. Pept. Res.* **60**, 300–303 (2002).

47. Zayas, J. F. Foaming Properties of Proteins. in *Functionality of Proteins in Food* (ed. Zayas, J. F.) 260–309 (Springer, 1997). doi:10.1007/978-3-642-59116-7_6.
48. Schneggenburger, P. E., Worbs, B. & Diederichsen, U. Azide reduction during peptide cleavage from solid support—the choice of thioscavenger? *J. Pept. Sci.* **16**, 10–14 (2010).
49. Nshanian, M., Lakshmanan, R., Chen, H., Ogorzalek Loo, R. R. & Loo, J. A. Enhancing Sensitivity of Liquid Chromatography–Mass Spectrometry of Peptides and Proteins Using Supercharging Agents. *Int. J. Mass Spectrom.* **427**, 157–164 (2018).
50. ARCHS4. https://maayanlab.cloud/archs4/gene/MMP2#tissueexpression.
51. Murphy, G. *et al.* Mechanisms for pro matrix metalloproteinase activation. *APMIS* **107**, 38–44 (1999).
52. ARCHS4. https://maayanlab.cloud/archs4/gene/MMP24.
53. Eckhard, U. *et al.* Active site specificity profiling of the matrix metalloproteinase family: Proteomic identification of 4300 cleavage sites by nine MMPs explored with structural and synthetic peptide cleavage analyses. *Matrix Biol. J. Int. Soc. Matrix Biol.* **49**, 37–60 (2016).
54. Vrettos, E. I. *et al.* Unveiling and tackling guanidinium peptide coupling reagent side reactions towards the development of peptide-drug conjugates. *RSC Adv* **7**, 50519–50526 (2017).
55. Edsparr, K., Basse, P. H., Goldfarb, R. H. & Albertsson, P. Matrix Metalloproteinases in Cytotoxic Lymphocytes Impact on Tumour Infiltration and Immunomodulation. *Cancer Microenviron.* **4**, 351–360 (2010).
56. Albertsson, P. *et al.* Matrix metalloproteinases of human NK cells. *Vivo Athens Greece* **14**, 269–276 (2000).

All websites last accessed at 20th of June 2022

11. Supplementary Information

11.1 Y9-N_3 final analysis

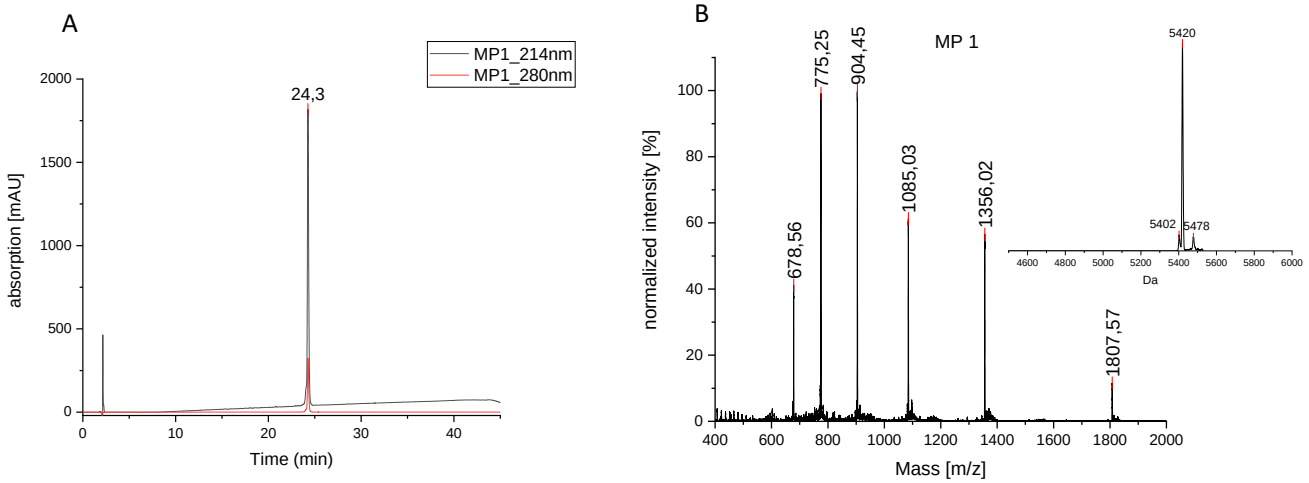

*S 1 A) RP- HPLC final analysis of Y9-N_3 MP1 at 214 and 280 nm **B)** Mass spectrogram of Y9-N_3 MP1 and the deconvoluted spectrum. MW_{calc}: 5420 Da*

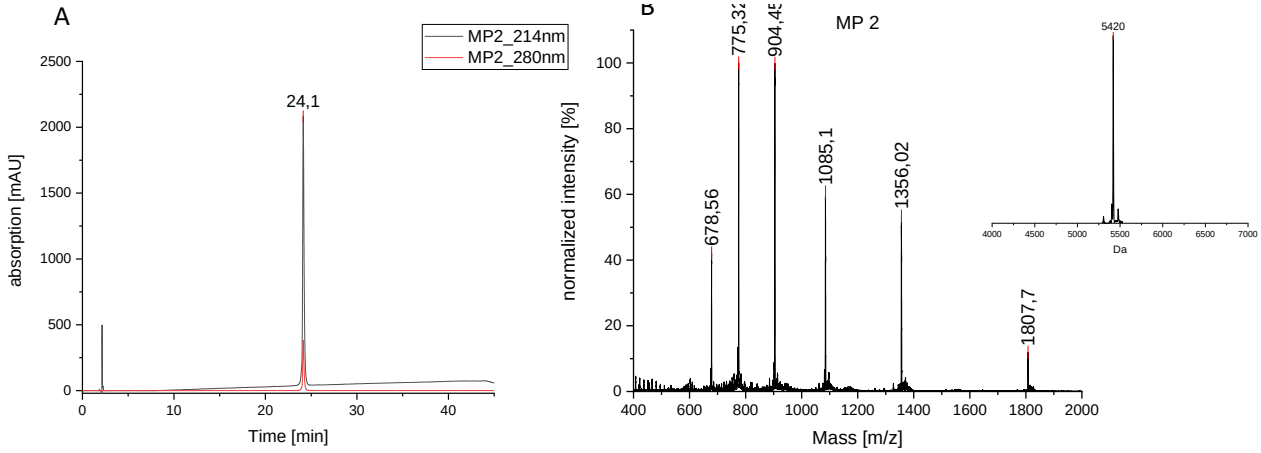

*S 2 A) RP- HPLC final analysis of Y9-N_3 MP2 at 214 and 280 nm **B)** Mass spectrogram of Y9-N_3 MP2 and the deconvoluted spectrum. MW_{calc}: 5420 Da*

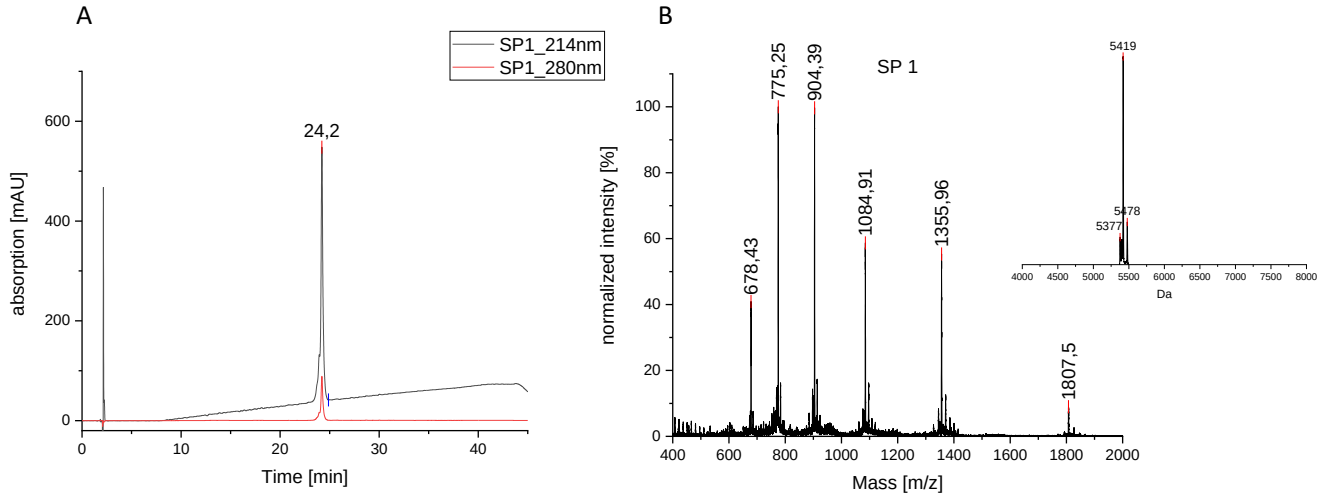

*S 3 A**)** RP- HPLC final analysis of Y9-N_3 SP1 at 214 and 280 nm **B)** Mass spectrogram of Y9-N_3 SP1 and the deconvoluted spectrum. MW_{calc}: 5420 Da*

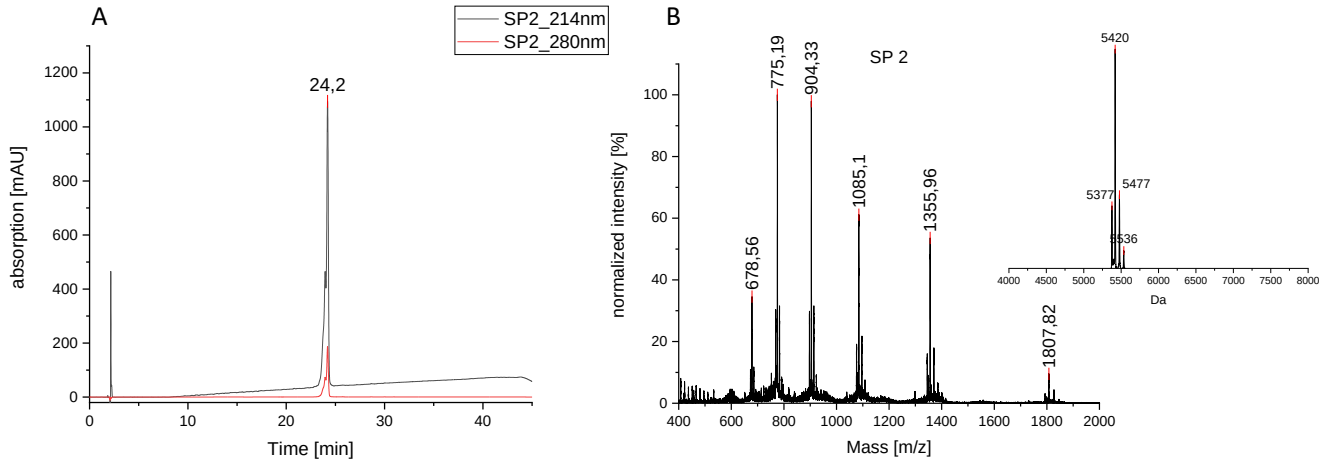

*S 4 A**)** RP- HPLC final analysis of Y9-N_3 SP1 at 214 and 280 nm **B)** Mass spectrogram of Y9-N_3 SP1 and the deconvoluted spectrum. MW_{calc}: 5420 Da*

11.2 Val- Cit final analysis

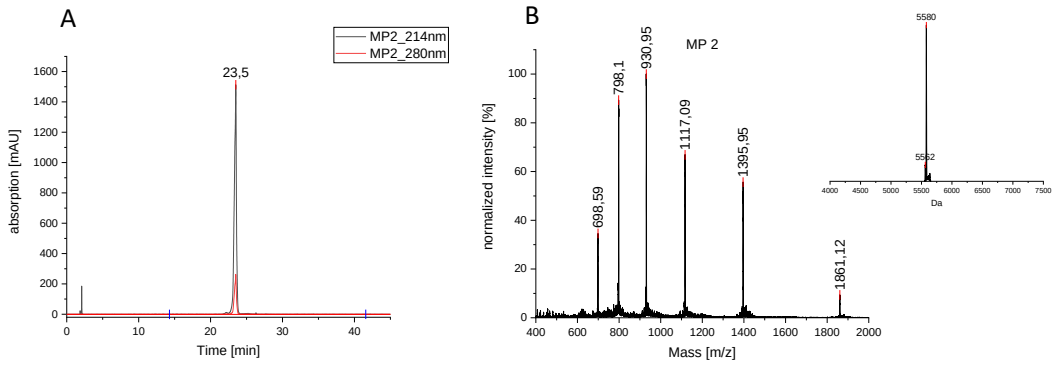

*S 5 **A)** RP- HPLC of a-ISEr Val-Cit from MP2. **B)** Mass spectrum and deconvoluted spectrum of a-ISEr Val-Cit MP2. Calculated mass: 5581 Da*

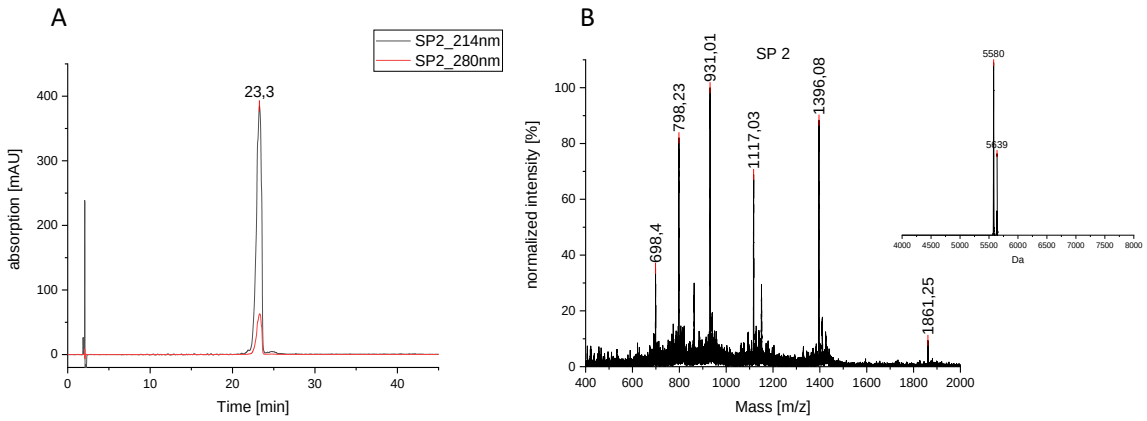

S 6 ***A)*** *RP- HPLC of a-ISEr Val-Cit from SP2.* ***B)*** *Mass spectrum and deconvoluted spectrum of a-ISEr Val-Cit SP2. Calculated mass: 5581 Da*

11.3 Y9-N3 Data from HT29 cell culture studies

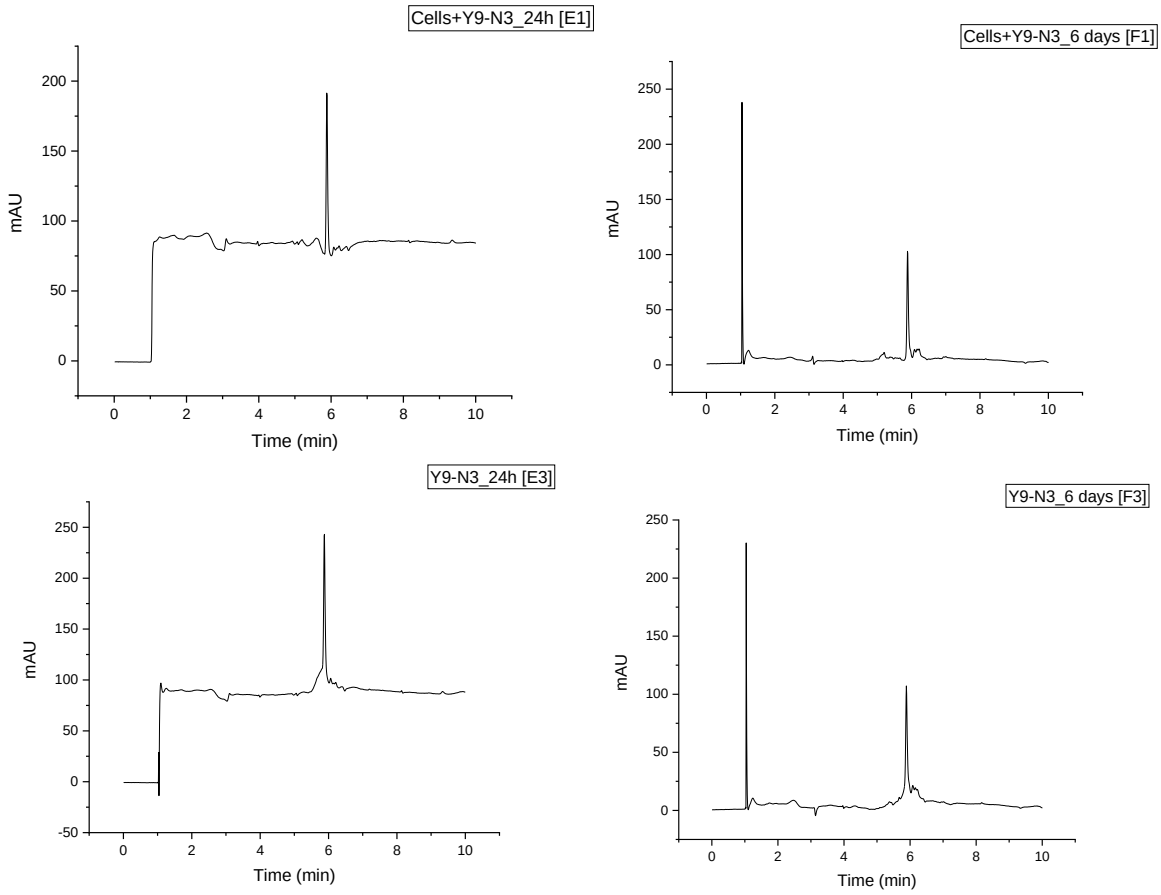

S 7 Y9-N$_3$ incubated with and without cells. Right hand side results after 24h. Left hand side results after 6 days

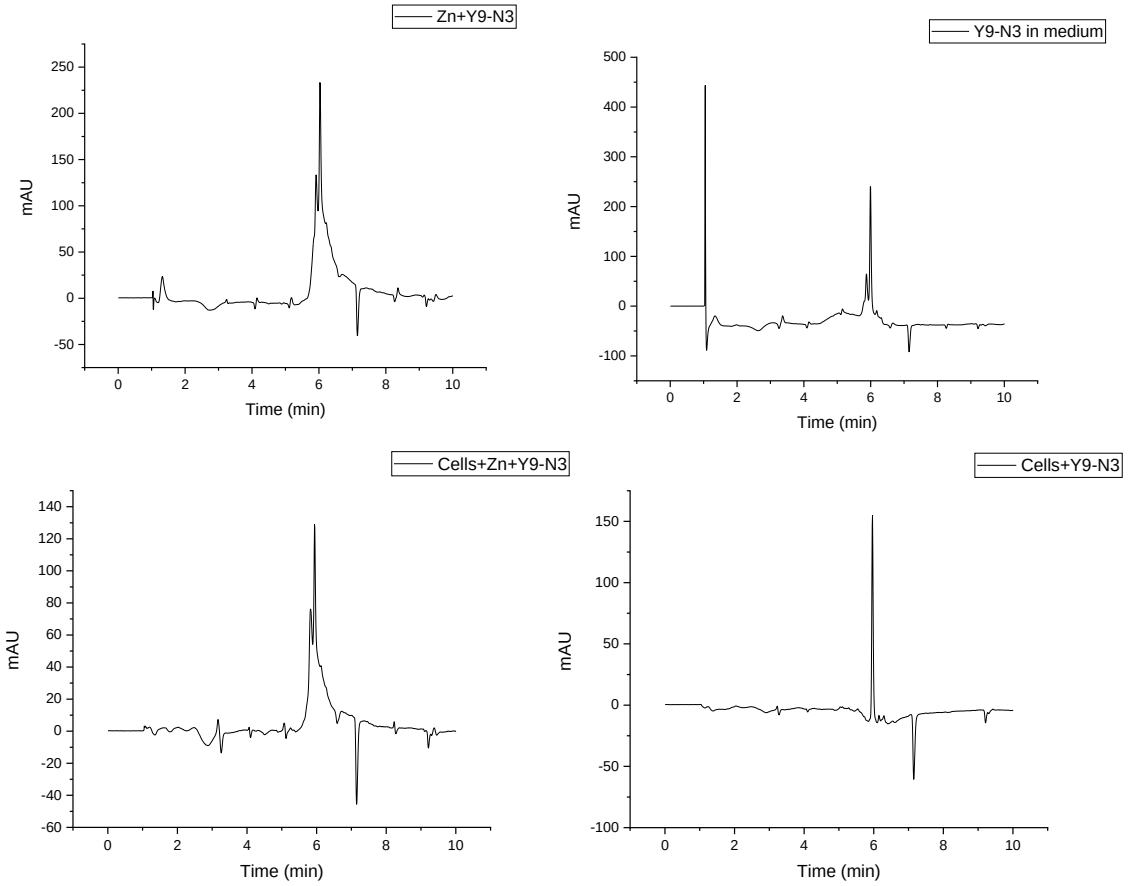

S 8 Y9-N_3 incubated with and without cells. Analysis after 24h incubation time. On the right hand side with the addition of the co-factor Zn^{2+}

11.4 Results from binder studies

A

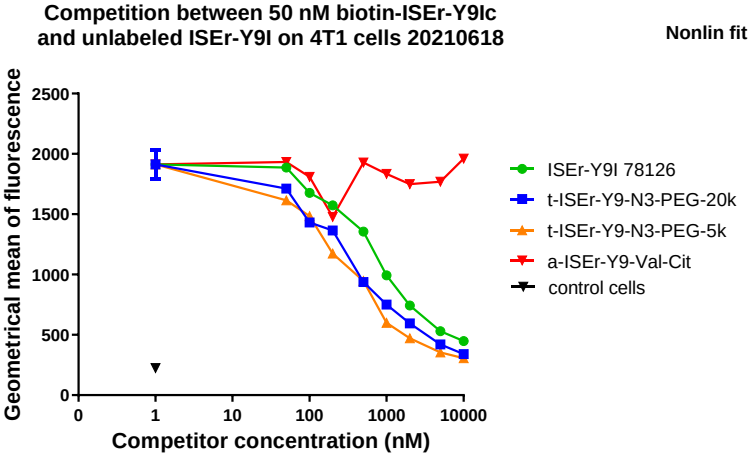

B

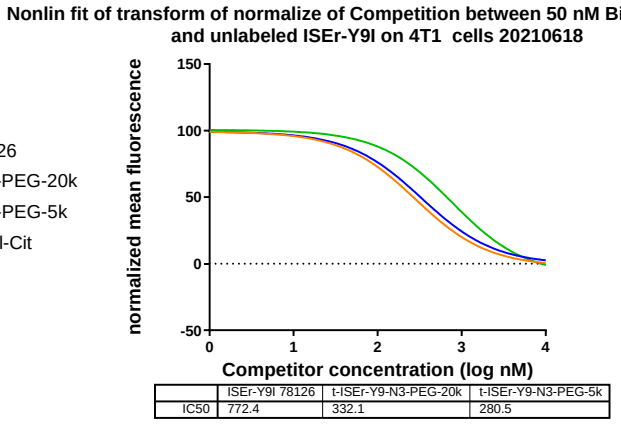

	ISEr-Y9l 78126	t-ISEr-Y9-N3-PEG-20k	t-ISEr-Y9-N3-PEG-5k
IC50	772.4	332.1	280.5

S 9 ***A)*** *measured fluorescence of 4T1 cell line after staining with 50 nm Biotin-ISEr_Y9lc against the competitor concentration. Measured fluorescence on the cells not incubated with peptide (background signal) is visible as a black triangle.* ***B)*** *Normalized fit of the data and the calculated IC50 values in nM. ISEr-Y9l 78126 (green), t-ISEr-Y9-N_3-20k-PEG (blue), t-ISEr Y9-N_3 5kPEG (orange)*

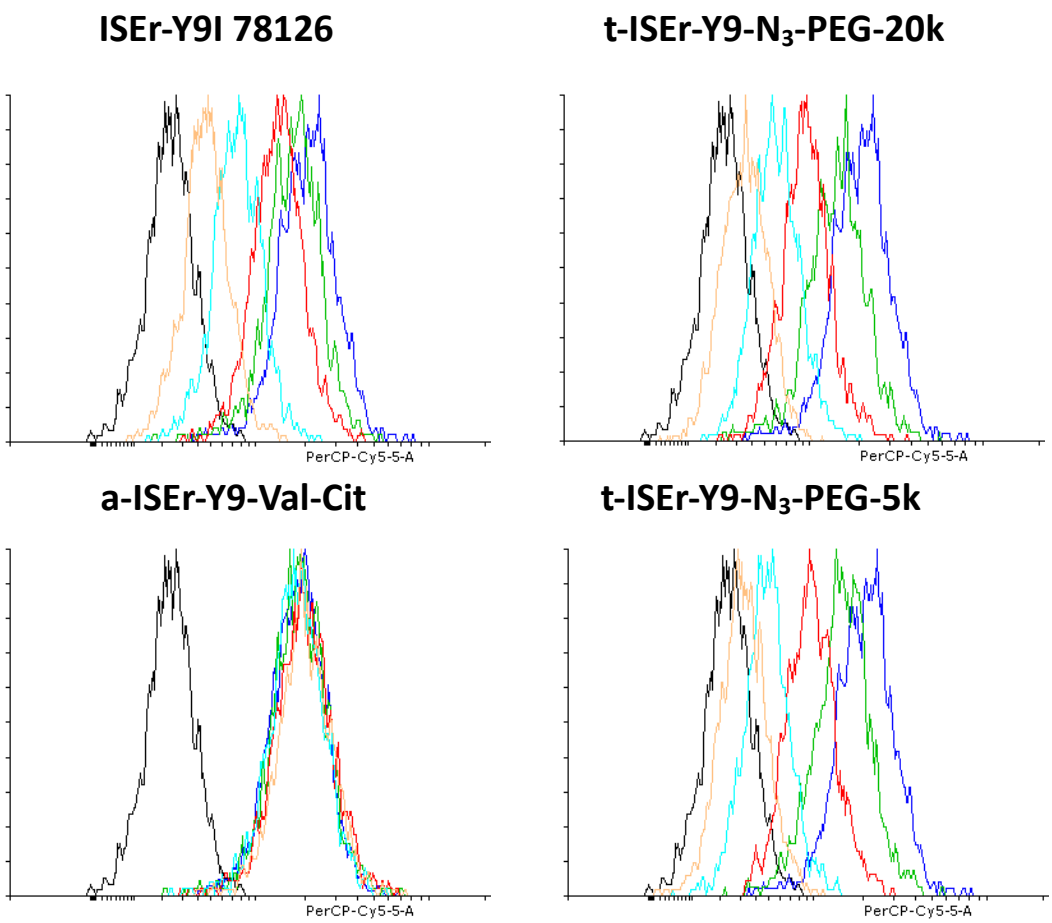

S 10 Overlay histograms of 4T1 cells incubated with 50 nM biotin-ISEr-Y9Ic along with 0 (blue), 100 nM (green), 500 nM (red), 2 µM (turquoise) or 10 µM (orange) of the different ISEr-Y9I variants, and stained with Streptavidin-PerCP-Cy5.5; black: no biotin-ISEr-Y9Ic

A

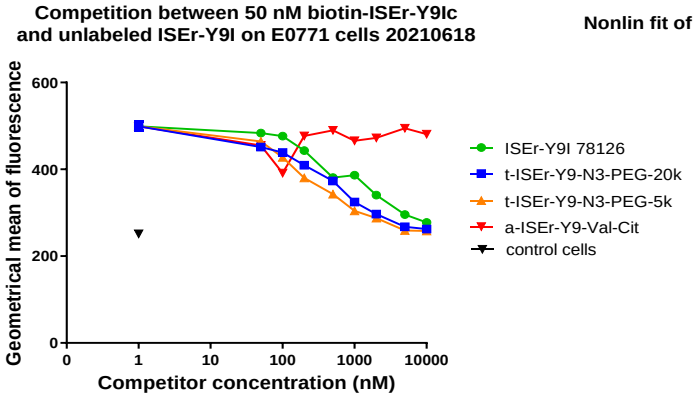

B

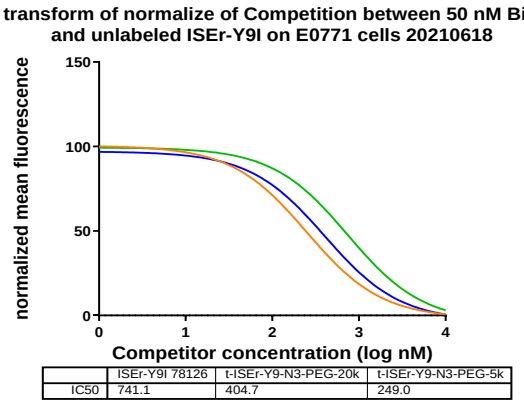

	ISEr-Y9I 78126	t-ISEr-Y9-N3-PEG-20k	t-ISEr-Y9-N3-PEG-5k
IC50	741.1	404.7	249.0

*S 11 **A)** measured fluorescence of E0771 cell line after staining with 50 nm Biotin-ISEr_Y9Ic against the competitor concentration. Measured fluorescence on the cells not incubated with peptide (background signal) is visible as a black triangle. **B)** Normalized fit of the data and the calculated IC50 values in nM. ISEr-Y9I 78126 (green), t-ISEr-Y9-N_3-20k-PEG (blue), t-ISEr Y9-N_3 5kPEG (orange)*

ISEr-Y9I 78126

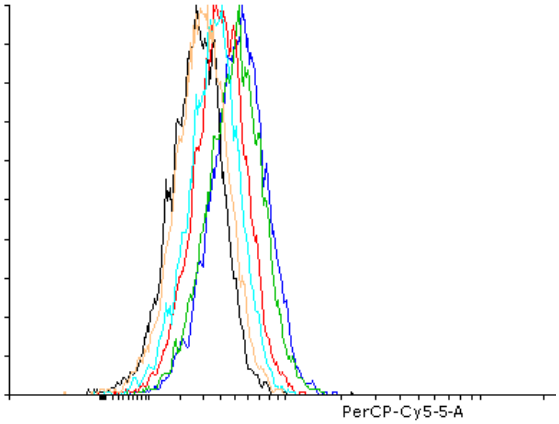

t-ISEr-Y9-N_3-PEG-20k

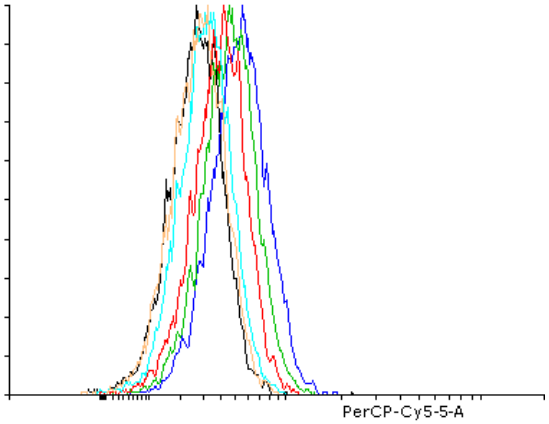

a-ISEr-Y9-Val-Cit

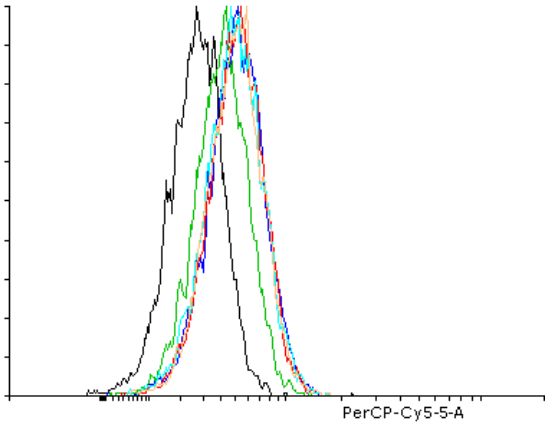

t-ISEr-Y9-N_3-PEG-5k

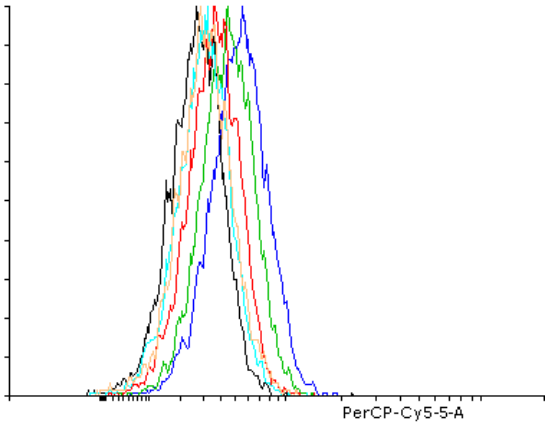

S 12 Overlay histograms of E0771 cells incubated with 50 nM biotin-ISEr-Y9Ic along with 0 (blue), 100 nM (green), 500 nM (red), 2 µM (turquoise) or 10 µM (orange) of the different ISEr-Y9I variants, and stained with Streptavidin-PerCP-Cy5.5; black: no biotin-ISEr-Y9Ic

11.5 Gated cells from DHR assay

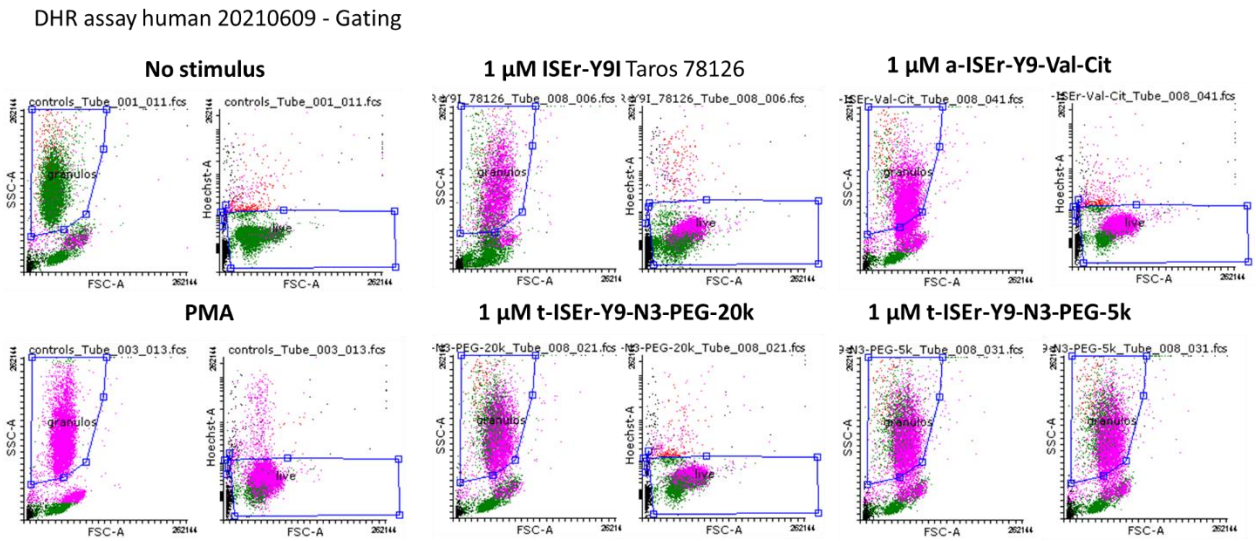

S 13 Gating strategy for live human blood-derived granulocytes after stimulation with buffer only, PMA, 1 µM ISEr-Y9l (78126), 1 µM t-ISErs, 1µM a-ISEr, or 1 µM ISEr-ssc Y9l 2020-004